

## **2.1 NOVEL HYBRID MATERIALS- METAL PHOSPHONATES**

### ***Introduction***

Metal Phosphonates are hybrid inorgano-organic compounds which have been extensively studied [1-6]. In them, the nature of the organic moiety may be designed to confer specific properties to arrive at compounds with different network such as, open framework, layered or pillared materials and even one dimensional solids. These hybrid materials have potential applications in catalysis, proton conductivity, as absorbents, ion exchangers, or as hosts in intercalation reactions [7-14].

Zirconium phosphate and titanium phosphate of the class of TMA salts are now well-known inorganic ion-exchange materials and have shown a number of advantages as ideal host lattices [15,16]. In the tetrahedral moiety of phosphoric acid,  $\text{PO}(\text{OH})_3$ , if H or OH is replaced by R (where R = alkyl or aryl), phosphonic acids are obtained, which when treated with tetravalent metals such as  $\text{Zr}^{4+}$ ,  $\text{Ti}^{4+}$ ,  $\text{Sn}^{4+}$ ,  $\text{Th}^{4+}$ ,  $\text{Ce}^{4+}$  etc. gives rise to metal phosphonates [17,18].

Metal phosphonates are often layered hybrid inorgano-organic compounds in which the inorganic part forms the central portion of the layer with pendant organic groups on both sides of this central layer [19]. The nature of the phosphonate can be shaped by the choice of the organic functionality such as when they possess ionogenic groups  $-\text{OH}$ ,  $-\text{COOH}$ ,  $-\text{SO}_3\text{H}$  etc. compounds that behave as ion exchangers and fast proton conductors are obtained [19].

Metal Phosphonates were first reported around 25 years ago by Yamanaka et al. [20,21] Since then, much effort has been put into the synthesis and chemistry of these materials, which has resulted in the development of new synthetic methods and strategies. Yamanaka's work, based on that of Clearfield and Smith and Alberti et al on layered zirconium hydrogen phosphonates, proved to be the first of thousands of papers that would be published on the subject of layered M(IV) phosphonates.

The structure of these materials can briefly be described as an inorganic layer, consisting of M(IV) ions octahedrally co-coordinated by  $\text{PO}_3$  groups, with the organic functional groups pendant in the interlayer region (**Figure 2.1**).

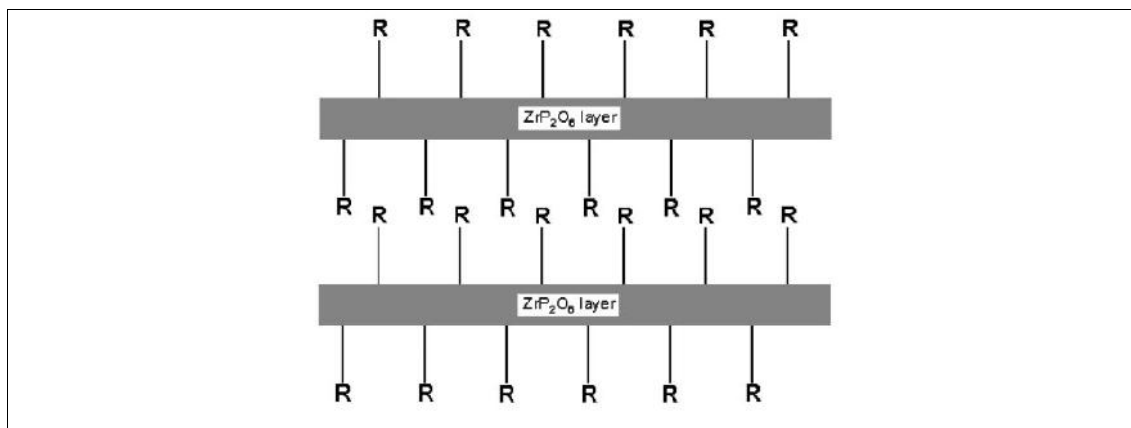


**Figure 2.1** Schematic representation of the arrangement of layers in Zirconium phosphonates [22]

There is now an enormous diversity in the organic functional groups that can be included in these materials. Early work was concerned with simple phosphonates, with R as an alkyl chain or phenyl group, whereas later studies have involved more complex groups.

$\alpha$ -zirconium phosphonates (**Figure 2.2**), of general formula  $Zr(O_3PR)_2$  are known since 1978. These compounds with layered structure is similar to that of the parent compound  $\alpha$ -ZrP (zirconium phosphate), where two organic R groups per zirconium atom point towards the interlayer region. The free area associated with each R group is  $24 \text{ \AA}^2$  ( $\alpha$ -type) and, in general, the interlayer space is filled by these organic groups, that are arranged in a compact double layer. Zirconium phosphonates  $Zr(O_3PR)_2$  can be synthesized using phosphonic acids instead of phosphoric acid. A generic phosphonate derivative of  $\alpha$ -zirconium phosphate has formula  $ZrPO_4[O_2P(OH)R]$ . In  $\beta$ -type structure the free area associated with each R group is  $36 \text{ \AA}^2$ . In this case also the organic groups tend to fill the interlayer region by a compact double layer [6].

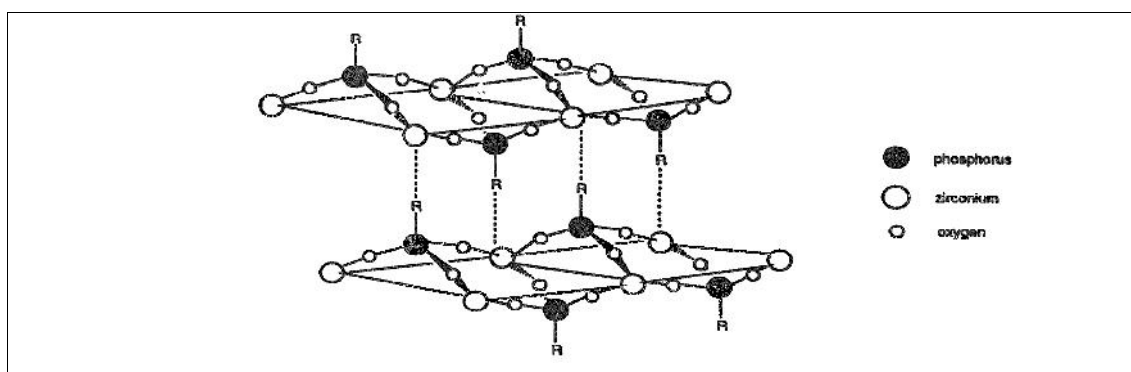


**Figure 2.2** Structure of Zirconium phosphonates [23]

An extensive literature on metal phosphonates exists today, which have been reviewed and detailed [1-6].

The most promising feature of these metal phosphonates is the ease with which pillared or intercalated structures can be obtained. However, because of the entrance of the guest molecules between the layers, there is a change in the interlayer distance [24].

The majority of these layered materials have a common method of synthesis, regardless of the functional group. The procedure involves the initial formation of a fluoride complex of the M(IV) cation in solution, which is subsequently decomposed at 60-70 °C in the presence of a phosphonic acid. The attraction of this method is its general applicability to the synthesis of a large number of metal phosphonates with a wide range of organic functional groups [22].

During the past few decades much effort has been dedicated to obtain metal phosphonate as porous materials by using organo-diphosphonate ligands ( $O_3P-R-PO_3$ )<sup>n-</sup> where R = organic moiety, whose combination with metal ions, generally [M(IV)] are expected to lead to 3D structures with open frame works without using organic templates. The use of alkyl/aryl diphosphonate would allow manipulation of the length of the carbon atom to increase and modulate the size of the pores [18]. The porosity of the final compound is related to the rigidity of the organic linkers. This method gives more chance to obtain microporosity or mesoporosity [8].

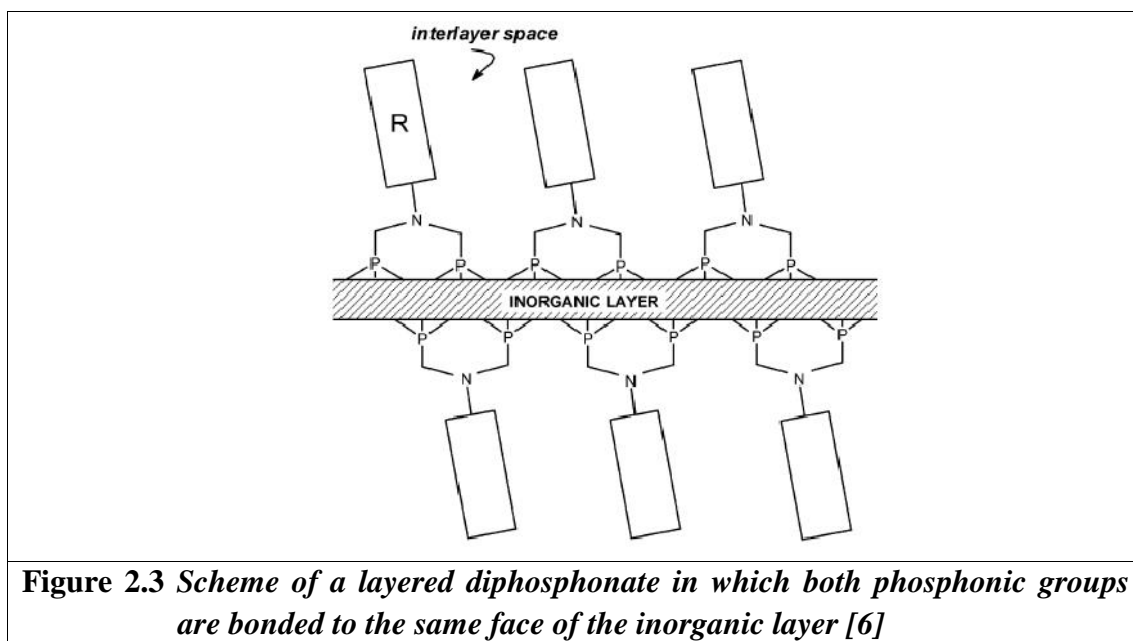
In M(IV) diphosphonates, these anions effectively form bridge between two metal atoms. In case of biphenyls that are fully pillared, no porosity is expected. With few exceptions, attempts to include porosity by interspersing smaller phosphate or phosphite groups between the pillars are reported to give rise to mesoporosity due to structural disorder. At best, the porosity is not uniform and broad pore size distributions are observed [22].

According to Clearfield et al., the stacking of unequally sized layers could yield the pores. Thus, uncontrolled stacking and randomly-sized layers are the intrinsic difficulties that prevent preparing highly ordered porous zirconium phosphonates [8].

### ***Amino phosphonates***

Amino phosphonic acids have received considerable attention [5, 6, 25] due to the diverse binding abilities/chelating ability/effectiveness of donor group in the

binding of tetravalent metal ions. Organo phosphonates containing multi-dentate building blocks e.g. tri/tetra/penta phosphonate groups, such as Claw molecules of the type Amino Tris Methylene Phosphonic Acid (ATMP), Ethylene Diamine Tetramethylene Phosphonic acid (EDTMP), Diethylene Triamine Pentamethylene Phosphonic acid (DETPMP), N, N' – diamino butyl tetra methyl phosphonic acid (DBTMP), and N, N' – diamino cyclohexyl tetra methyl phosphonic acid (DCTMP), etc, also contain Lewis bases as additional coordinating sites. These organo phosphonates when combined with tetravalent metal ions, can induce cross linking, the dimensions of which can be tailored by the right choice of interlinking organic groups. Further, the organic species incorporated in an inorganic phase, permits control of porosity, hydrophobicity/hydrophilicity, ion exchange characteristics (organic moiety containing ionogenic groups), using a sol-gel chimie douce approach. This creates a different strategy to reduce overcrowding of organic groups in the interlayer space. It consists in the use of selected building blocks that can connect both phosphonic groups to metal atoms on the same side of layers, as schematically shown in **Figure 2.3**. One organic residue is associated to each two phosphonate tetrahedra, through the amino group, allowing to accommodate large organic groups covalently bonded to the inorganic backbone [6].



## 2.2 LITERATURE SURVEY IN THE CURRENT AREA OF STUDY

Tian-Yi Ma et al have reported new periodic mesoporous titanium phosphonates, abbreviated as PMTP-1, PMTP-2, TPPH [26-28]. PMTP-1 was synthesized using ethylene diamine tetra (methylene phosphonic acid) (EDTMPS). The wastewater cleanup test shows that the synthesized PMTP-1 materials had large metal ion adsorption capacity and high photocatalytic activity. The further functionalization of the PMTP-1 materials would extend their performances non localized in adsorption and catalysis. PMTP-2 was synthesized by an autoclaving process combined with the evaporation-induced self-assembly (EISA) method, using the coupling molecule 1-hydroxy ethylidene-1,1-diphosphonic acid (HEDP). The synthesized PMTP-2 was functionalized by sulfation with  $\text{ClSO}_3\text{H}$ , leading to a large ion exchange capacity. The as-synthesized monoliths could be moulded into various macroscopic morphologies, which may potentially fulfill the qualifications for some industrial devices. The synthesized materials TPPH (F127, P123) were used as adsorbents for the liquid phase adsorption of  $\text{Cu}^{2+}$  ions in water and the gas phase adsorption of  $\text{CO}_2$ , showing high adsorption capacity and good reusability, which makes them promising adsorbents for practical application in environment remediation. Ma T. Y. et al have also reported adsorption of heavy metal ions and  $\text{CO}_2$  using TiHEDP [29] and TiATMP [30].

Guerrero G. et al have reported Titanium oxide/phenylphosphonate hybrids, prepared by a two-step sol-gel processing, involving first the nonhydrolytic condensation between titanium isopropoxide and phenylphosphonic acid (or the parent bis(trimethylsilyl) ester), followed by the hydrolysis and condensation of the remaining alkoxide groups. Partial hydrolysis led to the formation of  $\text{Ti}_4(\mu_3\text{-O})(\mu_2\text{-O}^i\text{Pr})_3(\text{O}^i\text{Pr})_5(\text{PhPO}_3)_3$ ; the potential use of this intermediate compound as a single-source precursor was explored [31].

Mehring M. et al reported the syntheses, characterizations and single-crystal x-ray structures of soluble titanium alkoxide phosphonates  $[\text{Ti}_4(\mu_3\text{-O})(\text{O}^i\text{Pr})_5(\mu\text{-O}^i\text{Pr})_3(\text{RPO}_3)_3]\cdot\text{DMSO}$  ( $\text{R} = \text{Ph}, \text{Me}, t\text{-Bu}, 4\text{-CNPh}$ ) and the titanium alkoxide phosphonate  $[\text{Ti}(\text{O}^i\text{Pr})_2(t\text{BuPO}_3)]_4$  [32].

Tsai T. Y. et al reported a new type of zirconium phosphonate derivative (Zr-P). This Zr-P is hybridized with an epoxy polymer to synthesize epoxy/zirconium

phosphate nano-composite. The material has a reasonably good optical property even with 10 wt% loading of layered material to the epoxy polymer matrix [33].

Zhang X. J. et al reported Titania-phosphonate hybrid porous materials using claw type molecules ethylene diamine tetra(methylene phosphonic acid) and diethylene triamine penta(methylene phosphonic acid) through anchoring process [34].

Zeng R. et al reported layered metal phosphonates zirconium benzylamino-N,N-dimethyl phosphonate phosphate materials [35].

Chessa et al reported  $\alpha$ -zirconium phosphonates using supports of N-heterocyclic carbines [36].

Ma X. et al reported novel type organosoluble and filiform zirconium phosphonate with the layered mesoporous backbone functionalized with hydroxyl and amino groups [37].

Shimizu G. K. H. et al have reviewed on “progress in phosphonates and sulphonates”. This review shows that their differences likely outweigh their similarities when it comes to their framework, structures and properties [38].

Wu Z. et al reported two porous zirconium methylphosphonates, microporous ZMPmi and mesoporous ZMPme, were prepared by using dibutyl methylphosphonate (DBMP) as the template [8].

Zhang B. et al reported new types of zirconium layered compounds containing the *N*-(phosphonomethyl) iminodiacetic acid group (PMIDAH<sub>2</sub>) that have been synthesized and characterized. In this paper, they have reported the reaction products formed by H<sub>2</sub>PMIDAH<sub>2</sub> and a zirconium salt in the presence of H<sub>3</sub>PO<sub>4</sub>, under varied conditions, and their intercalation properties. The ion-exchange behavior of these compounds is also discussed [19].

Ayyappan Subbiah et al reported a family of microporous materials formed by Sn(IV)phosphonate nanoparticles, e.g. Sn(O<sub>3</sub>PC<sub>6</sub>H<sub>5</sub>)<sub>2</sub>, Sn(O<sub>3</sub>PC<sub>6</sub>H<sub>5</sub>)(O<sub>3</sub>PCH<sub>3</sub>), Sn(O<sub>3</sub>PC<sub>12</sub>H<sub>8</sub>PO<sub>3</sub>), and Sn(O<sub>3</sub>PC<sub>6</sub>H<sub>4</sub>C<sub>6</sub>H<sub>5</sub>)(O<sub>3</sub>PCH<sub>3</sub>). A consequence of their very small particle size is that the particles aggregate into micron-sized spheres that create tunnels that represent micropores. The characteristic suggests their use in separations, not only by size but also by control of hydrophilic hydrophobic character or by chemical character [39].

Christian Serre et al reported hydrothermal synthesis and structure determination from powder data of new three-dimensional titanium(IV) diphosphonates -  $\text{Ti}(\text{O}_3\text{P}-(\text{CH}_2)_n-\text{PO}_3)$  [40].

Zhong-Yong Yuan et al reported cubic mesoporous titanium phosphonates with multifunctionality, by one pot hydrothermal autoclaving process, with the assistance of cationic surfactant cetyl trimethyl ammonium bromide. 1-hydroxyethylidene-1,1-diphosphonic acid was used as the coupling molecule and its application as adsorbent explored for heavy metal-ion adsorption and  $\text{CO}_2$  capture [41].

Faghihian H. et al reported synthesis and characterization of novel zirconium phosphonate using 4-carboxyphenylamino-bis-methylphosphonic acid, and reported its use as ion exchange material for removal of  $\text{Ni}^{2+}$ ,  $\text{Cu}^{2+}$  and  $\text{Zn}^{2+}$  from aqueous solution [42].

Zhong-Yong Yuan et al reported mesoporous zirconium phosphonate materials using 1-hydroxyethylidene-1,1-diphosphonic acid as coupling molecule and cetyl trimethyl ammonium bromide as template. The hydroxyethylidene-bridged mesoporous zirconium phosphonate was used as solid-acid catalyst for the synthesis of methyl-2,3-isopropylidene- $\beta$ -D-ribofuranoside from D-ribose [43].

Qinghong Xu et al reported mesoporous zirconium phosphonate hybrid material using nitrilotris(methylene)-triphosphonic acid (ATMP) and explored its application in removal of heavy metal ions (such as  $\text{Pb}^{2+}$ ,  $\text{Cu}^{2+}$  and  $\text{Cd}^{2+}$ ) [44].

Rachel A. Caruso et al reported surface functionalised nanofibre using titanium–zirconium oxide and amino tris(methylene phosphonic acid) (ATMPA) and explored its application as adsorbent for removal of heavy metal ions [45].

Marco Taddei, et al reported one dimensional, two-dimensional, and three-dimensional zirconium phosphonates based on glyphosate and glyphosine and studied its proton conductivity properties [46].

Grailot A. et al reported thermosensitive copolymer sorbents by free radical copolymerisation between the N-n-propylacryl amide (NnPAAm) and the (dimethoxyphosphoryl)methyl-2-methylacrylate(MAPC1), followed by a hydrolysis of the phosphonated esters into phosphonic diacid groups (h MAPC1). The thermosensitivity and sorption abilities of the resulting poly(NnPAAm-stat- $_h$  MAPC1) copolymers were studied [47].

Z. Wang et al reported synthesis of manganese phosphonate (NH<sub>4</sub>)Mn(hedpH) (hedp = 1-hydroxyethylidenediphosphonate) (denoted as MnP) under hydrothermal conditions, and reported its use for removal of heavy metal ions Pb(II), Cu(II) from aqueous solutions [48].

K. Demadis et al reported synthesis and characterization of Cu(II) phenylvinylphosphonate (PVP) [49].

Zhen-Gang Sun et al reported 2D layered cobalt (II) phosphonates using 2-hydroxyphosphonoacetic acid under hydrothermal conditions. The material exhibits surface photovoltage properties [50].

### 2.3 AIM AND SCOPE OF THE PRESENT WORK

Recently, interest has been generated in the preparation of some organic based inorganic ion exchangers, where there is a promise of developing new materials, giving rise to new, composite and interesting properties [4, 7, 51]. Tetravalent metal acid (TMA) salts are inorganic ion exchangers. The protons present in the structural hydroxyl groups can be exchanged for several cations and thus they behave as cation exchangers [52,53]. Anchoring of organic units on the backbone of TMA salts is of particular interest, since they have a rigid inorganic back bone and flexibility of the organic groupings. M(IV) phosphates where M(IV)= Zr or Ti of the class of TMA salts have been studied as ion exchangers for metal separations[54,55]. In the tetrahedral moiety of phosphoric acid, PO(OH)<sub>3</sub>, if H or OH is replaced by R (where R=alkyl or aryl possessing ionogenic groups such as -COOH, -OH, -SO<sub>3</sub>H etc.), phosphonic acid is obtained, which when treated with tetravalent metals such as Zr, Ti, Sn, Th, Ce etc. give rise to novel metal phosphonates[3,4,14,18,56].

Aminophosphonic acids possess effectiveness of donor groups in the binding of tetravalent metal ions, and have received considerable attention due to the diverse binding abilities [5, 6]. As discussed earlier in the text, several metal amino phosphonates have been synthesized and used for metal ion adsorption [26-28, 44, 45, 48].

From our laboratory we have reported the synthesis of zirconium and titanium based phosphonates such as ZrHEDP[54], TiHEDP[55], ZrTHEDP[57], ZrDETPMP[58] and TiDETPAMP[59] (where HEDP= hydroxy ethylidene diphosphonic acid and DETPMP=diethylene triamine penta(methylene phosphonic

acid). These materials have been used as cation exchangers for metal ion separations [54-59].

The present study is focused towards synthesis of amorphous novel hybrid metal amino phosphonates, ZrATMP and TiATMP (where, ATMP = amino tri(methylene phosphonic acid) using a sol-gel route and exploring the utility of these materials as ion exchangers in column operations. Amorphous materials are preferred [60] to crystalline materials as they can be obtained in a range of mesh sizes suitable for column operations. Crystalline materials have shown the disadvantage of small grain size, restricting their application in column operation. ATMP (**Figure 2.4a**), a claw type amino phosphonic acid (possessing six structural hydroxyl groups, compared to phosphoric acid  $H_3PO_4$  (**Figure 2.4b**) which has three structural hydroxyl groups) was used with the intention of obtaining higher cation exchange capacity in terms of pendant hydroxyl groups in the resulting metal phosphonate which would offer good affinity as well as selectivity for metal ions.

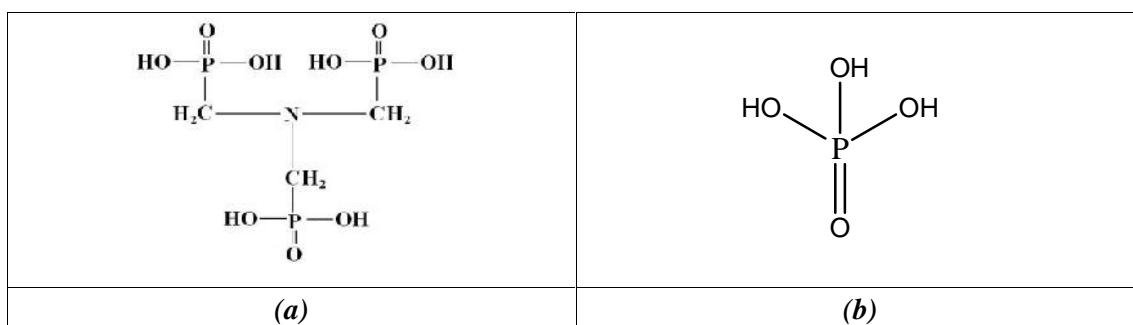


**Figure 2.4 (a) structure of ATMP (b) structure of phosphoric acid**

The present study deals with the synthesis and characterization of amorphous novel hybrid materials, metal phosphonates of the class of TMA (Tetravalent Metal Acid) salts,

- a) **Zirconium amino tris-methylene phosphonate (ZrATMP)**
- b) **Titanium amino tris-methylene phosphonate (TiATMP)**

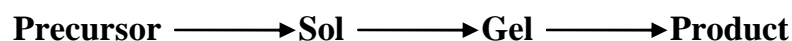
With an increasing concern around the world for green technologies, much attention is focused towards the development of alternate synthetic routes. Presently, soft chemistry routes involving low temperatures, popularly known as “Chimie Douce” by the French, are fast replacing the traditional ceramic (Brute force) methods. The traditional ceramic methods involve mixing and grinding powders of the constituents as oxides, nitrates, sulphates, chlorides or carbonates and heating

them at high temperatures and high pressures with intermediate grinding, mixing and rapid quenching. The present day trend is to avoid brute force methods in order to get a better control of the structure at molecular level, stoichiometry and phasic purity. Low temperature chemical routes and reactions which involve mild conditions are of great interest and more preferred because of the ensuing energy savings.

The materials ZrATMP and TiATMP have been synthesized by sol-gel route that represents the most essential component of soft chemistry routes.

## 2.4 SOL-GEL PROCESS

The sol-gel process is a wet-chemical technique for the fabrication of materials, employing low temperature, starting either from a chemical solution or colloidal particles (sol for solution or nanoscale particle) to produce an integrated network (gel). In general, sol-gel technique can be regarded as the preparation of the sol, gelation of the sol and removal of the solvent. The overall sol-gel process can be represented by the following sequence of transformations [61]:



*Precursors* are starting materials, in which the essential basic entities for further network formation are present in the correct stoichiometry. Typical precursors are metal alkoxides and metal chlorides.

*Sol* is a colloidal suspension of particles in a liquid, the particles typically ranging from 1-100 nm in diameter.

*Gel* is a semi-rigid solid, in which solvent is contained in a network/framework of the material, which is either colloidal (essentially a concentrated sol) or polymeric.

The name “sol-gel” is thus given to the process, because of the distinctive viscosity increase that occurs at a particular point in the sequence of steps. A sudden increase in viscosity is the common feature in sol-gel processing, indicating the onset of gel formation. Sol-gel process can be distinguished from precipitation by its specific property to stabilize a finely dispersed (mostly colloidal) phase in solution.

Typically, formation of a metal oxide involves connecting the metal centres with oxo (M-O-M) or hydroxo (M-OH-M) bridges, therefore generating metal-oxo or metal-hydroxo polymers in solution. The drying process serves to remove the liquid phase from the gel, thus forming a porous material, and then a thermal treatment

(firing) may be performed in order to favour further polycondensation and enhance mechanical properties.

Important steps involved in sol-gel synthesis are –

**Hydrolysis:** It involves reaction of inorganic or organometallic precursor with water or a solvent, at ambient or slightly elevated temperature. Acid or base catalysts are added to speed up the reaction.

**Polymerization:** This step involves condensation of adjacent molecules wherein water/alcohol are eliminated and metal oxide linkages are formed. Polymeric networks grow to colloidal dimensions in the liquid (sol) state.

**Gelation:** It leads to the formation of a three dimensional network throughout the liquid, by the linking up of polymeric networks.

**Aging:** Aggregation of smaller polymeric units to the main network progressively continues on ageing the gel. A continuous change in structure and properties of a completely immersed gel in liquid is called ageing. Solvent molecules however, remain inside the pores of the gel.

**Drying:** Here, solvent is removed at moderate temperatures ( $< 200\text{ }^{\circ}\text{C}$ ) leaving the residue behind.

**Dehydration:** This step is carried out between  $400\text{ }^{\circ}\text{C}$  and  $800\text{ }^{\circ}\text{C}$  to drive off the organic residues and chemically bound water.

**Densification:** Heating the porous gel at high temperatures, leads to formation of a dense oxide product. The densification temperature depends considerably on the dimensions of the pore network, the connectivity of the pores, and surface area.

Sol-gel processing is one of the promising routes to synthesis of inorgano organic hybrids using a “Chimie Douce”, low temperature approach, often from aqueous medium, with a possibility to introduce a large variety of organic moieties into an inorganic matrix. The mild reaction conditions used for the synthesis of metal phosphonates makes viable the incorporation of organic functional groups, without disturbing the inorganic backbone [24]. The currently employed synthesis routes to metal phosphonates are the use of hydro or solvothermal reactions [18, 22, 24]. The sol-gel method, offers the possibility to prepare solids with pre-determined structure. The choice of starting materials and reaction conditions are of great importance. Variation of the reaction temperature, the pH of the reaction mixture, metal salt to reactant ratio, nature of metal salt, relative concentration of reactants, mode of

addition (metal salt to phosphonic acid or vice versa), ageing period and solvents have influence on the final product formed. The preparation procedure thus affects the composition and structure, which is further reflected in the properties/performance such as porosity, surface polarity and crystallinity. Systematic investigation of these parameters, in conjunction with variations in the metal and organic functional groups can be exploited as a coherent strategy towards synthesis of novel hybrid materials. The various steps involved in the sol-gel technique described above may or may not be followed. In practice, however, a modified sol-gel route is followed.

### ***Advantages of Sol-Gel Process***

- ❖ High homogeneity –due to intimate mixing of raw materials
- ❖ High purity of products formed
- ❖ Low temperature processing (energy savings, minimize evaporation losses, minimize air pollution, no reaction with container)
- ❖ More uniform phase distribution in multicomponent systems
- ❖ Materials with improved and desired properties (tailor made materials) can be obtained
- ❖ Porous materials using templates

### ***Disadvantages of the Sol-Gel Process***

- ❖ Large shrinkage during processing
- ❖ Residual fine pores
- ❖ Residual hydroxyl groups when hydroxides are used
- ❖ Residual carbon (originating from templates)
- ❖ Health hazards of organic solvents
- ❖ Long processing times

## **2.5 EXPERIMENTAL**

**Materials:** Zirconium oxychloride ( $ZrOCl_2$ ) and Titanium tetrachloride ( $TiCl_4$ ) were procured from Loba Chemicals. 50% (~1.18 M) ATMP (Amino trismethylene phosphonic acid) with density = 1.3 g/cm<sup>3</sup> and molecular weight = 299.04 g (CAS No.6419-19-8) was obtained from Hydrochem India Pvt. Ltd. Appropriate/required concentration of ATMP was prepared from 50% (~1.18 M) ATMP solution for

synthesis of ZrATMP and TiATMP. Deionized water (DIW) was used for all the studies.

**Synthesis of ZrATMP and TiATMP:** The main objective was to prepare a material with maximum cation exchange capacity (CEC) and which is highly insoluble and chemically resistant to any media (where exchanger would be used). ZrATMP/TiATMP were synthesized by sol-gel method varying several conditions/parameters such as mole ratio of reactants, temperature, mode of mixing [metal salt solution to ATMP solution or vice versa], pH, aging and rate of mixing and synthesis conditions optimized, in each case using CEC as the indicative tool. Each sample synthesized was assessed for chemical stability/resistivity as well as preparative reproducibility. For performing ion exchange studies the material was synthesized at optimized conditions. **Tables 2.1** and **2.2** describe optimization of reaction conditions for synthesis of ZrATMP (Entry No.2) and TiATMP (Entry No.8).

**Synthesis of ZrATMP at optimized conditions:** ZrATMP was prepared by mixing aqueous solutions of ATMP (0.2M, 50 mL) and  $\text{ZrOCl}_2 \cdot 8\text{H}_2\text{O}$  (0.1M, 50 mL) at room temperature, dropwise (flow rate,  $1 \text{ mL} \cdot \text{min}^{-1}$ ) and with continuous stirring at optimized parameters as presented in **Table 2.1**. A gelatinous precipitate was obtained, and solution along with precipitate was stirred further for 1 h. The resulting gelatinous precipitate was allowed to age for 1h, then filtered, and washed with DIW till removal of chloride ions, followed by drying at room temperature. The material was then broken down to the desired particle size [30-60 mesh (ASTM)] by grinding and sieving. 5 g of the material was treated with  $\text{HNO}_3$  (1 M, 50 mL) for 30 min with occasional shaking. The material was then separated from acid by decantation and washed with DIW for removal of any adhering acid. This process (acid treatment) was repeated at least five times. After final washing, the material was dried at room temperature. This material was used for all studies.

**Table 2.1 Optimization of reaction conditions for synthesis of ZrATMP**

Parameters	No	Mole ratio Metal: Anion (M)	Volume ratio Metal: Anion (mL)	Temp. (°C)	Stirring time (h)	Aging time (h)	CEC (meq/g)
Concentration	1	0.1:0.1	50 : 50	RT	1 hr	1 hr	3.19
	2	<b>0.1:0.2</b>	<b>50 : 50</b>	<b>RT</b>	<b>1 hr</b>	<b>1 hr</b>	<b>3.61</b>
	3	0.2:0.1	50 : 50	RT	1 hr	1 hr	2.68
Volume	4	0.1:0.2	50 : 100	RT	1 hr	1 hr	2.46
	5	0.1:0.2	100 : 50	RT	1 hr	1 hr	2.24
Temperature	6	0.1:0.2	50:50	70	1 hr	1hr	3.19
Aging Time	7	0.1:0.2	50:50	RT	1 hr	15 hr	2.99
	8	0.1:0.2	50:50	RT	1 hr	3 hr	2.84
Stirring Time	9	0.1:0.2	50:50	RT	2hr	1 hr	2.61
	10	0.1: 0.2	50:50	RT	3 hr	1 hr	2.94
pH	11	0.1: 0.2	50:50	RT	1 hr	1hr	3.09
Mode of addition	12	0.1: 0.2	50:50	RT	1 hr	1hr	3.12*

\* Change in mode of addition - ZrOCl<sub>2</sub> added dropwise to ATMP, RT= Room Temperature (25°C)

**Table 2.2 Optimization of reaction conditions for synthesis of TiATMP**

Parameters	No	Mole ratio Metal: Anion (M)	Volume ratio Metal: Anion (mL)	Temp. (°C)	Stirring time (h)	Aging time (h)	CEC (meq/g)
Concentration	1	0.1:0.1	50 : 50	RT	1 hr	1 hr	3.21
	2	0.1:0.2	50 : 50	RT	1 hr	1 hr	3.89
	3	0.2:0.1	50 : 50	RT	1 hr	1 hr	2.68
Volume	4	0.1:0.2	50 : 100	RT	1 hr	1 hr	2.46
	5	0.1:0.2	100 : 50	RT	1 hr	1 hr	2.24
Temperature	6	0.1:0.2	50:50	70	1 hr	1hr	3.69
Aging Time	7	0.1:0.2	50:50	RT	1 hr	15 hr	2.99
	8	<b>0.1:0.2</b>	<b>50:50</b>	<b>RT</b>	<b>1 hr</b>	<b>3 hr</b>	<b>4.01</b>
Stirring Time	9	0.1:0.2	50:50	RT	2hr	1 hr	2.61
	10	0.1:0.2	50:50	RT	3 hr	1 hr	2.94
pH	11	0.1:0.2	50:50	RT	3 hr	1hr	3.12
Mode of addition	12	0.1:0.2	50:50	RT	1 hr	3hr	3.01*

\* Change in mode of addition – TiCl<sub>4</sub> added dropwise to ATMP. RT= Room Temperature (25°C).

**Synthesis of TiATMP at optimized conditions:** TiATMP was prepared by mixing aqueous solutions of ATMP (0.2 M, 50 mL) and TiCl<sub>4</sub> (0.1 M, 50 mL) (in 10% w/w H<sub>2</sub>SO<sub>4</sub> solution) at room temperature, dropwise (flow rate, 1 mL·min<sup>-1</sup>) and with continuous stirring at optimized parameters as presented in **Table 2.2**. A gelatinous precipitate was obtained, and solution along with precipitate was stirred further for 1 h. The resulting gelatinous precipitate was allowed to age for 3h, then filtered, and washed with DIW till removal of chloride ions, followed by drying at room temperature. The material was then broken down to the desired particle size [30-60 mesh (ASTM)] by grinding and sieving. The material was subjected to acid treatment as described above. This material was used for all studies.

## 2.6 MATERIAL CHARACTERIZATION

Metal phosphonates ZrATMP and TiATMP were subjected to physical, ion exchange and instrumental methods of characterization.

### 2.6.1 Physical Characteristics

Physical characteristics include appearance, percentage moisture content, particle size, apparent density, true density, nature of exchanger and chemical stability (**Tables 2.3 and 2.4**).

**Appearance:** The material was observed for physical appearance such as colour, opacity/transparency, hardness etc.

In the present study, ZrATMP was obtained as white hard granules while TiATMP was obtained as pale yellow hard granules.

**% Moisture content:** Percentage moisture content of an exchanger is the ability of the exchanger to hold moisture, and depends on the matrix structure - functional groups/ionogenic groups present in the exchanger.

For determining percentage moisture content, 1 g of the material was allowed to stand in DIW for 24 h. The material was then filtered and dried at room temperature to remove surface moisture and weighed. This material was then dried at 110 °C for 4 h and reweighed after cooling in a desiccator. The percentage moisture content was calculated using the formula,

$$\% \text{ Solid} = \frac{\text{Weight of dried material}}{\text{Weight of material before drying}} \times 100 \quad (\text{Eq. 2.1})$$

$$\% \text{ Moisture content} = 100 - (\% \text{ solid}) \quad (\text{Eq. 2.2})$$

**Particle size:** Ion exchange materials in general, are supplied as small round beads, having a diameter between 0.3 and 1.2 mm. Large beads are preferred for pressure drop advantage in column operations. However, large beads are subject to a greater rate of breakage than those having a smaller size. The most efficient ion-exchange processes occur when most of the functional groups can be accessed (equilibrated) within a short contact time between liquid and exchanger. The larger the particle size, the greater is the time required to access groups deeper in the particles. Thus, ion exchange rate will increase as the particle size decreases. The diffusion path lengths of the exchanging ions to exchanger and from the exchanged sites to electrolyte media are shorter with smaller particle sizes [62].

In the present study, ZrATMP, and TiATMP of particle size 0.25–0.59 mm [30-60 mesh (ASTM)] were used.

**Density and Specific gravity:** Density is characteristic of the exchanger. Most common of these is the apparent density or *bulk density* or *column density* in which the weight of the ion exchanger per unit volume is determined. Density is used to measure the performance of an ion exchanger in commercial units. A change in density after extended use is a signal that chemical degradation has occurred.

Specific gravity generally refers to the value determined for wet exchanger when using a pycnometer. This is also known as true density. Cation exchangers have a greater specific gravity than anion exchangers. To avoid floating of exchanger particles, true density should be more than 1. The true density of commercial exchangers is generally between 1.1 to 1.5 g·mL<sup>-1</sup>.

**Apparent density ( $D_{col}$ ):** For apparent density measurements, exact weight of exchanger is taken in a calibrated glass column. After backwashing, water is drained and exchanger material allowed to settle. Apparent density is determined using the equation,

$$\text{Apparent density} = \frac{\text{Weight of ion exchanger}}{\text{Volume of ion exchange bed}} \quad (\text{Eq. 2.3})$$

**True density ( $D_{ie}$ ):** The true density is determined by first weighing specific gravity bottle ( $W$ ). The bottle is weighed again along with the ion exchanger ( $W_i$ ). The bottle is now filled with water along with ion exchange material and weighed ( $W_{iw}$ ). The weight of the specific gravity bottle containing water is also noted ( $W_w$ ). The true density is calculated by using equation,

$$D_{ie} = \frac{(W_i - W)}{(W_w - W_{iw}) + (W_i - W)} \quad (\text{Eq. 2.4})$$

**Nature of exchanger:** The nature of exchanger, weak or strong, can be determined by *pH* titration curve. Acid sites in a material can be titrated against an alkali hydroxide (used for neutralization) and a salt solution of same alkali metal (used as a supporting electrolyte). A plot of *pH* versus number of milliequivalents of  $\text{OH}^-$  ions, is termed as the “*pH* titration curve” or the “potentiometric curve”, which gives an idea regarding the acidic nature of material, weak or strong [63].

0.5 g of the material was placed in NaCl (0.1 M, 100 mL) solution. This solution mixture was titrated against NaOH (0.1 M) solution. After addition of every 0.5 mL of titrant, sufficient time was provided for establishment of equilibrium, till the *pH* is constant. A *pH* titration curve is obtained by plotting *pH* versus volume of NaOH/number of milliequivalents of  $\text{OH}^-$  ions. *pH* titration curves (**Figures 2.5A and 2.5B**) indicate that ZrATMP and TiATMP are weak cation exchangers.

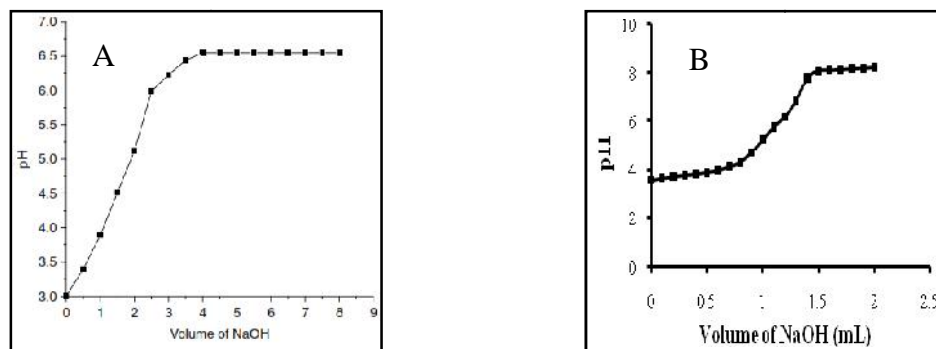


**Figure 2.5** *pH* titration curves for (A) ZrATMP and (B) TiATMP

**Chemical stability:** A study of the chemical resistivity/stability of materials in mineral acids, bases and organic solvent media is both useful and important while using the material for various applications in varied environments.

Chemical resistivity/stability in various media - acids (varying concentration of  $\text{H}_2\text{SO}_4$ ,  $\text{HNO}_3$ ,  $\text{HCl}$ ), bases (varying concentration of  $\text{NaOH}$  and  $\text{KOH}$ ) and organic solvents (ethanol, toluene, xylene and acetic acid) was studied by taking 0.5 g of the material in 50 mL of the particular medium and allowing to stand for 24 h. The change in colour, nature, weight as well as solubility was observed. Further, to confirm the stability/solubility of the material in particular media, supernatant liquid was checked qualitatively for respective elements of the material. Maximum tolerable limits evaluated in a particular medium have been presented in **Tables 2.3 and 2.4**. In general, ZrATMP and TiATMP are stable in acids and organic solvent media but not so stable in base medium.

## **2.6.2 Ion Exchange Characteristics**

Ion exchange characteristics include cation exchange capacity, effect of calcination on CEC, void volume fraction/porosity, concentration of fixed ionogenic groups, volume capacity of the resin, etc. (**Tables 2.3 and 2.4**)

**Cation Exchange Capacity (CEC):** Capacity in general can be described as a measure of the quantity of ions, acid or base, removed/exchanged by an ion-exchange material. Capacity and related data are primarily used for two purposes (a) for the characterization of ion exchange materials (b) for use in numerical calculations of ion exchange-operations. The term ion exchange capacity is intended to describe the total available exchange capacity of an ion exchanger, as described by the number of functional groups on it. This value is constant for a given ion exchange material and is expressed in milli equivalents per gram, based on dry weight of material in given form (such as H<sup>+</sup> or Cl<sup>-</sup>). For the characterization of ion exchangers, two capacity parameters are commonly used: the total static exchange capacity (which is determined by batch method) and dynamic exchange capacity (which is determined by column method). The exchange capacity depends on the functional groups per gram of exchanger, while the extent of the total exchange capacity depends on the level of ionization of the functional groups of the exchanger and on the chemical and physical conditions of the process. Likewise it is recommended to use sodium acetate for weak acid ion exchangers, NaCl for neutral ion exchangers and NH<sub>4</sub>Cl for acidic ion exchangers, for the determination of CEC. The Na<sup>+</sup> CEC of materials is generally determined by the column method [64], by varying concentration and volume of electrolyte solution at a fixed flow rate to find optimum concentration and volume required for complete exchange.

In the present study, the Na<sup>+</sup> cation exchange capacity (CEC) of ion exchangers ZrATMP and TiATMP were determined by the column method [64] by optimizing volume and concentration of sodium acetate solution (**Figure 2.6(a-d)**).

Firstly, a fixed volume (250 mL) of sodium acetate solution of varying concentration (0.1 M, 0.2 M, 0.3 M, 0.4 M, 0.5 M, 0.6 M, 0.7 M) was passed through a glass column (30 cm × 1 cm internal diameter) containing 0.5 g of the exchanger, maintaining a flow rate of 0.5 mL·min<sup>-1</sup> and effluent (containing H<sup>+</sup> ions eluted out) titrated against 0.1 M NaOH solution. The optimum concentration of eluant is thus determined. Now, eluent of optimum concentration was used and 10 mL fractions

passed through the column maintaining a flow rate  $0.5 \text{ mL}\cdot\text{min}^{-1}$ . This experiment was conducted to find out the minimum volume necessary for a complete elution of the  $\text{H}^+$  ions, which reflects the efficiency of the column. Using these optimized parameters  $\text{Na}^+$  CEC was determined, using the formula  $aV/W$ , where  $a$  is molarity,  $V$  the amount of alkali used during titration, and  $W$  is the weight of the exchanger. The CEC values for ZrATMP and TiATMP are presented in **Table 2.3 and 2.4**.

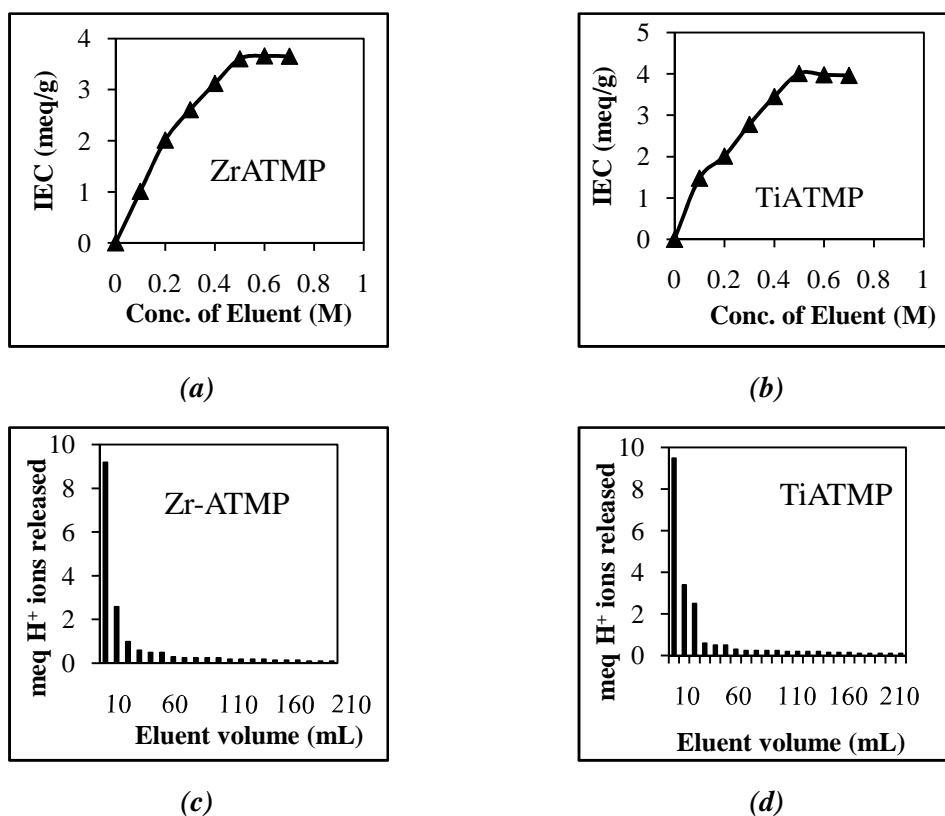


**Figure 2.6(a-d) Concentration and eluent volume optimization for determination of CEC using ZrATMP and TiATMP**

**Effect of calcination on CEC:** There are several important ion exchange processes that occur at high temperatures. For such cases, thermal stability is one of the most important requirements of a good ion exchanger. The exchanger in use should be able to withstand the temperature of the reaction system. Ion-exchange materials should not be used at temperatures above those recommended by the manufacturer. Functional groups are lost from both cation- and anion- exchange resins, when the temperature limit is exceeded. The rate of weight loss increases exponentially as the temperature rises above the upper limit.

A study on the effect of calcination on the exchanger material, would give information regarding the utility of the material for high temperature applications. The

effect of calcination on CEC was studied using 1 g of each sample, calcined in the temperature range 100 °C - 500 °C at an interval of 50 °C for 2 h, cooled to room temperature in desiccator and CEC determined by the column method [64]. The values of Na<sup>+</sup> CEC of calcined samples of ZrATMP and TiATMP are presented in **Tables 2.3 and 2.4**.

The Na<sup>+</sup> CEC of the calcined materials shows that CEC values decrease with increasing temperature. Decrease in CEC in temperature range 100-200 C is attributed to loss of moisture/hydrated water. Further, decrease in CEC beyond 200 C could be attributed to condensation of structural hydroxyl groups and decomposition of organic moiety.

**Void volume fraction/porosity:** The porosity of an ion exchanger is related to the degree of cross-linking and the network formed as a result. The porosity also influences ion exchange properties, particularly the capacity and selectivity. The capacity would be much lower than it really is, if the exchanger had no porous structure and if only the functional groups at the surface were active for ion exchange. The high cation exchange capacity obtained in case of porous materials, is due to active functional groups located in the interior of the pores also [65]. Ion-exchange materials are generally microporous or macroporous. Microporous materials are more commonly referred to as gel or gel type exchanger. Porosity in such materials cannot be measured by standard techniques. Such exchanger particles swell with water or a solvent. There is no porosity when the material is dry. Macroporous materials have a measurable porosity which does not disappear when the exchanger is dry. Void volume fraction, concentration of fixed ionogenic group ( $C_r$ ) and volume capacity of the resin ( $Q$ ) are calculated using following equations,

**Void volume fraction**

$$\text{Void volume fraction} = 1 - \frac{D_{col}}{D_{ie}} \quad (\text{Eq. 2.5})$$

**Concentration of fixed ionogenic group ( $C_r$ )**

$$C_r = \frac{D_{ie} \times (100 - \% \text{ moisture}) \times IEC}{100} \quad (\text{Eq. 2.6})$$

**Volume capacity of the resin ( $Q$ )**

$$Q = (1 - \text{void volume fraction}) \times C_r \quad (\text{Eq. 2.7})$$

### **2.6.3 Instrumental Methods of Characterization**

**Elemental analysis:** In the present study, elemental analysis (Zr,Ti,P) was performed on ICP-AES spectrometer (Labtam, 8440 Plasmalab). Carbon, hydrogen and nitrogen contents have been determined using Thermo finnigan, Flash EA 1112 series. The concentration of different elements is measured at ppm level, which is then converted into the % weight of the element, by incorporating the dilution factor. These values are then converted into moles of each element.

**Energy dispersive X-ray analysis (EDX):** EDX of samples were scanned on Jeol JSM-5610-SLV scanning microscope. EDX has been used in coordination with and as supportive analysis with ICP-AES which is more accurate compared to EDX.

Elemental analysis of ZrATMP and TiATMP, performed by ICP-AES, C, H, N analysis and EDX presented in **Tables 2.3 and 2.4**. EDX data for Zr and Ti are presented in (**Figure 2.7a**) for ZrATMP and (**Figure 2.8a**) for TiATMP. The ICP-AES and C, H, N analysis data is well supported by EDX data for both materials.

**Fourier Transform Infrared Spectroscopy (FTIR):** FTIR spectra was obtained using KBr wafer on a Shimadzu (Model 8400S). The FTIR spectra for ZrATMP and TiATMP have been presented in **Figures 2.7b and 2.8b** respectively. The FTIR spectrum of these materials exhibit broad band in the region  $\sim 3400\text{ cm}^{-1}$  which is attributed to symmetric and asymmetric O – H stretching vibrations due to residual water and presence of structural hydroxyl groups,  $\text{H}^+$  of the – OH being cation exchange sites. These sites are also referred to as defective P – OH groups [53]. A sharp medium band at  $\sim 1636\text{ cm}^{-1}$  is attributed to aquo H – O – H bending [66]. The broad band at  $\sim 1034\text{ cm}^{-1}$  is attributed to M – O – P framework vibrations [30]. The band at  $\sim 1428\text{ cm}^{-1}$  is due to overlapped C – H bending of –  $\text{CH}_2$  groups, P – C stretching vibrations and presence of tertiary amine [34]. Slade et al. attribute the band at  $\sim 1400\text{ cm}^{-1}$  to be due to  $\text{P} - \text{OH}$  stretching vibrations referred to as defective P – OH groups responsible for cation exchange capacity [67].

**Thermal analysis:** TGA was performed on a Shimadzu, DT-30 thermal analyzer at a heating rate of  $10^\circ\text{C}$  per minute. TGA of ZrATMP and TiATMP presented in **Figure 2.7c** and **Figure 2.8c** respectively reveals that ZrATMP exhibits the first weight loss  $\sim 10\%$  in temperature range ( $30\text{-}120^\circ\text{C}$ ) and second weight loss  $\sim 7\%$  in temperature range ( $120\text{-}500^\circ\text{C}$ ) while TiATMP exhibits the first weight loss  $\sim 12\%$  ( $30\text{-}150^\circ\text{C}$ ) and the second weight loss  $\sim 15\%$  ( $150\text{-}500^\circ\text{C}$ ). The first weight loss in the

temperature range ~30-150 °C is attributed to loss of moisture/hydrated water, while second weight loss ~150-500 °C is attributed to condensation of structural hydroxyl groups and decomposition of organic moiety.

Based on the elemental analysis ICP-AES, CHN data and TGA data, ZrATMP and TiATMP are formulated as  $(\text{ZrO})(\text{C}_3\text{H}_{10}\text{NP}_3\text{O}_9)_{0.9} \cdot 2\text{H}_2\text{O}$  and  $\text{Ti}(\text{C}_3\text{H}_{12}\text{NP}_3\text{O}_9)_{0.9} \cdot 2\text{H}_2\text{O}$  respectively. The number of water molecules in each case is calculated using Alberti and Torracca (1968) formula [29, 34]. In formulating the composition of amorphous metal phosphonates [29], it is assumed that the hydroxyl protons are lost, to coordinate with the tetravalent metal, forming M-O-P bonds. Formulation is thus based on metal phosphorous ratio.

**X-ray diffraction studies:** XRD was performed on an X-ray diffractometer (Bruker AXS D8) using Cu-K $\alpha$  radiation (X-ray source of wavelength 1.5418 Å) with a nickel filter. The absence of sharp peaks in the X-ray diffractogram of ZrATMP (**Figure 2.7d**) and TiATMP (**Figure 2.8d**) indicate amorphous nature of the materials.

**Scanning electron microscopy (SEM):** SEM provides information about the general morphology of the material. SEM was scanned on Jeol JSM-5610-SLV scanning electron microscope. SEM of ZrATMP and TiATMP are presented in **Figures 2.7e and 2.8e** respectively. Variation in surface morphology as well as irregular particle size of ZrATMP and TiATMP also indicate amorphous nature.

### ***Summarizing structure and properties of ZrATMP and TiATMP***

Based on physico-chemical and ion exchange characterization, and instrumental methods of analysis, it can be concluded that both ZrATMP and TiATMP possess the characteristics of ideal ion exchangers. The presence of structural hydroxyl groups ( $\text{H}^+$  of the -OH being exchangeable sites) are responsible for cation exchange.  $\text{Na}^+$  CEC values for ZrATMP is  $3.61 \text{ meq.g}^{-1}$  and TiATMP is  $4.01 \text{ meq.g}^{-1}$ . The materials are amorphous in nature, very insoluble in almost any media and possess granular nature that is suitable for column operations. The above conclusions indicate good potential for ZrATMP and TiATMP to be explored as cation exchangers.

**Table 2.3 Characterization of ZrATMP**

<b>Physico-chemical and Ion Exchange Characterization</b>					
Appearance	White opaque granules	Cation exchange capacity(CEC) and effect of calcination on CEC	Temperatures (°C)	CEC (meq.g <sup>-1</sup> )	
Particle size	0.25 - 0.59 mm		RT	3.61	
% Moisture content	6.49 %		100	2.93	
True density	1.78 g·mL <sup>-1</sup>		200	2.11	
Apparent density	0.35 g·mL <sup>-1</sup>		300	2.26	
Void volume fraction	0.79		400	2.73	
Concentration of fixed ionogenic group	6.30 mmol·g <sup>-1</sup>		500	1.76	
Volume capacity of resin	1.26 mL·g <sup>-1</sup>	Chemical Stability (Maximum tolerable limits)	Acids	18N H <sub>2</sub> SO <sub>4</sub> , 16N HNO <sub>3</sub> , 11.3N HCl	
Nature of exchanger	Weak cation exchanger		Bases	0.01 N NaOH, 0.01 N KOH	
			Organic Solvents	Ethanol, Toluene, Acetic Acid, Xylene	
<b>Instrumental methods of characterization</b>					
<b>ZrATMP</b>		<b>Elements</b>			
		<b>Zr (wt. %)</b>		<b>P (wt. %)</b>	
<b>ICP-AES</b>	Theoretical values	22.19		20.37	
	Practical values	22.22		20.31	
<b>EDX</b>	Practical values	22.02		20.51	
		<b>C (wt. %)</b>	<b>H (wt. %)</b>	<b>N (wt. %)</b>	
<b>CHN Analysis</b>	Theoretical values	8.00	3.16	3.07	
	Practical values	8.03	3.45	2.96	
<b>EDX</b>	Practical values	-	-	2.16	
<b>Proposed Formula</b>		<b>(ZrO)(C<sub>3</sub>H<sub>10</sub>NP<sub>3</sub>O<sub>9</sub>)<sub>0.9</sub>·2H<sub>2</sub>O</b>			
<b>FTIR</b>	Peak (cm <sup>-1</sup> )	~ 3400	~ 1636	~ 1034	~ 1428
	Group assigned	-OH <sub>stretching</sub>	-OH <sub>bending</sub>	P=O <sub>stretching</sub>	-CH <sub>bending</sub>
<b>TGA</b>	% Weight loss	~ 10 %			
	Temperature range (°C)	30 -120			
	% Weight loss	~ 7%			
	Temperature range (°C)	120 -500			
<b>XRD</b>	Nature of material	Amorphous			
<b>SEM</b>	Size of particles	Amorphous material			

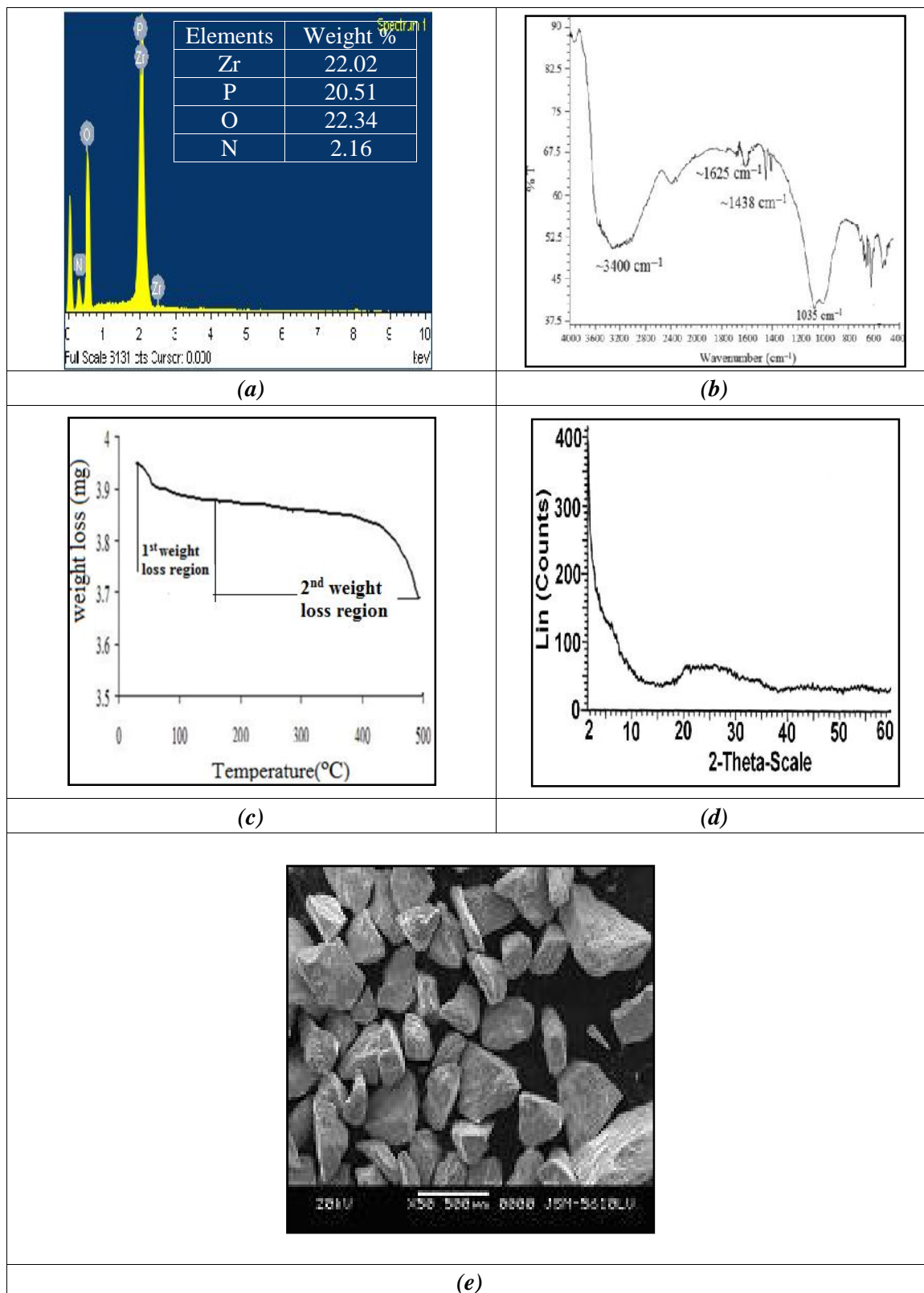


Figure 2.7 (a) EDX; (b) FTIR; (c) TGA; (d) XRD and (e) SEM of ZrATMP

**Table 2.4 Characterization of TiATMP**

<b>Physico-chemical and Ion Exchange Characterization</b>					
Appearance	Pale yellow opaque granules	Cation exchange capacity(CEC) and effect of calcination on CEC	Temperatures (°C)	CEC (meq.g <sup>-1</sup> )	
Particle size	0.25 - 0.59 mm		RT	4.01	
% Moisture content	11.52 %		100	3.93	
True density	1.80 g.mL <sup>-1</sup>		200	3.22	
Apparent density	0.27 g.mL <sup>-1</sup>		300	3.07	
Void volume fraction	0.70		400	2.26	
Concentration of fixed ionogenic group	1.05 mmol.g <sup>-1</sup>		500	1.13	
Volume capacity of resin	0.29 meq.mL <sup>-1</sup>	Chemical Stability (Maximum tolerable limits)	Acids	18N H <sub>2</sub> SO <sub>4</sub> , 16N HNO <sub>3</sub> , 11.3N HCl	
Nature of exchanger	Weak cation exchanger		Bases	0.02 N NaOH, 0.02 N KOH	
			Organic Solvents	Ethanol, Toluene, Acetic Acid, Xylene	
<b>Instrumental methods of characterization</b>					
<b>TiATMP</b>		<b>Elements</b>			
		<b>Ti (% Wt)</b>		<b>P (% Wt)</b>	
<b>ICP-AES</b>	Theoretical values	12.93		22.50	
	Practical values	13.01		21.12	
<b>EDX</b>	Practical values	13.62		20.50	
		<b>C (% Wt)</b>		<b>H (% Wt)</b>	
<b>CHN Analysis</b>	Theoretical values	8.70		4.50	
	Practical values	7.89		4.54	
<b>EDX</b>	Practical values	-		2.99	
<b>Proposed Formula</b>		<b>Ti(C<sub>3</sub>H<sub>12</sub>NP<sub>3</sub>O<sub>9</sub>)<sub>0.9</sub>·2H<sub>2</sub>O</b>			
<b>FTIR</b>	Peak (cm <sup>-1</sup> )	~ 3400	~ 1638	~1050	~1428
	Group assigned	- OH <sub>stretching</sub>	-OH <sub>bending</sub>	P=O <sub>stretching</sub>	CH <sub>bending</sub>
<b>TGA</b>	% Weight loss	~ 12 %			
	Temperature range(°C)	30-150			
	% Weight loss	~ 15 %			
	Temperature range(°C)	150-500			
<b>XRD</b>	Nature of material	Amorphous			
<b>SEM</b>	Size of particles	Amorphous material			

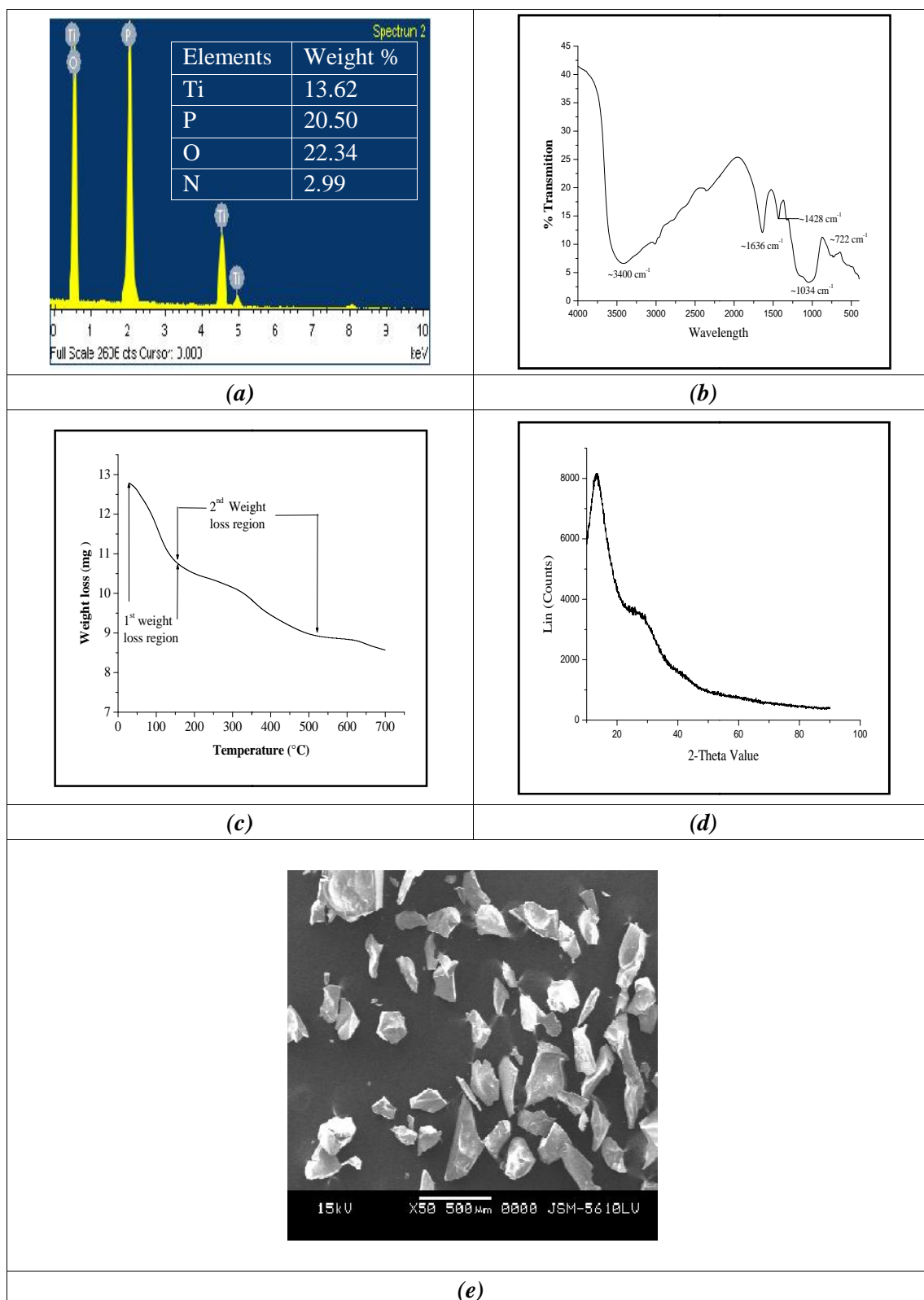


Figure 2.8 (a) EDX; (b) FTIR; (c) TGA; (d) XRD and (e) SEM of TiATMP

## 2.7 THERMODYNAMICS, KINETICS AND ADSORPTION STUDIES

### Introduction

Ion-exchange equilibrium is attained when an ion exchanger (spherical ion exchanger beads of uniform size containing the counter ion A) is placed in an electrolyte solution BY, containing a counter ion which is different from that in the ion exchanger. Ion A in the exchanger is partially replaced by B expressed as,



where R is the exchanger matrix and A and B are exchanging ions presented in **Figure 2.9**.

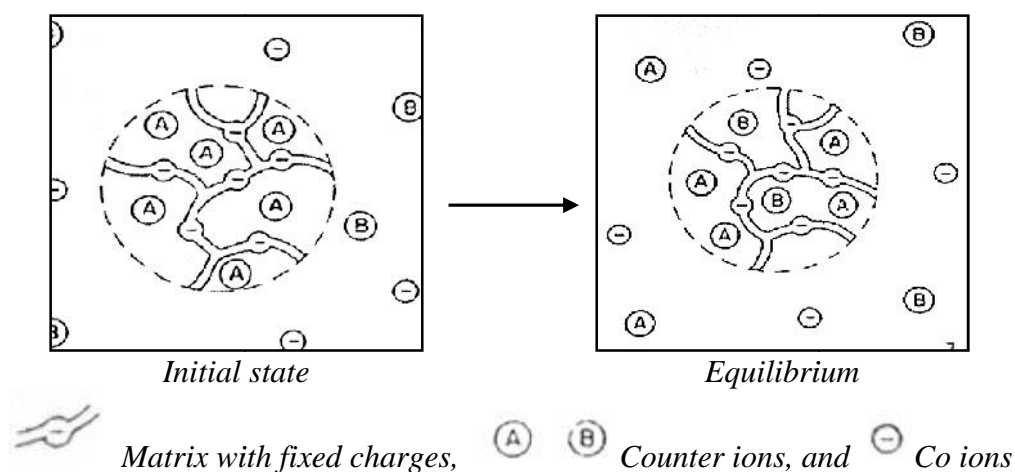


**Figure 2.9 Ion exchange equilibrium [63]**

As equilibrium is approached, A ions diffuse out of the beads into the solution, and B ions diffuse from the solution into the beads. This interdiffusion of counter ions is called ion exchange.

Ion exchange is inherently a stoichiometric process. Any counter ions, which leave the ion exchanger, is replaced by an equivalent amount of other counter ions. This is a consequence of electro neutrality requirement. When a counter ion moves out into the solution, the ion exchanger is left with an electric surplus charge which it must compensate by taking up another counter ion. The total counter ion content thus remains constant, irrespective of ionic composition.

Apparent deviations from stoichiometric behaviour can occur because of electrolyte sorption and desorption which may accompany ion exchange and which change the co-ion content of the ion exchanger. Under normal conditions, however,

Donnan exclusion keeps co-ions, in substantial amounts, from entering the ion exchanger during the entire process, however, this does not hinder the exchange of counter ions.

The exchange is, as a rule, reversible. Thus, it makes no difference from which side equilibrium is approached, that is, whether A is exchanged for B, or B for A. The final equilibrium distribution of the counter ions is the same in either case, provided that the amounts of all the components in the system are the same.

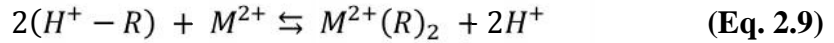
At equilibrium, the concentration ratios of the competing counter ion species, in the ion exchanger and in the solution are not the same. The ion exchanger prefers one species to the other. This shows that the redistribution of the counter ions is not purely statistical. The preference for one species may have several causes. The most important of these are,

- a) The electrostatic interactions between the charged framework and the counter ions, depends on the size and, in particular, on the valence of the counter ion.
- b) In addition to the electrostatic forces, other interactions between the ions and their environment are effective.
- c) Large counter ions may be sterically excluded from the narrow pores of the ion exchanger.

The above mentioned factors depend on the nature of the counter ion and thus may lead to preferential uptake of a species by the ion exchanger. The ability of the ion exchanger to distinguish between various counter ion species is called selectivity. A theoretical background of thermodynamics and kinetics of exchange combined with operating parameters notably temperature, pressure, concentration of electrolyte etc. is thus very important to improve selectivity, and efficiency of the exchange process. When characterizing the ion exchange properties of ion exchange materials, the feasibility and mechanism of the ion exchange process is very important. Thermodynamics and kinetics of exchange enable us to understand the viability of an ion exchange material in separation technology.

***Thermodynamics of exchange:*** Thermodynamics is a powerful tool to study an ion exchange reaction at equilibrium and determines feasibility of the exchange process. The importance of a thermodynamic study is its ability to predict correlations among experimental results in the absence of detailed knowledge of the structure of the system [68].

The ion-exchange process occurring on the surface of an ion exchanger, can be represented by the equation:



where  $M^{2+}$  = bivalent metal ion and  $R$  = Ion exchange material.

This equation can also be written in a generalized form as:



where the barred and unbarred quantities represent the concentrations in the exchanger and solution phases, respectively. The equivalent ionic fractions of the counter-ions in the exchanger and solution phases ( $\bar{X}_M, \bar{X}_H, X_M$  and  $X_H$ ) are calculated from the expressions:

$$\bar{X}_M = \frac{\bar{C}_M}{\bar{C}}, X_M = \frac{C_M}{C}, \bar{X}_H = \frac{\bar{C}_H}{\bar{C}}, X_H = \frac{C_H}{C} \quad (\text{Eq. 2.11})$$

where  $\bar{C}$  and  $C$  are the total electrolyte concentrations in the solid ( $\bar{C} = \bar{C}_M + \bar{C}_H$ ) and solution phases ( $C = C_M + C_H$ ).

For equilibrium as presented in (Eq. 2.11), the selectivity coefficient ( $K_c$ ) is calculated from the expression,

$$K_c = \frac{\bar{X}_M(X_H)^2}{(\bar{X}_H)^2 X_M} \quad (\text{Eq. 2.12})$$

The corrected selectivity coefficient ( $K_c'$ ) is defined by,

$$K_c' = \frac{\bar{X}_M(X_H)^2}{(\bar{X}_H)^2 X_M} \frac{(\gamma_H)^2}{\gamma_M} \quad (\text{Eq. 2.13})$$

where,  $\bar{X}_M$  and  $\bar{X}_H$  are equivalent ionic fractions of metal ions and hydrogen ions in the ion exchanger phase and  $X_M$  and  $X_H$  are equivalent ionic fractions of metal ions and hydrogen ions in solution phase, respectively.  $\gamma_M$  and  $\gamma_H$  are the activity coefficients of metal ion and hydrogen ion, respectively, in the solution phase and  $n$  is the valence of the metal ion. The solution phase activity coefficients for hydrogen and metal ions are calculated using the Debye-Hückel limiting law.

$$\log \gamma_i = -A Z_i^2 \sqrt{\mu_i} \quad (\text{Eq. 2.14})$$

Where,  $\gamma_i$  is the activity coefficient,  $A$  is a constant, the values of which have been taken from the table of Manov [69],  $Z_i$  is charge of the ions and  $\mu_i$  is the ionic strength. The thermodynamic equilibrium constant  $K$  is calculated at different temperatures from plots of  $\ln K_c'$  versus equivalent ionic fractions of metal ions in the exchanger phase  $\bar{X}_M$ , following the expression given by Gaines and Thomas [70].

$$\ln K = (Z_M - Z_H) + \int_0^1 \ln K'_C d\bar{X}_M \quad (\text{Eq. 2.15})$$

where,  $Z_M$  and  $Z_H$  are charges on the competing metal and hydrogen ions. The integrals are evaluated from the areas under the curve of  $\ln K'_C$  versus  $\bar{X}_M$  using the computer (curxpt) software.

The standard Gibbs free energy,  $G^\circ$ , is calculated from the thermodynamic equilibrium constant  $K$ , using the general equation,

$$\Delta G^\circ = \frac{-RT \ln K}{Z_M Z_H} \quad (\text{Eq. 2.16})$$

The standard enthalpy change,  $H^\circ$ , is calculated from the van't Hoff isochor,

$$\Delta H^\circ = [\ln K_2 - \ln K_1] \left[ \frac{T_1 T_2}{T_2 - T_1} \right] R \quad (\text{Eq. 2.17})$$

The standard entropy change,  $S^\circ$ , is calculated using the expression,

$$\Delta S^\circ = \frac{(\Delta H^\circ - \Delta G^\circ)}{T} \quad (\text{Eq. 2.18})$$

where,  $R$  is the gas constant,  $K_1$  and  $K_2$  are equilibrium constants at the temperatures  $T_1$  and  $T_2$ , respectively.

For an ion exchange process in aqueous medium, the most important factor is size of the cation and hence the hydrated ionic radii. Smaller the size of the cation, more heavily it is hydrated, with the result that the hydrated ionic radius is large. The values of  $\Delta G^\circ$ ,  $\Delta H^\circ$  and  $\Delta S^\circ$  appear to be a function of the hydrated ionic radii of the exchanging metal ions.

When a solid ion exchanger is in contact with electrolyte solution, mainly two reactions may take place, either ion exchange or sorption. As physical forces are responsible for sorption, the value of equilibrium constant ( $K$ ) may decrease with increasing temperature [71-73]. Ion exchange being a chemical reaction, some energy is required for crossing the barrier (energy of activation). In such cases therefore, as the temperature increases metal ion exchange will increase. Therefore, the interaction is temperature dependent.

A negative enthalpy change ( $H^\circ$ ) indicates that the exchange reaction is exothermic while a positive enthalpy change indicates that the exchange reaction is endothermic. The enthalpy change ( $H^\circ$ ) for an ion exchange reaction can be either of the reasons or a net effect of the following factors: (1) the heat consumed in bond breaking, as  $H^+$  is released from the resin (2) the heat released in the formation of bonds with the incoming cation (3) the heat corresponding to the energy required for

crossing the barrier (distance between exchange phase and solution phase) (4) the enthalpy change accompanying hydration and dehydration of exchanging ion in the solution. As dehydration is a must for ion exchange to occur, some energy must be supplied, to the cations, as it leaves the hydration sphere to undergo ion exchange [74].

The entropy change ( $S^\circ$ ) normally depends on the extent of hydration of the exchangeable and exchanging ions along with any change in water structure around ions that may occur when they pass through the channels of the exchanger, introducing a high degree of disorder into the resin matrix due to the ion exchange process.

In general, Gibbs free energy change ( $\Delta G^\circ$ ) values decrease with increase in temperature which shows increase in feasibility and spontaneity of the sorption/ion exchange process with rise in temperature. Negative values of Gibbs free energy change ( $G^\circ$ ) indicate that the exchange process is feasible and spontaneous in nature and attainment of a more stable energy level after ion exchange of metal ions.  $G^\circ$  depends on temperature, as well as heat consumed and released during  $M^{2+}$ - $H^+$  exchange in terms of hydration and dehydration as well as the size of the hydrated cationic radii.

**Kinetics of exchange:** A kinetic approach can very well explain the exchange mechanism and rate of the exchange reaction, which is of recognized importance for economic and industrial applications. When designing an ion exchange system, it is desirable to have an appreciable rate of ion exchange. Kinetic measurements performed under particular conditions, could be useful to elucidate a mechanism.

A kinetic study gives information pertaining to the rate laws obeyed by the system, prediction of ion exchange rates, rate determining step of the ion exchange process as well as the mechanism of exchange.

Most of the studies are based on the  $B_t$  criteria proposed by Boyd et al [75], which is of limited use because of different mobility of the competing ions. The criteria are useful only for the isotopic exchange i.e. the ions having similar effective diffusion co-efficient.

The use of Nernst Planck equation is suggested [1] for non-isotopic exchange to obtain more precise values of the various kinetic parameters. Energy and entropy of activation are the fundamental properties of a system. These parameters are important

to understand the mechanism of interactions on the surface during adsorption or ion exchange [76]. The knowledge of the sign and magnitude of entropy changes of ion exchange reactions are of great value for understanding the nature of ion binding by ion exchangers [77]. The exchange reaction may be expressed as,



where,  $A^+$  and  $B^+$  are the exchanging monovalent cations, and R is exchanger matrix.

The overall transport of mass is divided into five steps –

- a) Diffusion of  $B^+$  through the solution up to the exchanger particle.
- b) Diffusion of  $B^+$  through the exchanger particle.
- c) Chemical exchange between  $A^+$  and  $B^+$  at the exchanging position in the interior of the particle.
- d) Diffusion of the displaced cation  $A^+$  out of the interior of the exchanger (Reverse of step b).
- e) Diffusion of the displaced cation  $A^+$  through the solution away from the exchanger particle (Reverse of step a).

This shows that ion exchange, as a rule, is purely a diffusion phenomenon. The anions/coions present in solution do not participate in the exchange to an appreciable extent, considering Donnan equilibrium [63].

#### ***The Rate Determining Step:***

In the course of ion exchange, a counter ion A must migrate from its place within the ion exchanger into the solution. Simultaneously, a counter ion B must go the other way and occupy the place left by ion A. There is a transfer of ions in both the ion exchanger and the solution. In the bulk solution, any concentration differences are constantly leveled out by agitation. Agitation, however, affects neither the interior of the beads nor a liquid layer, which adheres to the bead surfaces. Within the beads and through this layer, the so-called “film”, transport can occur by diffusion only. Thus we come across two potential rate-determining steps:

- a) Interdiffusion of counter ions within the ion exchanger itself (particle diffusion).
- b) Interdiffusion of counter ions in the adherent films (film diffusion).

The rate controlling mechanism can be film diffusion, if the slow step is diffusion across the hydrodynamic film that surrounds the exchanger particles, or

particle diffusion, if the slow step is diffusion inside the exchanger beads themselves. In the first case, a concentration gradient is set up within the liquid film, whereas inside the exchanger, a uniform concentration of ion, prevails. In the second case, the concentration gradient occurs within the exchanger, while the film has a uniform composition. A high metal ion concentration, relatively large particle size of the exchanger and a vigorous shaking of the exchanging mixture favours a particle diffusion controlled process [63, 78].

**Particle Diffusion Controlled Exchange:** The kinetics of ion exchange can be explained with respect to fractional attainment of equilibrium  $U(\tau)$ . For a particle diffusion controlled phenomenon [79],

$$U(\tau) = 1 - \left( \frac{Q_A(t)}{Q_A^0} \right) = \left[ \frac{C_o - C_t}{C_o - C_\infty} \right] \quad (\text{Eq. 2.20})$$

where  $Q_A(t)$  and  $Q_A^0$  are the amount of A at time t and initial amount of A in the ion exchanger respectively (A being the counter ion), while  $C_t$ ,  $C_r$  and  $C_o$  are metal ion concentration at time t, equilibrium metal ion concentration and initial metal ion concentration respectively.  $U(\tau)$  is seen to be dependant only on the magnitude of the dimensionless time parameter  $\tau$ . According to the explicit approximation [80, 81],  $U(\tau)$  for a particle diffusion controlled phenomenon is given by,

$$U(\tau) = \{1 - \exp[\pi^2(f_1(\alpha)\tau + f_2(\alpha)\tau^2 + f_3(\alpha)\tau^3)]\}^{1/2} \quad (\text{Eq. 2.21})$$

where,  $\tau = D_A t / r_0^2$  and (mobility ratio) =  $D_A / D_B$ .  $D_A$  and  $D_B$  are diffusion coefficients of counter ions A and B respectively in the ion exchanger phase,  $r_0$  = bead radius and  $t$  = time.  $\tau$  versus  $t$  for different metal ion concentrations are plotted. The concentration at which, plot of  $\tau$  versus  $t$  is a straight line passing through the origin, confirms a particle diffusion controlled exchange [63]. This concentration is thus the minimum concentration for a particle diffusion controlled exchange.

**Evaluation of the Energy and Entropy of Activation:**

The plots of † vs.  $t$  at different temperatures for minimum metal ion concentration are plotted. The slope (S) of various † vs.  $t$  plots are calculated. They are related to  $D_A$  as follows [78],

$$S = D_A / r_0^2 \quad (\text{Eq. 2.22})$$

The values of  $\ln D_A$  obtained using above equation are plotted against  $1/T$ . These plots are straight lines verifying the validity of the Arrhenius relation,

$$D_A = D_o \exp (-E_a/RT) \quad (\text{Eq. 2.23})$$

The energy of activation ( $E_a$ ) and the pre-exponential constant ( $D_o$ ) are evaluated from the slope and intercept of these plots. The entropy of activation ( $US^*$ ) is then calculated [82] by substituting  $D_o$  in the equation,

$$D_o = 2.72 d^2 kT / h \exp (US^*/R) \quad (\text{Eq.2.24})$$

where,  $d$  is ionic jump distance (an average distance between two exchanging sites) taken as 5 Å,  $k$  and  $h$  are Boltzmann and Planck's constant respectively, and  $T = 273$  K.

Since the exchanger is not dynamic, ion exchange process depends on mobility of the exchanging ions. Since Self-diffusion coefficient ( $D_o$ ) gives an idea about the mobility of the migrating ions, it therefore depends on the size and charge of the ion and on the extent of hydration in aqueous medium. Ions with large ionic radius are less hydrated and therefore its self-diffusion co-efficient should be highest.

The minimum energy required for the exchange is expressed as energy of activation ( $E_a$ ). The main factor on which  $E_a$  value is dependent is, ease of dehydration of a hydrated ion, to occupy a site on the exchanger.

The entropy reflects the changes in hydration sphere of the exchanging cation during the ion exchange process. When ion exchange occurs, cation of high entropy in the external aqueous phase, passes to one of lower entropy in the exchanger phase [83], which results in a significant negative contribution of entropy change.

During exchange, the orientation of the exchanger sites and mobile ions are equally important and expressed as orientation factor. Orientation factor being related to randomness, is given by entropy of activation ( $S^*$ ). The overall rate of exchange thus depends on  $D_o$ ,  $E_a$  and  $S^*$ . The larger the  $D_o$  and  $S^*$ , and smaller the  $E_a$ , faster is the rate of exchange.

**Adsorption:** The phenomenon of higher concentration of any molecular species at the surface than in the bulk of a solid is known as adsorption. Adsorption is a general term that refers to the disappearance of solutes from solution with the presumption of adsorption on a solid phase. It is the accumulation at the solid-solution interface, and may result from either physical or chemical interaction with the surface. Adsorption refers to attraction and bonding onto a surface, while absorption is a process in which the solute is taken up throughout the bulk.

In some cases distinction is difficult and the generic term *sorption* has been used. Sorption is determined by the extent of solute removal from solution in either batch studies or in elution studies with columns of adsorptive materials. Sorption is the process in which both adsorption and absorption take place simultaneously. Adsorption is not necessarily a physical phenomena always. It may be a process involving chemical interaction between adsorbent and adsorbate. This type of adsorption is known as chemisorption. Physisorption is a relatively weak bonding to the surface, while chemisorption is a stronger interaction which involves ionic or covalent bonding, in addition to van der Waal's and dispersion forces operative in physical adsorption.

A typical technique is to supply a known concentration of sorbate to a known mass of adsorbent. After the solution and solid have come to equilibrium, solution concentration is then measured and the difference between the initial concentration and final equilibrium concentration adjusted for the solution volume is assumed to be the amount of sorption per unit mass of the sorbent.

Adsorption models deal with the equilibrium between the ions, adsorption solution and exchange matrix. It is well understood that the adsorption phenomena for a given pair of ions and a solid surface is mainly a function of the particular ion concentration and the concentration of other ions, especially the H<sup>+</sup> ions (pH) [84]. Sorption of ions, mainly depends on the degree of surface heterogeneity due to the existence of crystal edges, broken bonds and imperfection on the surfaces. In the modeling of ion adsorption, effects of surface heterogeneity have been taken into account in the last decade [84].

Equilibrium behaviour is described in terms of equilibrium isotherms which depend on the system temperature, concentration of the solution, contact time and pH [85, 86]. Adsorption equilibrium is usually established when the concentration of an adsorbate (metal ions) in a bulk solution is in dynamic balance with that of the adsorbent (exchanger) interface. The variation in adsorption with concentration and temperature is generally expressed in terms of adsorption isotherms - Langmuir and Freundlich adsorption isotherms.

Generally, both Langmuir and Freundlich isotherms are used for explaining the adsorption of metal ions on materials, since they are simple and have an ability to describe experimental results in a wide range of concentrations. Linear regression is

the widely used method for fitting the transformed forms of original Langmuir and Freundlich isotherm equations [84]. Both isotherm models can be easily transformed into linear forms to obtain adjustable parameters, just by graphical means or by linear regression analysis. The application of Langmuir and Freundlich models have been further extended, considering the influence of adsorption sites and the competition between different ions for adsorption on the available sites. Kinniburgh et al [87] derived the competitive Langmuir isotherm characterized by site affinity, maximum adsorption capacity and a parameter describing mutual replacement of  $H^+$  and  $M^{2+}$  on an adsorbing site [84].

**Langmuir Isotherm:** The Langmuir relationship has originally been derived for the adsorption of gases onto solid surfaces but it can be applied to solution systems as well. It is based on a model with the following basic assumptions:

- There is only a mono-molecular layer of adsorbed molecules.
- The equilibrium is characterized by the fact that the rates of adsorption and desorption are equal.

The linearized form of the Langmuir isotherm equation is given as:

$$C_e/(X/m) = 1/(bV_m) + C_e/V_m, \quad (\text{Eq. 2.25})$$

where  $X$  is the amount of adsorbate,  $m$ , the amount of adsorbent,  $C_e$ , the equilibrium concentration of the adsorbate in the solution. 'b' is a constant that represents adsorption bond energy, which is related to the affinity between the adsorbent and adsorbate which is also a direct measure for the intensity of the sorption process.  $V_m$  is a constant related to the area occupied by a monolayer of sorbate, reflecting the maximum adsorption capacity [85, 86]. A dimensionless constant equilibrium parameter  $R_L$  can also be used to express an essential characteristic of the Langmuir isotherm. The  $R_L$  value indicates the shape of the isotherm and is expressed as  $R_L = 1/(1 + bC_0)$ . A value  $0 < R_L < 1$  indicates favourable adsorption,  $R_L = 0$  irreversible adsorption and  $R_L = 1$  means linear adsorption while a value,  $R_L > 1$  indicates an unfavorable adsorption [85].

**Fruendlich Isotherm:** The Fruendlich isotherm is applied to deduce the adsorption intensity of the adsorbent and towards the adsorbate. Unlike Langmuir isotherm, the Fruendlich isotherm assumes that the removal of metal ions occurs on a heterogeneous surface involving a multilayer adsorption of metal ions. Fruendlich

equation is an empirical relationship describing the sorption of solutes from a liquid to a solid surface. It gives relationship between the magnitude of adsorption and concentration, and can be expressed mathematically by an empirical equation known as Freundlich adsorption isotherm. Freundlich isotherm is expressed as,

$$\log(X/m) = \log K + (1/n)\log C_e, \quad (\text{Eq. 2.26})$$

where,  $X$  and  $m$  have the same meaning as described in Langmuir isotherm,  $K$  and  $1/n$  are the Freundlich constants, describing the adsorption capacity and intensity respectively. A value,  $0 < 1/n < 1$  indicates a normal isotherm, while  $1/n > 1$  is indicative for cooperative sorption, for  $n = 1$  the partition between the two phases is independent of the concentration [85, 86].

The isotherm constants are important in understanding the adsorption mechanism and their subsequent application for prediction of some important design parameters. Plots of  $C_e/(X/m)$  vs  $C_e$  and  $\log(X/m)$  vs  $\log C_e$  are drawn for Langmuir and Freundlich isotherms respectively which are straight lines from which the constants can be determined by the slopes and intercepts. In order to decide which type of isotherm fits better, the  $R^2$  values (goodness of fit criterion) computed by linear regression for both type of isotherms and a value  $0 < R^2 < 1$  indicates that the isotherm provides a good fit to the sorption experimental data where  $R^2$  values should be close to unity.

In order to explore the feasibility of ZrATMP and TiATMP as cation exchanger, towards transition metal ions ( $\text{Co}^{2+}$ ,  $\text{Ni}^{2+}$ ,  $\text{Cu}^{2+}$ ,  $\text{Zn}^{2+}$ ) and heavy metal ions ( $\text{Cd}^{2+}$ ,  $\text{Hg}^{2+}$ ,  $\text{Pb}^{2+}$ ) following studies were under taken.

- ✓ The equilibrium exchange of metal ions with  $\text{H}^+$  ions contained in ZrATMP and TiATMP have been studied varying temperature, at constant ionic strength. On the basis of the exchange isotherms, thermodynamic parameters equilibrium constant ( $K$ ), standard Gibbs free energy change ( $G^\circ$ ), entropy change ( $S^\circ$ ) and enthalpy change ( $H^\circ$ ) have been evaluated and correlated.
- ✓ Ion exchange kinetics of transition metal ions ( $\text{Co}^{2+}$ ,  $\text{Ni}^{2+}$ ,  $\text{Cu}^{2+}$ ,  $\text{Zn}^{2+}$ ) and heavy metal ions ( $\text{Cd}^{2+}$ ,  $\text{Hg}^{2+}$ ,  $\text{Pb}^{2+}$ ) ions with  $\text{H}^+$  ions contained in ZrATMP and TiATMP has been studied varying temperature, applying the Nernst-Planck equation. Kinetic parameters such as self-diffusion coefficient ( $D_o$ ), energy of activation ( $E_a$ ) and entropy of activation ( $S^*$ ) have been evaluated (under the conditions favouring a particle diffusion-controlled mechanism) and correlated.

- ✓ Adsorption isotherms (Langmuir and Freundlich) have been studied by varying metal ion concentration, pH, contact time and temperature. Langmuir constants ( $b$  and  $V_m$ ) and Freundlich constants ( $K$  and  $1/n$ ) have been evaluated using Langmuir and Freundlich isotherms respectively.  $R^2$  value (goodness of fit criterion) has been computed by linear regression for both types of isotherms.

## 2.8 EXPERIMENTAL

**Materials and Methods:** Chloride and nitrate salts of transition metal ions ( $\text{Co}^{2+}$ ,  $\text{Ni}^{2+}$ ,  $\text{Cu}^{2+}$ ,  $\text{Zn}^{2+}$ ) and heavy metal ions ( $\text{Cd}^{2+}$ ,  $\text{Hg}^{2+}$ ,  $\text{Pb}^{2+}$ ) of AR grade were obtained from E Merck, India. Disodium salt of ethylene diamine tetra acetic acid (EDTA) was procured from Fluka. Indicators and reagents used are of AR grade. DIW was used for all the studies. ZrATMP and TiATMP have been synthesized and characterized, as discussed earlier in text, **Sections 2.6** and **2.7**. For thermodynamic, kinetic and adsorption studies the exchanger (ZrATMP and TiATMP) particles of definite mesh size [30 - 60 mesh (ASTM)] in  $\text{H}^+$  form was used and experiments performed using shaker bath having a temperature variation of  $\pm 0.5$  °C.

### 2.8.1 Thermodynamic studies

**Equilibrium time determination:** This experiment was performed for  $\text{Cu}^{2+}$  and the results obtained, utilized for other metal ions under study. 0.1 g of exchanger ZrATMP or TiATMP (in  $\text{H}^+$  form) was shaken with 0.002 M metal ion solution in stoppered conical flasks, varying time in the range of 30 min to 6 h, with 30 min interval at a particular temperature (303 K) After every prescribed time interval, the metal ion concentration was evaluated by EDTA titration. A plot of the fractional attainment of equilibrium versus time (t) gives indication about maximum equilibrium time.

**Equilibrium experiments:** The equilibrium experiments were performed by shaking 0.1 g of the exchanger particles at the desired temperature (303 K to 333 K with 10 K interval) in a shaker bath for optimum equilibrium time 6 h with 20 ml of a mixture of solution containing 0.06 M HCl and the appropriate metal ion of varying volume ratios (1, 3, 5,...19 ml 0.02 M metal ion solution and 19, 17, 15,...1 ml of 0.06 M HCl, respectively were prepared) having constant ionic strength (0.06 M). After every prescribed time interval metal ion concentration was determined by EDTA titration. From this experiment, thermodynamic parameters equilibrium constant ( $K$ ), standard

Gibbs free energy change ( $G^\circ$ ), enthalpy change ( $H^\circ$ ) and entropy change ( $S^\circ$ ) have been determined.

### 2.8.2 Kinetic studies

**Varying metal ion concentration:** The concentration effect on the mechanism of exchange was studied by taking metal ion solution of different concentrations (varied from 0.002 to 0.018 M with interval of 0.002 M) for the ion exchange process. 20 mL metal ion solutions of each concentration were shaken with 0.2g of exchanger (in  $H^+$  form) in stoppered conical flasks at 303 K for different time intervals (0.5, 1.0, 2.0, 3.0, 4.0 min). After every prescribed time interval the metal ion concentration was evaluated by EDTA titration.

**Varying reaction temperature:** 20 mL, 0.02 M metal ion solution was shaken with 0.2g of exchanger in stoppered conical flasks at desired temperatures (303, 313, 323, 333 K) for different time intervals (0.5, 1.0, 2.0, 3.0, 4.0 min). After every prescribed time interval the metal ion concentration was evaluated by EDTA titration.

### 2.8.3 Adsorption studies

**Effect of pH, contact time and temperature:** Adsorption/ion exchange of metal ions  $Co^{2+}$ ,  $Ni^{2+}$ ,  $Cu^{2+}$ ,  $Zn^{2+}$  (transition metal ions) and  $Cd^{2+}$ ,  $Hg^{2+}$ ,  $Pb^{2+}$  (heavy metal ions) using ZrATMP/TiATMP was studied in the pH range (1–7) by batch method. To 0.1g of the exchanger ZrATMP/TiATMP, 10 mL of 0.002 M metal ion solution was added, pH adjusted (using  $HNO_3$  and  $NaOH$  in acidic range and alkaline range respectively) and the mixture shaken for 30 min after which metal ion concentration was determined by EDTA titrations. The % uptake has been calculated using formula,

$$[(C_o - C_e)/C_o] \times 100 \quad \text{(Eq. 2.27)}$$

where  $C_o$  is the initial concentration of metal ion in mg/L and  $C_e$  is the final concentration of metal ion in mg/L.

The metal ion solution (10 mL) of 0.002M concentration were equilibrated in stoppered conical flasks at the desired temperatures (303 K to 333 K with 10 K interval) at specific time intervals with increments of 10 min. (10 – 200 min). In each case, the pH of the solution was adjusted to the value at which maximum sorption of respective metal ion takes place, using 0.1 g of ion exchanger. After each prescribed time interval the metal ion concentration was evaluated by EDTA titrations.

## 2.9 RESULTS AND DISCUSSION-PART I

### *Thermodynamic studies using ZrATMP*

Thermodynamics of ion exchange has been studied for  $\text{Co}^{2+}$ ,  $\text{Ni}^{2+}$ ,  $\text{Cu}^{2+}$ ,  $\text{Zn}^{2+}$  (transition metal ions) and  $\text{Cd}^{2+}$ ,  $\text{Hg}^{2+}$ ,  $\text{Pb}^{2+}$  (heavy metal ions). Equilibrium constant ( $K$ ), standard Gibbs free energy ( $G^\circ$ ), enthalpy ( $H^\circ$ ) and entropy ( $S^\circ$ ) have been evaluated using standard equations (Eqs. 2.16-2.18) [63, 88] discussed earlier in text and results presented in (Table 2.5).

A plot of the fractional attainment of equilibrium  $U(t)$  versus time ( $t$ ) **Figure 2.10** shows that the exchange equilibrium for ZrATMP appears to have attained within 6 h and hence all the equilibrium studies were performed, allowing a maximum equilibrium time of 6h.

Equilibrium constant ( $K$ ) values increase with increase in temperature for all metal ions under study (Table 2.5), indicating that the metal ions have higher affinity for the exchanger and that the mechanism is ion exchange [89].

In the present study, free energy change ( $G^\circ$ ) for all metal exchange reactions is negative, over the entire temperature range, indicating feasibility of the ion exchange process and that the exchanger has a greater preference for metal ions than  $\text{H}^+$  ions. The  $G^\circ$  values become more negative with increasing temperature, confirming that the exchange is favoured with increasing temperature.

Enthalpy change ( $H^\circ$ ) is positive in all cases indicating the exchange process to be endothermic. Higher/positive values of enthalpy change indicate more endothermicity of the exchange process and requirement of more energy for dehydration to occur. As dehydration is a must for ion exchange to occur, some energy must be supplied, to the cation, as it leaves the hydration sphere to undergo ion exchange [90]. The  $H^\circ$  values indicate that probably complete dehydration occurs in case of  $\text{Cu}^{2+}$  amongst transition metal ions and  $\text{Pb}^{2+}$  amongst heavy metal ions.  $S^\circ$  also follows same trend as  $H^\circ$  for all metal ions.

Higher  $S^\circ$  values also observed in case of  $\text{Cu}^{2+}$  and  $\text{Pb}^{2+}$  are attributed to greater dehydration, which indicates the greater disorder produced during the exchange.

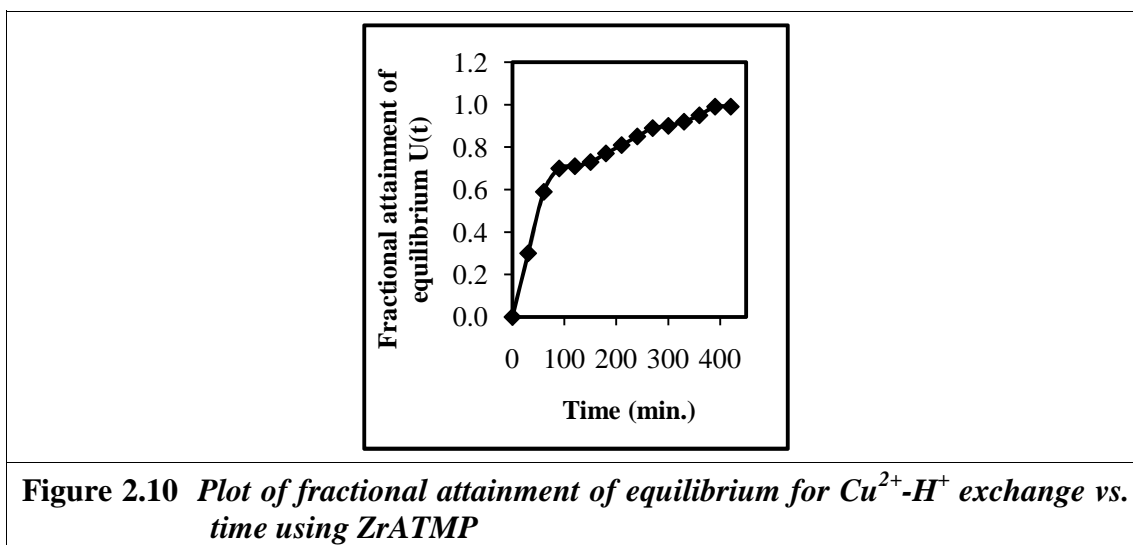


Table 2.5 Thermodynamic parameters evaluated for  $\text{M}^{2+}$  -  $\text{H}^+$  exchange at various temperatures using ZrATMP

Metal ions	Temperature (K)	K	$G^\ddagger$ ( $\text{kJ}\cdot\text{mol}^{-1}$ )	* $H^\ddagger$ ( $\text{kJ}\cdot\text{mol}^{-1}$ )	$S^\ddagger$ ( $\text{J}\cdot\text{mol}^{-1}\cdot\text{K}^{-1}$ )
$\text{Co}^{2+}$ - $\text{H}^+$	303	2.63	-4.57	28.17	108.88
	313	2.98	-5.17		107.33
	323	3.40	-5.90		106.27
	333	3.65	-6.40		104.67
$\text{Ni}^{2+}$ - $\text{H}^+$	303	2.12	-3.90	31.05	115.44
	313	2.98	-5.17		115.74
	323	3.09	-5.49		113.09
	333	3.27	-5.91		110.58
$\text{Cu}^{2+}$ - $\text{H}^+$	303	0.47	-1.85	100.0	336.4
	313	1.02	-2.62		329.9
	323	3.87	-6.44		328.1
	333	4.06	-7.00		321.6
$\text{Zn}^{2+}$ - $\text{H}^+$	303	1.07	-2.60	8.8	37.80
	313	1.18	-2.83		37.32
	323	1.35	-3.15		37.15
	333	1.39	-3.30		36.50
$\text{Cd}^{2+}$ - $\text{H}^+$	303	2.06	-3.85	24.40	93.25
	313	2.21	-4.17		91.30
	323	2.27	-4.39		89.14
	333	2.90	-5.39		89.49
$\text{Hg}^{2+}$ - $\text{H}^+$	303	4.57	-7.02	13.12	66.46
	313	4.82	-7.57		66.12
	323	4.99	-8.04		65.53
	333	5.05	-8.37		64.56
$\text{Pb}^{2+}$ - $\text{H}^+$	303	0.41	-1.17	76.78	259.15
	313	0.99	-2.58		253.47
	323	2.11	-4.10		250.49
	333	3.12	-5.70		247.60

### ***Kinetic studies using ZrATMP***

As a representative, plot of  $\tau$  versus  $t$  for the  $\text{Cu}^{2+}\text{-H}^+$  exchange process has been presented in **Figure 2.11**. For metal ion concentrations  $\geq 0.014\text{ M}$ , straight lines passing through the origin are obtained, confirming a particle diffusion controlled exchange at these concentrations [79]. For further kinetic studies, this minimum concentration ( $0.014\text{ M}$  for  $\text{M}^{2+}\text{-H}^+$  exchange process) was used for all metal ions under study, since at this concentration the Donnan exclusion is predominant, which prevents the interference of co-ion in the exchange process [80].

The plots of  $\dagger$  versus  $t$  for  $\text{M}^{2+} - \text{H}^+$  (where  $\text{M}^{2+} = \text{Co}^{2+}, \text{Ni}^{2+}, \text{Cu}^{2+}, \text{Zn}^{2+}, \text{Cd}^{2+}, \text{Hg}^{2+}$  and  $\text{Pb}^{2+}$ ) exchanges at different temperatures and plots of  $\ln D_A$  versus  $1/T$  are presented in **Figures 2.12 and 2.13** respectively. It is observed that the plots of  $\ln D_A$  versus  $1/T$  are straight lines verifying the validity of the Arrhenius relation.

The values of the self-diffusion co-efficient ( $D_0$ ), energy of activation ( $E_a$ ) and entropies of activation ( $S^*$ ) have been evaluated using standard equations (**Eqs. 2.22-2.24**) discussed earlier in text and results summarized in (**Table 2.6**). It is observed that for all metal ions under study the equilibrium values increase with increasing temperature. This may be due to increase in mobility of the ions with increasing temperature.

In the present study the observed order for  $D_0$ ,  $E_a$  and  $S^*$  is  $\text{Cu}^{2+} > \text{Ni}^{2+} > \text{Co}^{2+} > \text{Zn}^{2+}$  (for transition metal ions) and  $\text{Pb}^{2+} > \text{Cd}^{2+} > \text{Hg}^{2+}$  (for heavy metal ions). The sizes of transition metal ions follows the order  $\text{Cu}^{2+} > \text{Zn}^{2+} > \text{Co}^{2+} > \text{Ni}^{2+}$  and amongst heavy metal ions  $\text{Pb}^{2+} > \text{Hg}^{2+} > \text{Cd}^{2+}$ . Since larger ions are less hydrated, the  $\text{Cu}^{2+}\text{-Zn}^{2+}$  pair having larger ionic radii should be less hydrated and thus its self diffusion coefficient should be higher compared to  $\text{Co}^{2+}\text{-Ni}^{2+}$  pair while heavy metal ions should follow the order  $\text{Pb}^{2+} > \text{Hg}^{2+} > \text{Cd}^{2+}$ . Deviation from expected order in both cases could be attributed to electrostatic interaction of metal ions with the exchange sites, which increases with the increase in charge density [91], site acidity, pore size and size of exchanger particle etc. which could be the decisive factors in certain cases [92]. The order of  $D_0$  mentioned above could be due to a net contribution of all these factors.

For an ion exchanger,  $E_a$  values depend on the ease of dehydration of a hydrated ion, for it to occupy a site on the exchanger.  $E_a$  values also depend on several factors such as columbic barrier, geometry of exchanger particle, charge of the

incoming ions etc. The overall  $E_a$  value is a result of contribution of the above-mentioned factors. Based on ion size,  $E_a$  should follow the order  $\text{Co}^{2+} \text{ Ni}^{2+} > \text{Cu}^{2+} \text{ Zn}^{2+}$  and  $\text{Cd}^{2+} > \text{Hg}^{2+} > \text{Pb}^{2+}$ . It has been observed earlier that  $E_a$  values are in the 20.9-41.8  $\text{kJmol}^{-1}$  range for organic resins whereas in the 41.8-123.2  $\text{kJmol}^{-1}$  range for zeolites [93]. In the present study,  $E_a$  values are in the range 40.4-62.1  $\text{kJmol}^{-1}$  for all metal ions under study. The apparently low values indicate a low diffusion barrier for the metal ion, when it passes through the structural channels during ion exchange. The low  $E_a$  values are also indicative of the fact that the metal ion exchange studied herein is diffusion-controlled as observed earlier [94]. However, in the present study the observed order of  $E_a$  is similar to trends in  $D_0$  values.  $E_a$  values also reflect on the  $UH$  values that follow the same order.

The entropy reflects the changes in hydration sphere of the exchanging cation during the ion exchange process. When ion exchange occurs, cation of high entropy in the external aqueous phase, passes to one of lower entropy in the exchanger phase, which results in a significant negative contribution of entropy change. In the present study, the entropy of activation  $S^*$  has been found to be negative for both transition metal and heavy metal ions (Table 2.6). Negative values of  $S^*$  indicate the decrease in the degree of randomness at the surface of the exchanger during metal ion exchange process.

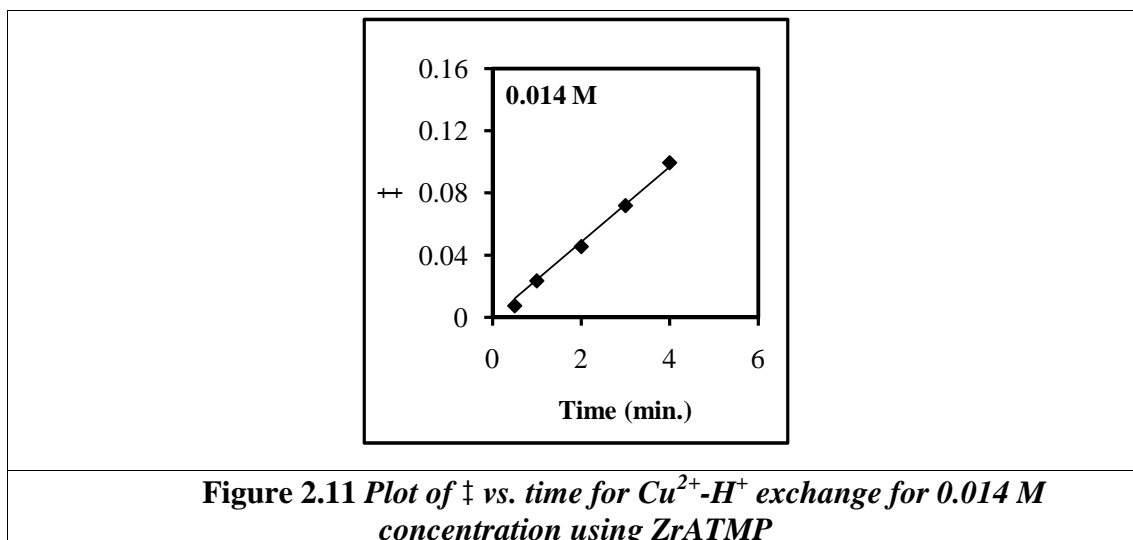
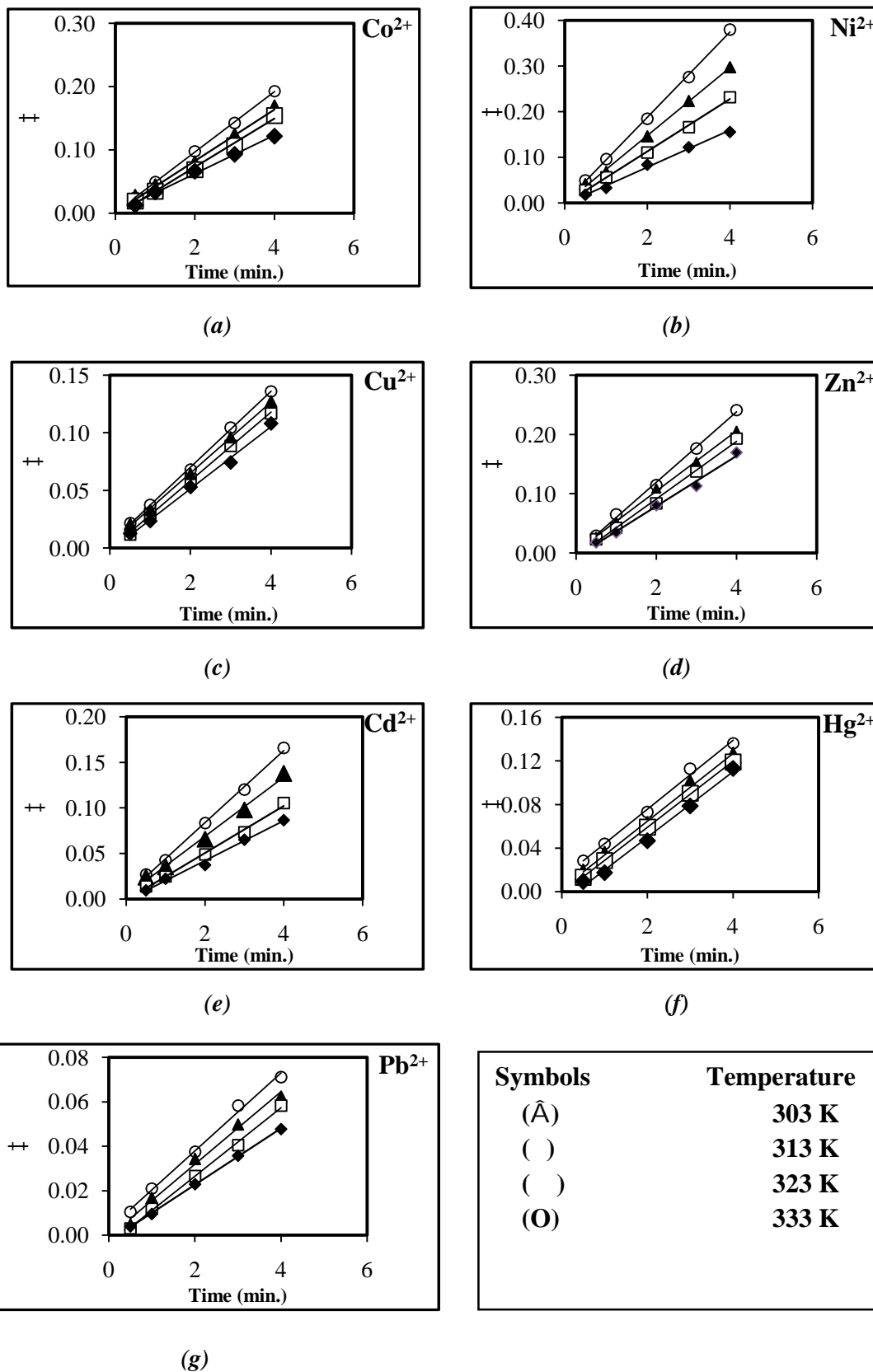


Figure 2.11 Plot of † vs. time for  $\text{Cu}^{2+}$ - $\text{H}^+$  exchange for 0.014 M concentration using ZrATMP

Table 2.6 Kinetic parameters evaluated for  $\text{M}^{2+}$ - $\text{H}^+$  exchange using ZrATMP

Exchanging ion	Equilibrium Values (meq.g <sup>-1</sup> )				Ionic radii (Å)	$D_0$ (m <sup>2</sup> ·s <sup>-1</sup> )	$E_a$ (kJ·mol <sup>-1</sup> )	$S^*$ (kJ·mol <sup>-1</sup> )
	303 K	313 K	323 K	333 K				
$\text{Co}^{2+}$	0.39	0.59	0.72	0.91	0.72	$2.50 \times 10^{-10}$	45.85	-90.90
$\text{Ni}^{2+}$	0.45	0.56	0.86	1.02	0.72	$3.90 \times 10^{-10}$	54.23	-84.67
$\text{Cu}^{2+}$	0.49	0.76	0.86	0.94	0.74	$4.33 \times 10^{-10}$	62.13	-73.78
$\text{Zn}^{2+}$	0.42	0.52	0.67	0.74	0.74	$2.46 \times 10^{-10}$	43.92	-102.54
$\text{Cd}^{2+}$	0.32	0.56	0.76	0.89	0.97	$4.59 \times 10^{-11}$	53.51	-94.14
$\text{Hg}^{2+}$	0.91	0.99	1.08	1.10	1.10	$4.55 \times 10^{-11}$	40.47	-94.39
$\text{Pb}^{2+}$	0.77	0.8	0.92	1.04	1.44	$4.65 \times 10^{-11}$	60.23	-23.45



**Figure 2.12** Plots of  $\ddagger$  vs. time at different temperatures for (a)  $\text{Co}^{2+}$ - $\text{H}^+$  (b)  $\text{Ni}^{2+}$ - $\text{H}^+$  (c)  $\text{Cu}^{2+}$ - $\text{H}^+$  (d)  $\text{Zn}^{2+}$ - $\text{H}^+$  (e)  $\text{Cd}^{2+}$ - $\text{H}^+$  (f)  $\text{Hg}^{2+}$ - $\text{H}^+$  (g)  $\text{Pb}^{2+}$ - $\text{H}^+$  exchanges using ZrATMP

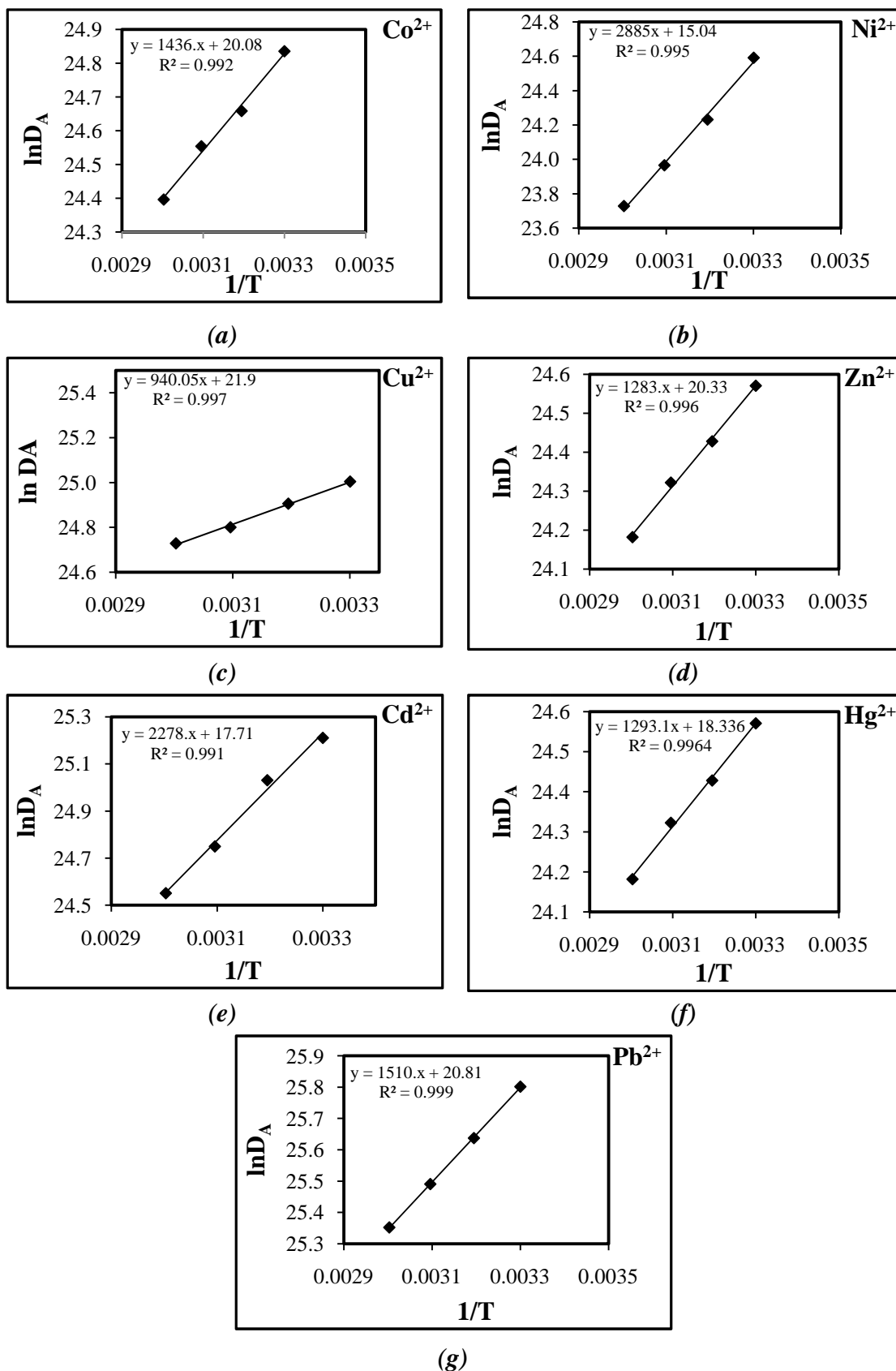


Figure 2.13(a-g) Arrhenius plots  $\ln D_A$  versus  $1/T$  for (a)  $\text{Co}^{2+} - \text{H}^+$  (b)  $\text{Ni}^{2+} - \text{H}^+$  (c)  $\text{Cu}^{2+} - \text{H}^+$  (d)  $\text{Zn}^{2+} - \text{H}^+$  (e)  $\text{Cd}^{2+} - \text{H}^+$  (f)  $\text{Hg}^{2+} - \text{H}^+$  (g)  $\text{Pb}^{2+} - \text{H}^+$  exchanges using ZrATMP

### **Adsorption studies using ZrATMP**

The effect of experimental conditions such as pH, contact time and temperature were studied to set the conditions for maximum adsorption/ion exchange for the metal ions by the ion exchanger.

The effect of pH on the sorption behaviour of metal ions (under study) have been presented in **Table 2.7**. At pH values less than ~3, very less sorption has been observed for all metal ions. The lack of sorption at low pH could be attributed to high concentration of hydrogen ions competing with the metal ions for sorption/exchange sites. A precipitation was observed in case of  $\text{Cu}^{2+}$ ,  $\text{Ni}^{2+}$ ,  $\text{Zn}^{2+}$ ,  $\text{Pb}^{2+}$  and  $\text{Cd}^{2+}$  at pH 7, while in case of  $\text{Co}^{2+}$  and  $\text{Hg}^{2+}$  precipitation was observed at pH 8. The observed order for % uptake of metal ion at optimum pH, is  $\text{Cu}^{2+} > \text{Ni}^{2+} > \text{Co}^{2+} > \text{Zn}^{2+}$  (amongst transition metal ions) and  $\text{Pb}^{2+} > \text{Cd}^{2+} > \text{Hg}^{2+}$  (amongst heavy metal ions) (**Table 2.7**).

The time taken for attainment of equilibrium for each metal ion in  $\text{mg}\cdot\text{L}^{-1}$  has been presented in (**Table 2.8**). Sorption of metal ions varying contact time and temperature has been presented in (**Tables 2.9 to 2.15**) and illustrated in (**Figures 2.14 to 2.20**) [plot of uptake (%) versus time]. It is observed that sorption increases gradually with increase in contact time and reaches a maximum value after which randomness is observed. Increase in % uptake could be attributed to two different sorption processes, namely, a fast ion exchange followed by chemisorption [54, 55]. It is observed that % uptake of each metal ion increases with increase in temperature, which indicates the uptake to be an ion exchange mechanism. When solid ion exchanger is in contact with electrolyte solution, mainly two reactions may take place, either ion exchange (inside the pores of the exchanger) or sorption. As physical forces are responsible for sorption, the value of  $k_c$  (equilibrium constant) may decrease with increasing temperature. Ion exchange being a chemical reaction, some energy is required for crossing the barrier (energy of activation). In such cases therefore, as the temperature increases, the ion exchange may increase. Increase in  $k_c$  with increase in temperature, thus indicates the mechanism to be probably ion exchange.

Langmuir constants ( $b$  and  $V_m$ ) and Freundlich constants ( $K$  and  $1/n$ ) obtained from the slopes and intercepts of the linear plots [**Figures 2.21(a-g)** and **2.22(a-g)**] are presented in **Table 2.16**. It is observed that  $R^2$  values are found to be close to unity for

both isotherms and provides a good fit to the experimental data for sorption of all the metal ions studied. Variation in  $R^2$  values is attributed to the fact that the surface adsorption is not a monolayer with single site. Two or more sites with different affinities may be involved in metal ion sorption [53]. In the present study, low values of  $b$  indicate favorable adsorption.  $V_m$  values, reflect maximum adsorption capacity of metal ions towards the exchanger. It is observed that with an increase in temperature, the maximum adsorption capacity  $V_m$  increased [54]. The values of  $1/n$  and  $R_L$  are obtained between 0 and 1 which indicates normal isotherm and favourable adsorption.

**Table 2.7 % Uptake of metal ions varying pH using ZrATMP**

pH	(% ) Uptake of metal ion						
	Co <sup>2+</sup>	Ni <sup>2+</sup>	Cu <sup>2+</sup>	Zn <sup>2+</sup>	Cd <sup>2+</sup>	Hg <sup>2+</sup>	Pb <sup>2+</sup>
1	11.54	37.07	17.78	21.20	16.67	3.85	17.78
2	19.28	47.50	36.00	22.35	28.00	19.28	28.00
3	29.55	<b>55.65</b>	<b>67.68</b>	31.87	<b>47.47</b>	<b>29.55</b>	35.35
4	43.00	50.42	55.45	37.89	44.55	22.00	<b>62.38</b>
5	49.00	48.41	45.10	<b>40.00</b>	34.31	18.00	34.31
6	<b>53.00</b>	50.36	34.95	37.00	25.24	11.00	22.33
7	51.00	-	-	-	-	5.00	-

Maximum deviation in % uptake of metal ion =  $\pm 2\%$

**Table 2.8 Equilibrium time determination (varying temperature) using ZrATMP**

Metal ion	Equilibrium time (min)			
	303 K	313 K	323 K	333 K
Co <sup>2+</sup>	90	80	70	60
Ni <sup>2+</sup>	160	130	110	90
Cu <sup>2+</sup>	190	170	120	100
Zn <sup>2+</sup>	60	50	50	50
Cd <sup>2+</sup>	110	90	70	70
Hg <sup>2+</sup>	60	50	50	50
Pb <sup>2+</sup>	170	150	130	110

**Table 2.9 % Uptake of  $\text{Co}^{2+}$  using ZrATMP**

Time Mins	% Uptake of $\text{Co}^{2+}$			
	303 K	313 K	323 K	333 K
10	9.1	13.2	23.3	39.1
20	14.5	17.3	28.9	42.9
30	22.1	25.7	34.7	49.7
40	26.9	29.3	42.9	51.8
50	31.9	35.8	45.5	53.7
60	38.8	40.1	49.2	54.2
70	40.1	45.7	53.2	
80	45.7	52.1		
90	46.1			

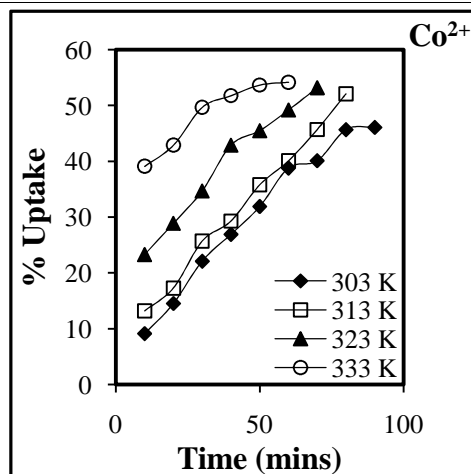


**Figure 2.14 % Uptake of  $\text{Co}^{2+}$**

**Reaction conditions:** Amount of ZrATMP, 0.1 g; metal ion concentration, 0.001 M; total volume of metal ion, 10 mL; pH, 6;

**Table 2.10 % Uptake of  $\text{Ni}^{2+}$  using ZrATMP**

Time Mins	% Uptake of $\text{Ni}^{2+}$			
	303 K	313 K	323 K	333 K
10	16.2	20.3	31.2	40.1
20	19.2	26.9	37.1	42.9
30	21.1	29.2	42.2	49.5
40	23.5	32.9	51.8	55.5
50	25.1	35.5	59.8	62.9
60	29.8	39.8	64.8	69.2
70	34.89	40.4	68.8	70.2
80	39.8	49.1	70.1	73.8
90	42.9	53.9	70.1	74.1
100	45.9	59.3	70.1	
110	51.9	67.8	72.9	
120	55.8	69.1		
130	59.1	70.1		
140	63.9			
150	67.3			
160	68.0			

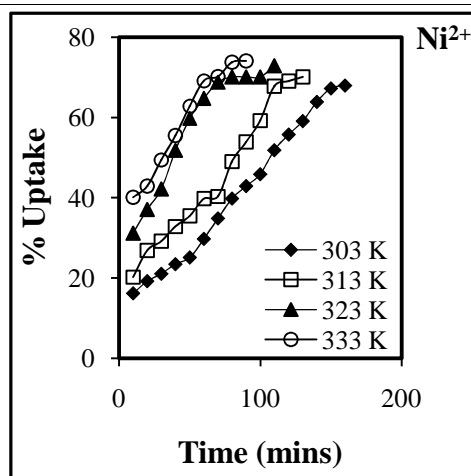


**Figure 2.15 % Uptake of  $\text{Ni}^{2+}$**

**Reaction conditions:** Amount of ZrATMP, 0.1 g; metal ion concentration, 0.001M; total volume of metal ion, 10 mL; pH, 3;

**Table 2.11 % Uptake of  $\text{Cu}^{2+}$  using ZrATMP**

Time Mins	% Uptake of $\text{Cu}^{2+}$			
	303 K	313 K	323 K	333 K
10	15.1	34.3	39.1	48.4
20	22.5	43.6	48.9	58.2
30	33.5	46.3	57.4	63.9
40	41.8	51.8	62.4	72.3
50	46.2	56.8	68.9	78.2
60	48.4	56.8	71.1	79.9
70	52.0	58.7	74.2	81.4
80	56.7	62.8	78.7	83.7
90	59.1	65.3	80.5	84.6
100	61.9	65.1	81.8	86.9
110	63.0	68.4	82.8	
120	64.9	70.5	84.0	
130	66.9	72.8		
140	68.4	74.5		
150	70.1	77.5		
160	72.4	78.8		
170	76.9	82.0		
180	79.9			
190	79.9			

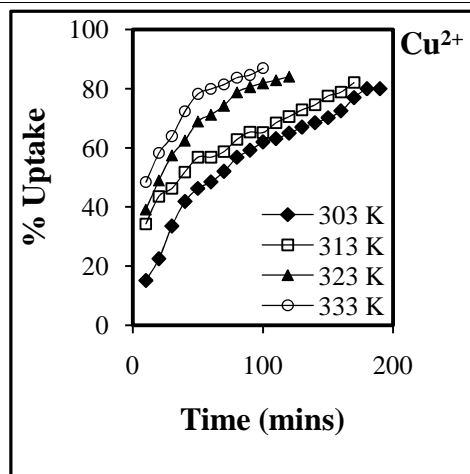


**Figure 2.16 % Uptake of  $\text{Cu}^{2+}$**

**Reaction conditions:** Amount of ZrATMP, 0.1 g; metal ion concentration, 0.001M; total volume of metal ion, 10 mL; pH, 3;

**Table 2.12 % Uptake of  $\text{Zn}^{2+}$  using ZrATMP**

Time Mins	% Uptake of $\text{Zn}^{2+}$			
	303 K	313 K	323 K	333 K
10	12.9	14.4	20.1	22.1
20	19.2	22.9	29.4	33.2
30	25.7	30.1	37.9	39.1
40	30.2	35.4	40.2	40.4
50	34.7	36.1	41.1	41.9
60	35.1			

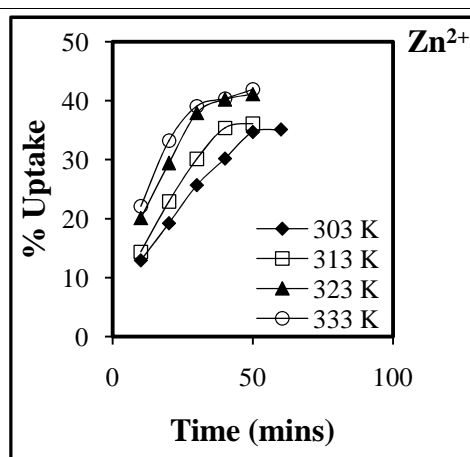


**Figure 2.17 % Uptake of  $\text{Zn}^{2+}$**

**Reaction conditions:** Amount of ZrATMP, 0.1 g; metal ion concentration, 0.001M; total volume of metal ion, 10 mL; pH, 5;

**Table 2.13 % Uptake of Cd<sup>2+</sup> using ZrATMP**

Time Mins	% Uptake of Cd <sup>2+</sup>			
	303 K	313 K	323 K	333 K
10	15.4	16.9	20.1	22.2
20	20.2	22.2	25.5	28.7
30	22.5	28.5	29.9	31.4
40	29.3	33.2	39.4	40.5
50	34.7	37.6	45.3	49.3
60	39.9	42.9	49.9	50.2
70	41.1	44.8	50.3	51.1
80	42.3	48.7		
90	44.9	49.5		
100	45.3			
110	45.3			

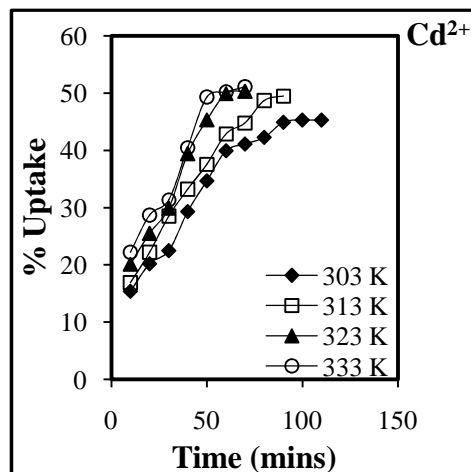


**Figure 2.18 % Uptake of Cd<sup>2+</sup>**

**Reaction conditions:** Amount of ZrATMP, 0.1 g; metal ion concentration, 0.001M; total volume of metal ion, 10 mL; pH, 3;

**Table 2.14 % Uptake of Hg<sup>2+</sup> using ZrATMP**

Time Mins	% Uptake of Hg <sup>2+</sup>			
	303 K	313 K	323 K	333 K
10	7.9	13.2	14.1	14.6
20	12.6	19.2	20.2	20.8
30	18.4	26.6	28.5	29.1
40	23.2	28.9	29.9	30.1
50	28.5	30.3	31.2	32.1
60	29.3			

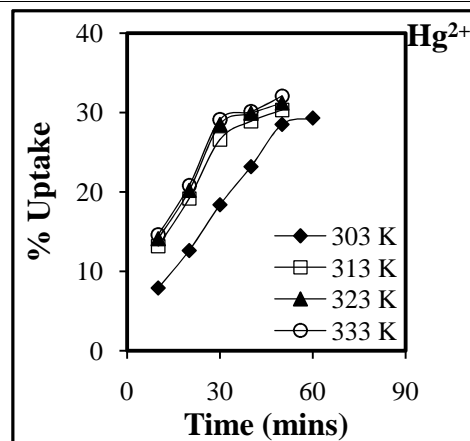


**Figure 2.19 % Uptake of Hg<sup>2+</sup>**

**Reaction conditions:** Amount of ZrATMP, 0.1 g; metal ion concentration, 0.001M; total volume of metal ion, 10 mL; pH, 3;

**Table 2.15 % Uptake of Pb<sup>2+</sup> using ZrATMP**

Time Mins	% Uptake of Pb <sup>2+</sup>			
	303 K	313 K	323 K	333 K
10	15.1	18.9	20.9	25.4
20	21.3	24.4	27.9	31.7
30	32.9	34.5	36.8	39.8
40	41.3	42.6	44.8	46.8
50	44.8	46.5	51.8	53.9
60	48.5	49.8	52.2	54.8
70	50.1	51.2	54.4	57.9
80	57.3	52.2	57.3	63.2
90	60.1	56.5	58.7	69.7
100	61.7	59.6	63.2	75.5
110	63.2	64.3	69.8	76.8
120	65.5	68.7	73.2	
130	67.2	71.1	75.5	
140	69.9	73.3		
150	70.1	74.8		
160	72.4			
170	72.9			

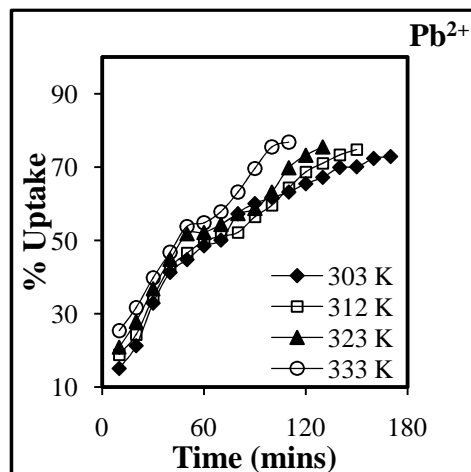


**Figure 2.20 % Uptake of Pb<sup>2+</sup>**

**Reaction conditions:** Amount of ZrATMP, 0.1 g; metal ion concentration, 0.001M; total volume of metal ion, 10 mL; pH, 4;

**Table 2.16 Langmuir and Freundlich constants evaluated for transition and heavy metal ions using ZrATMP**

Metal Ion	Temperature (K)	Langmuir Constants				Freundlich Constants		
		$R^2$	$b$ ( $\text{dm}^3 \cdot \text{mg}^{-1}$ )	$V_m$ ( $\text{mg} \cdot \text{g}^{-1}$ )	$R_L$ Values	$R^2$	$K$	$1/n$
Co <sup>2+</sup>	303	0.997	0.0047	17.21	0.988	0.856	2.633	0.905
	313	0.952	0.0090	18.48	0.993	0.950	2.699	0.949
	323	0.996	0.0079	21.45	0.980	0.968	2.776	0.975
	333	0.995	0.0071	23.80	0.995	0.971	3.144	0.738
Ni <sup>2+</sup>	303	0.990	0.0055	27.70	0.982	0.991	1.148	0.504
	313	0.995	0.0542	30.67	0.991	0.995	9.720	0.438
	323	0.990	0.0693	31.64	0.988	0.985	10.480	0.526
	333	0.994	0.0107	34.12	0.998	0.999	16.390	0.824
Cu <sup>2+</sup>	303	0.999	0.0045	30.00	0.990	0.972	3.403	0.531
	313	0.993	0.0053	44.09	0.999	0.987	4.399	0.643
	323	0.992	0.0036	38.02	0.999	0.997	6.429	0.808
	333	0.996	0.0018	86.95	0.993	0.989	4.009	0.603
Zn <sup>2+</sup>	303	0.991	0.0221	5.050	0.972	0.815	1.651	0.217
	313	0.992	0.0079	11.96	0.983	0.953	2.851	0.455
	323	0.995	0.0071	14.92	0.997	0.977	3.054	0.485
	333	0.998	0.0061	21.27	0.989	0.993	3.415	0.533
Cd <sup>2+</sup>	303	0.982	0.0022	19.72	0.856	0.908	2.843	0.453
	313	0.991	0.0023	29.23	0.950	0.958	2.494	0.397
	323	0.988	0.0015	55.86	0.968	0.997	3.196	0.504
	333	0.998	0.0014	76.33	0.971	0.991	3.636	0.560
Hg <sup>2+</sup>	303	0.988	0.0002	23.52	0.997	0.997	5.620	1.333
	313	0.993	0.0006	20.57	0.952	0.988	3.826	1.715
	323	0.980	0.0003	40.98	0.996	0.991	5.749	1.316
	333	0.995	0.0007	52.63	0.995	0.978	3.811	1.720
Pb <sup>2+</sup>	303	0.990	0.0047	63.29	0.991	0.995	2.686	0.277
	313	0.999	0.0065	64.51	0.995	0.962	2.968	0.272
	323	0.999	0.0078	70.42	0.985	0.938	3.397	0.265
	333	0.993	0.0065	89.28	0.999	0.991	3.972	0.293

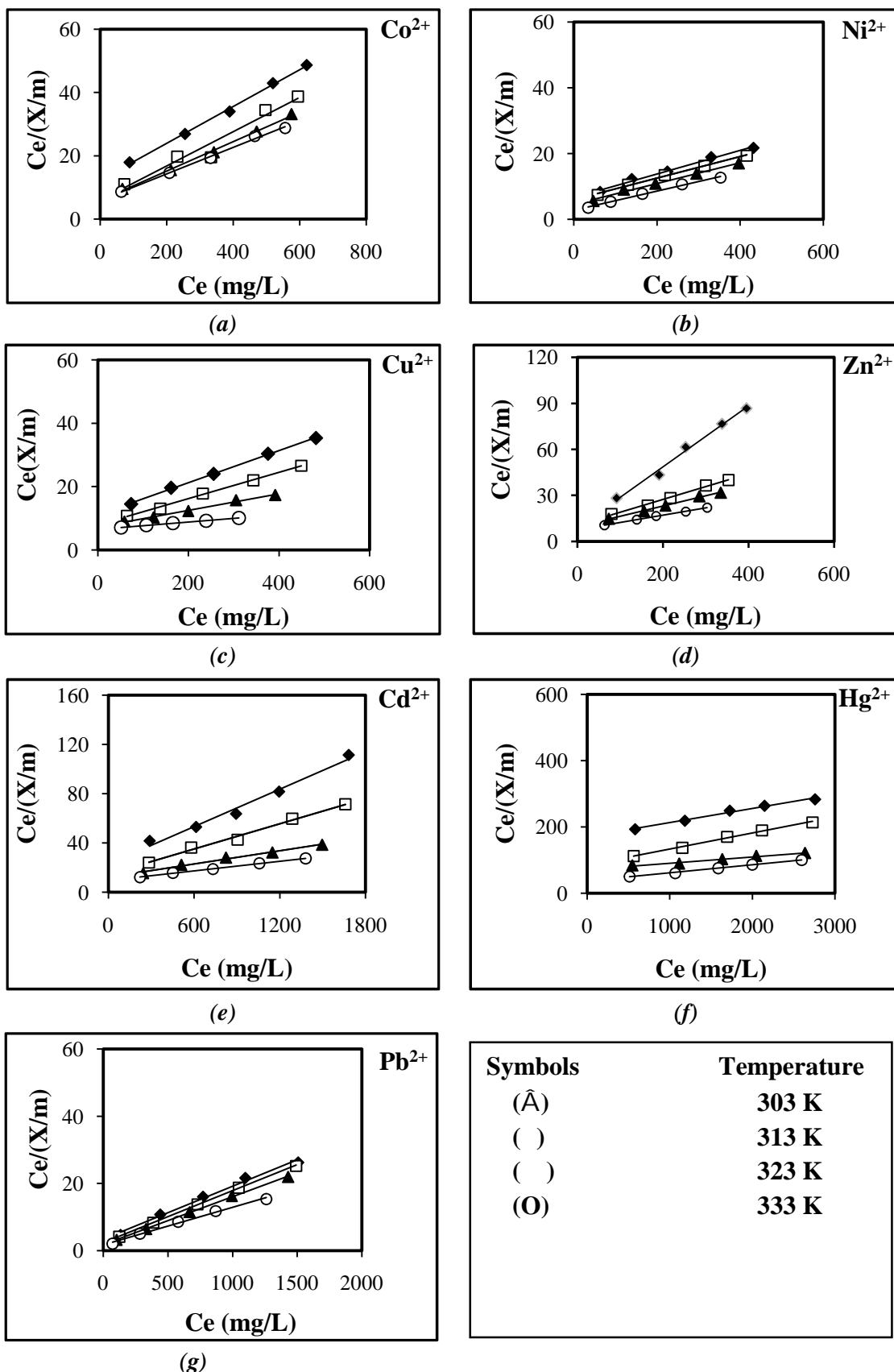


Figure 2.21(a-g) Langmuir plots for transition metal ions (a)  $Co^{2+}$ ; (b)  $Ni^{2+}$ ; (c)  $Cu^{2+}$ ; (d)  $Zn^{2+}$  and heavy metal ions (e)  $Cd^{2+}$ ; (f)  $Hg^{2+}$ ; (g)  $Pb^{2+}$  using ZrATMP

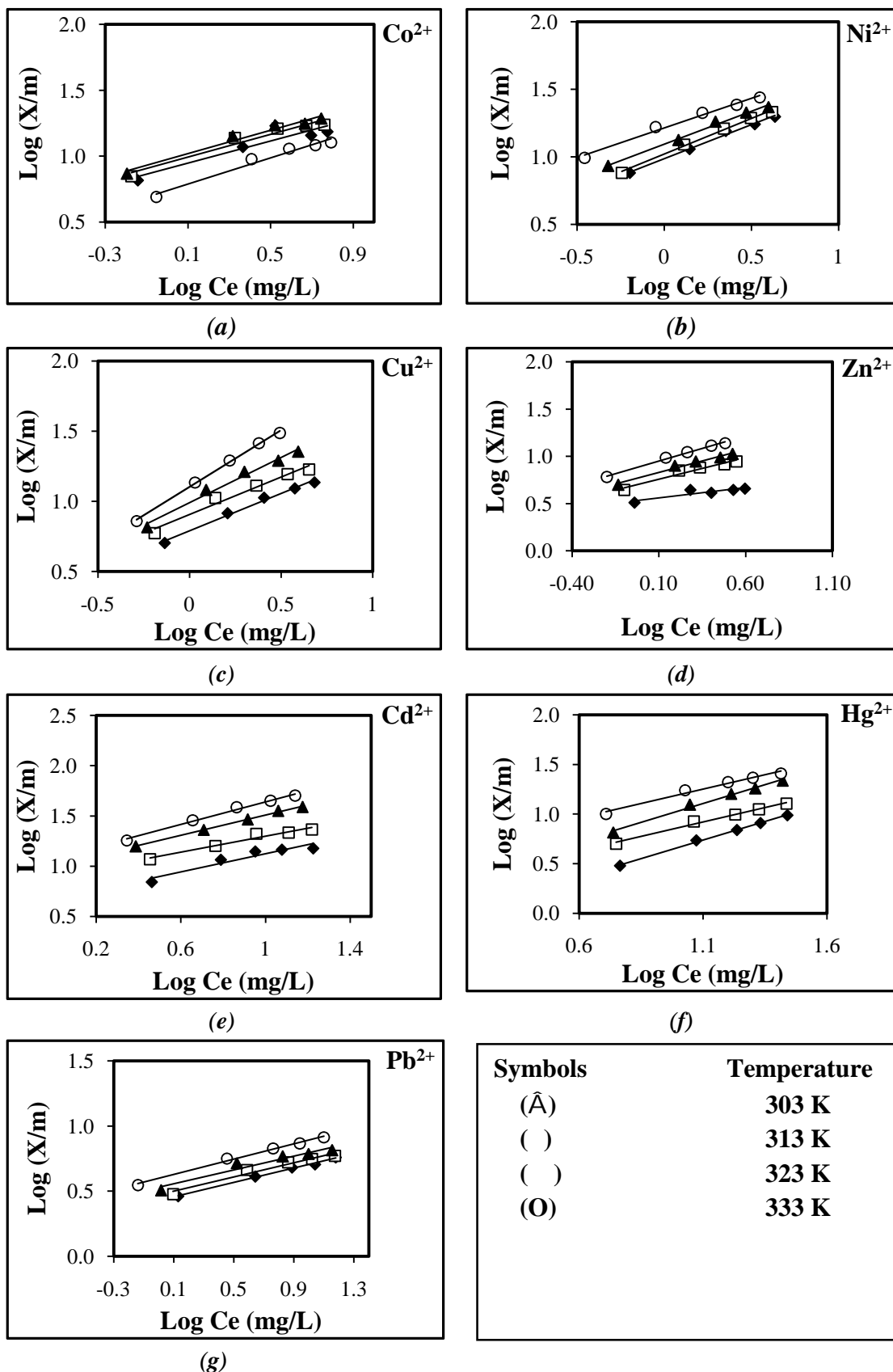


Figure 2.22(a-g) Freundlich plots for transition metal ions (a)  $\text{Co}^{2+}$ ; (b)  $\text{Ni}^{2+}$ ; (c)  $\text{Cu}^{2+}$ ; (d)  $\text{Zn}^{2+}$  and heavy metal ions (e)  $\text{Cd}^{2+}$ ; (f)  $\text{Hg}^{2+}$ ; (g)  $\text{Pb}^{2+}$  using ZrATMP

## 2.10 RESULTS AND DISCUSSION-PART II

### *Thermodynamic studies using TiATMP*

Thermodynamics of ion exchange has been studied for  $\text{Co}^{2+}$ ,  $\text{Ni}^{2+}$ ,  $\text{Cu}^{2+}$ ,  $\text{Zn}^{2+}$  (transition metal ions) and  $\text{Cd}^{2+}$ ,  $\text{Hg}^{2+}$ ,  $\text{Pb}^{2+}$  (heavy metal ions). Equilibrium constant ( $K$ ), standard Gibbs free energy ( $G^\circ$ ), enthalpy ( $H^\circ$ ) and entropy ( $S^\circ$ ) have been evaluated using standard equations (Eq. 2.16-2.18) [63, 88] discussed earlier in text and results presented in (Table 2.17).

A plot of the fractional attainment of equilibrium  $U(\dagger)$  versus time ( $t$ ) (Figure 2.23) shows that the exchange equilibrium for TiATMP appears to have attained within 6 h and hence all the equilibrium studies were performed, allowing a maximum equilibrium time of 6h.

Equilibrium constant ( $K$ ) values increase with increase in temperature for all metal ions under study (Table 2.17), indicating that the metal ions have higher affinity for the exchanger and that the mechanism is ion exchange [89].

In the present study, free energy change ( $G^\circ$ ) for all metal exchange reactions is negative, over the entire temperature range indicating feasibility of the ion exchange process and that the exchanger has a greater preference for metal ions than  $\text{H}^+$  ions. The  $G^\circ$  values become more negative with increasing temperature, confirming that the exchange is favoured with increasing temperature.

Enthalpy change ( $H^\circ$ ) is positive in all cases indicating the process to be endothermic. Higher/positive values of enthalpy change indicate more endothermicity of the exchange process and requirement of more energy for dehydration to occur. As dehydration is a must for ion exchange to occur, some energy must be supplied, to the cation, as it leaves the hydration sphere to undergo ion exchange [90]. The  $H^\circ$  values indicate that probably complete dehydration occurs in case of  $\text{Cu}^{2+}$  amongst transition metal ions and  $\text{Pb}^{2+}$  amongst heavy metal ions.

Higher  $S^\circ$  values also observed in case of  $\text{Cu}^{2+}$  and  $\text{Pb}^{2+}$  are attributed to greater dehydration, which indicates the greater disorder produced during the exchange.

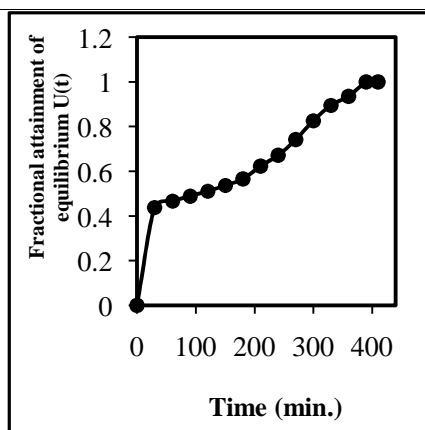


Figure 2.23 Plot of the fractional attainment of equilibrium for  $\text{Cu}^{2+}\text{-H}^+$  exchange vs. time using TiATMP

Table 2.17 Thermodynamic parameters evaluated for  $\text{M}^{2+}\text{-H}^+$  exchange at various temperatures using TiATMP

Metal ions	Temperature K	K	$G^\circ$ ( $\text{kJ}\cdot\text{mol}^{-1}$ )	* $H^\circ$ ( $\text{kJ}\cdot\text{mol}^{-1}$ )	$S^\circ$ ( $\text{J}\cdot\text{mol}^{-1}\cdot\text{K}^{-1}$ )
$\text{Co}^{2+}\text{-H}^+$	303	1.77	-3.4	17.07	67.8
	313	1.98	-3.8		66.9
	323	2.35	-4.4		66.8
	333	2.39	-4.6		65.3
$\text{Ni}^{2+}\text{-H}^+$	303	1.23	-2.8	8.95	38.8
	313	1.38	-3.0		38.5
	323	1.40	-3.2		37.7
	333	1.55	-3.5		37.5
$\text{Cu}^{2+}\text{-H}^+$	303	2.96	-4.9	151.07	514.9
	313	3.12	-5.3		499.6
	323	4.02	-6.7		488.4
	333	8.1	-12.9		491.3
$\text{Zn}^{2+}\text{-H}^+$	303	1.52	-3.1	23.17	86.9
	313	1.98	-3.8		86.3
	323	2.29	-4.4		85.3
	333	2.37	-4.6		83.5
$\text{Cd}^{2+}\text{-H}^+$	303	0.36	1.29	49.24	155.6
	313	1.45	-0.48		153.9
	323	1.58	-0.61		190.2
	333	1.93	-0.91		197.1
$\text{Hg}^{2+}\text{-H}^+$	303	1.13	-0.15	12.04	25.0
	313	1.48	-0.51		36.9
	323	1.68	-0.70		39.7
	333	1.95	-0.92		40.2
$\text{Pb}^{2+}\text{-H}^+$	303	4.31	-6.6	139.01	481.0
	313	5.5	-8.4		471.3
	323	6.9	-10.6		463.3
	333	9.2	-14.1		460.0

### ***Kinetic studies using TiATMP***

As representative, plots of  $\tau$  versus  $t$  for the  $\text{Cu}^{2+}\text{-H}^+$  exchange process has been presented in **Figure 2.24**. For metal ion concentrations  $\geq 0.014\text{ M}$ , straight lines passing through the origin were obtained, confirming a particle diffusion controlled exchange at these concentrations [79]. For further kinetic studies, this minimum concentration ( $0.014\text{ M}$  for  $\text{M}^{2+}\text{-H}^+$  exchange process) was used, for all metal ions under study, since at this concentration the Donnan exclusion is predominant, which prevents the interference of co-ion in the exchange process [80].

The plots of  $\dagger$  versus  $t$  for  $\text{M}^{2+} - \text{H}^+$  (where  $\text{M}^{2+} = \text{Ni}^{2+}, \text{Co}^{2+}, \text{Zn}^{2+}, \text{Cu}^{2+}, \text{Pb}^{2+}, \text{Cd}^{2+}$  and  $\text{Hg}^{2+}$ ) exchanges at different temperatures and plots of  $\ln D_A$  versus  $1/T$  are presented in (**Figures 2.25 and 2.26**) respectively. It is observed that the plots of  $\ln D_A$  versus  $1/T$  are straight lines verifying the validity of the Arrhenius relation.

The values of the self-diffusion co-efficient ( $D_0$ ), energy of activation ( $E_a$ ) and entropies of activation ( $S^*$ ) have been evaluated using standard equations (**Eq. 2.22-2.24**) discussed earlier in text and results summarized in (**Table 2.18**). It is observed that for all metal ions under study the equilibrium values increase with increasing temperature. This may be due to increase in mobility of the ions with increasing temperature.

In the present study the observed order for  $D_0$ ,  $E_a$  and  $S^*$  is  $\text{Cu}^{2+} > \text{Zn}^{2+} > \text{Co}^{2+} > \text{Ni}^{2+}$  (for transition metal ions) and  $\text{Pb}^{2+} > \text{Cd}^{2+} > \text{Hg}^{2+}$  (for heavy metal ions). The sizes of transition metal ions follow the order  $\text{Cu}^{2+} > \text{Zn}^{2+} > \text{Co}^{2+} > \text{Ni}^{2+}$  and amongst heavy metal ions  $\text{Pb}^{2+} > \text{Hg}^{2+} > \text{Cd}^{2+}$ . Since larger ions are less hydrated, the  $\text{Cu}^{2+}\text{-Zn}^{2+}$  pair having larger ionic radii should be less hydrated and thus its self diffusion coefficient should be higher compared to  $\text{Co}^{2+}\text{-Ni}^{2+}$  pair while heavy metal ions should follow the order  $\text{Pb}^{2+} > \text{Hg}^{2+} > \text{Cd}^{2+}$ . Deviation from expected order in both cases could be attributed to electrostatic interaction of metal ions with the exchange sites, which increases with the increase in charge density [91], site acidity, pore size and size of exchanger particle etc. which could be the decisive factors in certain cases [92]. The order of  $D_0$  mentioned above could be due to a net contribution of all these factors.

For an ion exchanger,  $E_a$  values depend on the ease of dehydration of a hydrated ion, for it to occupy a site on the exchanger.  $E_a$  values also depend on several factors such as columbic barrier, geometry of exchanger particle, charge of the

incoming ions etc. The overall  $E_a$  value is a result of contribution of the above-mentioned factors. Based on ion size,  $E_a$  should follow the order  $\text{Co}^{2+} \text{ Ni}^{2+} > \text{Cu}^{2+} \text{ Zn}^{2+}$  and  $\text{Cd}^{2+} > \text{Hg}^{2+} > \text{Pb}^{2+}$ . It has been observed earlier that  $E_a$  values are in the 20.9-41.8  $\text{kJmol}^{-1}$  range for organic resins whereas in the 41.8-123.2  $\text{kJmol}^{-1}$  range for zeolites [93]. In the present study,  $E_a$  values are in the range 7.82-23.99  $\text{kJ mol}^{-1}$  for transition metal ions and 12.91-25.48  $\text{kJ mol}^{-1}$  for heavy metal ions. The apparently low values indicate a low diffusion barrier for the metal ion, when it passes through the structural channels during ion exchange. The low  $E_a$  values are also indicative of the fact that the metal ion exchange studied herein is diffusion-controlled as observed earlier [94]. However, in the present study the observed order of  $E_a$  is similar to trends in  $D_0$  values.  $E_a$  values also reflect on the  $UH$  values that follow the same order.

The entropy reflects the changes in hydration sphere of the exchanging cation during the ion exchange process. When ion exchange occurs, cation of high entropy in the external aqueous phase, passes to one of lower entropy in the exchanger phase, which results in a significant negative contribution of entropy change. In the present study, the entropy of activation  $S^*$  has been found to be negative for both transition metal and heavy metal ions (Table 2.18). Negative values of  $S^*$  indicate the decrease in the degree of randomness at the surface of the exchanger during metal ion exchange process.

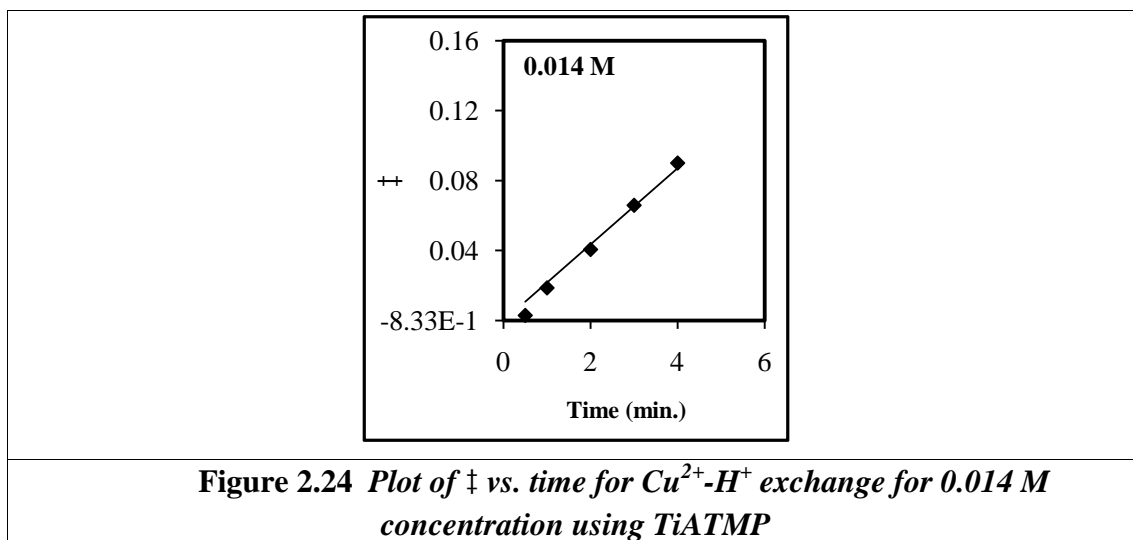


Table 2.18 Kinetic parameters evaluated for  $\text{M}^{2+}$ - $\text{H}^+$  exchange using TiATMP

Exchanging ion	Equilibrium Values (meq.g <sup>-1</sup> )				Ionic radii (Å)	$D_0$ (m <sup>2</sup> ·s <sup>-1</sup> )	$E_a$ (kJ·mol <sup>-1</sup> )	$S^*$ (kJ·mol <sup>-1</sup> )
	303 K	313 K	323 K	333 K				
$\text{Co}^{2+}$	0.49	0.53	0.56	0.60	0.72	$1.90 \times 10^{-9}$	10.67	-65.38
$\text{Ni}^{2+}$	0.47	0.50	0.52	0.54	0.72	$1.48 \times 10^{-9}$	7.82	-78.43
$\text{Cu}^{2+}$	0.54	0.63	0.70	0.75	0.74	$3.09 \times 10^{-9}$	23.99	-21.41
$\text{Zn}^{2+}$	0.55	0.58	0.62	0.65	0.74	$2.94 \times 10^{-9}$	11.94	-63.30
$\text{Cd}^{2+}$	0.33	0.35	0.39	0.43	0.97	$2.04 \times 10^{-8}$	18.95	-43.60
$\text{Hg}^{2+}$	0.28	0.21	0.33	0.49	1.10	$1.09 \times 10^{-8}$	12.91	-69.37
$\text{Pb}^{2+}$	0.42	0.46	0.53	0.57	1.44	$9.20 \times 10^{-8}$	25.48	-20.34

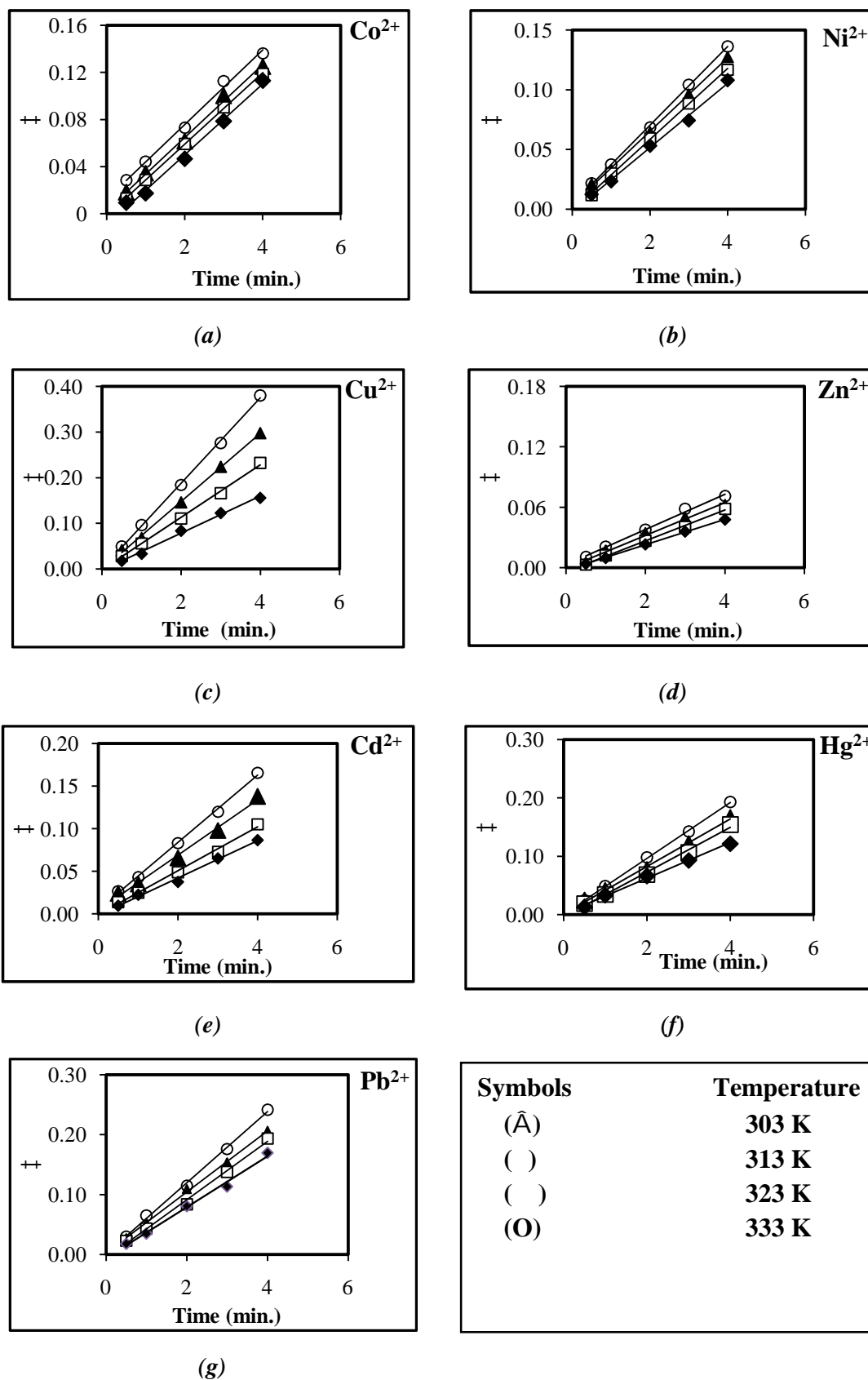


Figure 2.25 Plots of  $\ddagger$  vs. time at different temperatures for (a)  $\text{Co}^{2+}\text{-H}^+$  (b)  $\text{Ni}^{2+}\text{-H}^+$  (c)  $\text{Cu}^{2+}\text{-H}^+$  (d)  $\text{Zn}^{2+}\text{-H}^+$  (e)  $\text{Cd}^{2+}\text{-H}^+$  (f)  $\text{Hg}^{2+}\text{-H}^+$  (g)  $\text{Pb}^{2+}\text{-H}^+$  exchanges using TiATMP

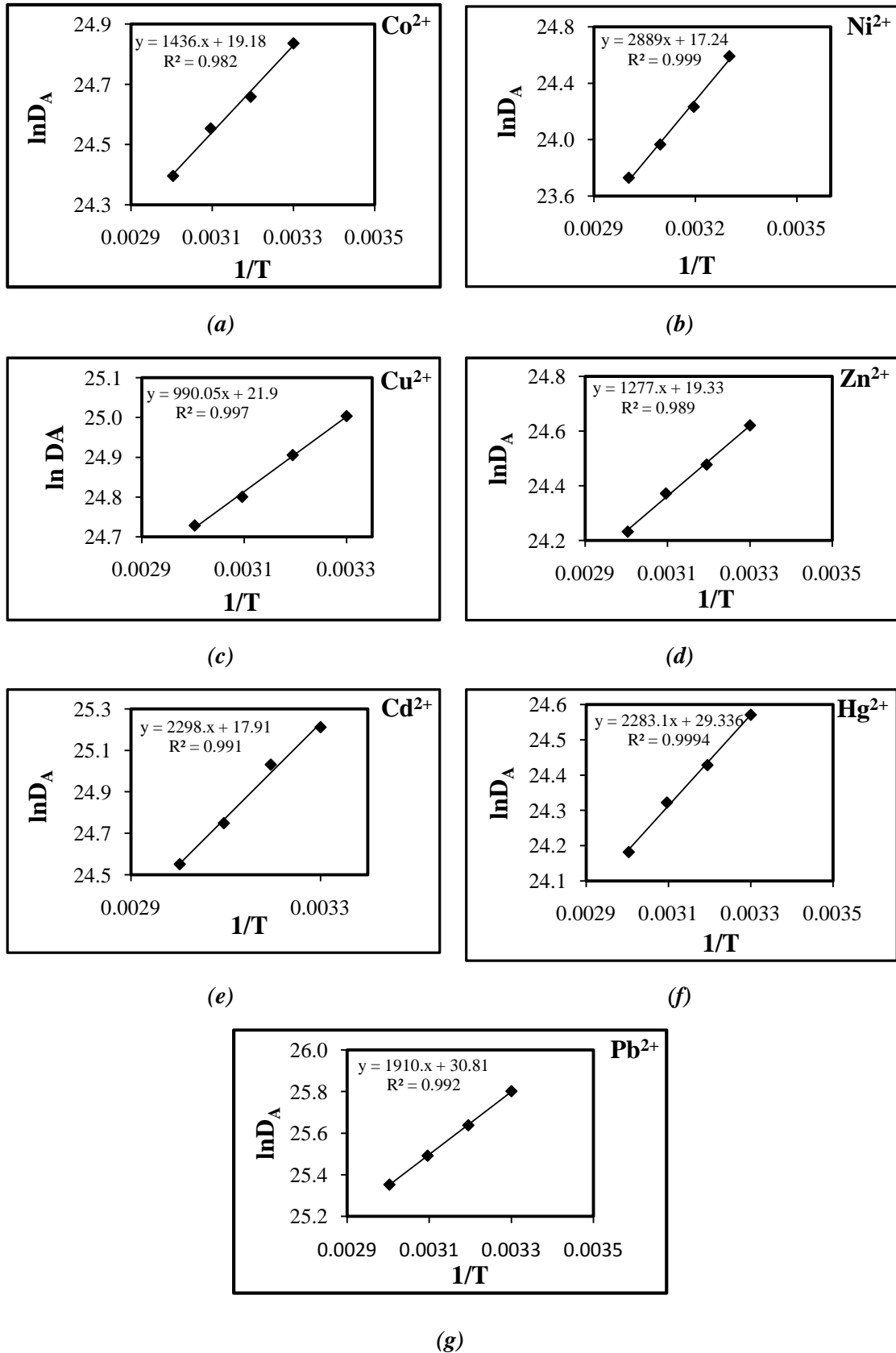


Figure 2.26(a-g) Arrhenius plots  $\ln D_A$  versus  $1/T$  for (a)  $\text{Co}^{2+} - \text{H}^+$  (b)  $\text{Ni}^{2+} - \text{H}^+$  (c)  $\text{Cu}^{2+} - \text{H}^+$  (d)  $\text{Zn}^{2+} - \text{H}^+$  (e)  $\text{Cd}^{2+} - \text{H}^+$  (f)  $\text{Hg}^{2+} - \text{H}^+$  (g)  $\text{Pb}^{2+} - \text{H}^+$  exchanges using TiATMP

### **Adsorption studies using TiATMP**

The effect of experimental conditions such as pH, contact time and temperature were studied to set the conditions for the maximum sorption/ion exchange of the metal ions by the ion exchanger.

The effect of pH on the sorption behaviour of metal ions (under study) have been presented in (**Table 2.19**). At pH values less than ~3, very less sorption has been observed for all metal ions. The lack of sorption at low pH could be attributed to the high concentration of hydrogen ions competing with the metal ions for sorption / exchange sites. A precipitation was observed in case of  $\text{Cu}^{2+}$ ,  $\text{Ni}^{2+}$ ,  $\text{Zn}^{2+}$ ,  $\text{Pb}^{2+}$  and  $\text{Cd}^{2+}$  at pH 7, while in case of  $\text{Co}^{2+}$  and  $\text{Hg}^{2+}$  precipitation was observed at pH 8. The observed order for % uptake of metal ion at optimum pH, is  $\text{Cu}^{2+} > \text{Zn}^{2+} > \text{Co}^{2+} > \text{Ni}^{2+}$  (amongst transition metal ions) and  $\text{Pb}^{2+} > \text{Cd}^{2+} > \text{Hg}^{2+}$  (amongst heavy metal ions)(**Table 2.19**).

The time taken for attainment of equilibrium for each metal ion in  $\text{mg}\cdot\text{L}^{-1}$  has been presented in (**Table 2.20**). Sorption of metal ions varying contact time and temperature has been presented in (**Tables 2.21 to 2.27**) and illustrated in (**Figures 2.27 to 2.33**) [plot of uptake (%) versus time]. It is observed that sorption increases gradually with increase in contact time and reaches a maximum value after which randomness is observed. Increase in % uptake could be attributed to two different sorption processes, namely, a fast ion exchange followed by chemisorption [54, 55]. It is observed that % uptake of each metal ion increases with increase in temperature, which indicates the uptake to be an ion exchange mechanism. When solid ion exchanger is in contact with electrolyte solution, mainly two reactions may take place, either ion exchange (inside the pores of the exchanger) or sorption. As physical forces are responsible for sorption, the value of  $k_c$  (equilibrium constant) may decrease with increasing temperature. Ion exchange being a chemical reaction, some energy is required for crossing the barrier (energy of activation). In such cases therefore, as the temperature increases, the ion exchange may increase. Increase in  $k_c$  with increase in temperature, thus indicates the mechanism to be probably ion exchange.

Langmuir constants ( $b$  and  $V_m$ ) and Freundlich constants ( $K$  and  $1/n$ ) obtained from the slopes and intercepts of the linear plots {**Figures 2.34(a-g) and 2.35(a-g)**} are presented in (**Table 2.28**). It is observed that  $R^2$  values are found to be close to

unity for both isotherms and provides a good fit to the experimental data for sorption of all the metal ions studied. Variation in  $R^2$  values is attributed to the fact that the surface adsorption is not a monolayer with single site. Two or more sites with different affinities may be involved in metal ion sorption [53]. In the present study, low values of  $b$  indicate favorable adsorption.  $V_m$  values, reflect maximum adsorption capacity of metal ions towards exchanger. It is observed that with an increase in temperature, the maximum adsorption capacity ( $V_m$ ), increased [54]. The values of  $1/n$  and  $R_L$  are obtained between 0 and 1 which indicates normal isotherm and favourable adsorption.

**Table 2.19 % Uptake of metal ions varying pH using TiATMP**

pH	(%) Uptake of metal ion						
	Co <sup>2+</sup>	Ni <sup>2+</sup>	Cu <sup>2+</sup>	Zn <sup>2+</sup>	Cd <sup>2+</sup>	Hg <sup>2+</sup>	Pb <sup>2+</sup>
1	11.54	7.88	17.78	37.93	16.67	3.85	17.78
2	19.28	7.06	36.00	42.50	28.00	19.28	28.00
3	29.55	13.19	<b>68.69</b>	46.77	<b>52.53</b>	<b>32.95</b>	35.35
4	44.00	18.95	55.45	<b>56.30</b>	44.55	22.00	<b>69.31</b>
5	<b>49.00</b>	<b>29.00</b>	45.10	45.24	34.31	18.00	34.31
6	41.00	23.00	34.95	43.17	25.24	11.00	22.33
7	37.00	-	-	-	-	5.00	-

Maximum deviation in % uptake of metal ion =  $\pm 2\%$

**Table 2.20 Equilibrium time determination (varying temperature) using TiATMP**

Metal ion	Equilibrium time (min)			
	303 K	313 K	323 K	333 K
Co <sup>2+</sup>	80	70	60	60
Ni <sup>2+</sup>	70	60	60	50
Cu <sup>2+</sup>	150	110	80	80
Zn <sup>2+</sup>	130	110	100	100
Cd <sup>2+</sup>	90	80	80	70
Hg <sup>2+</sup>	70	60	50	50
Pb <sup>2+</sup>	110	100	80	80

**Table 2.21 % Uptake of  $Co^{2+}$  using TiATMP**

Time Mins	% Uptake of $Co^{2+}$			
	303 K	313 K	323 K	333 K
10	7.7	21.1	25.5	30.2
20	11.9	29.5	34.4	39.4
30	15.5	31.9	41.1	45.5
40	18.4	38.5	48.9	49.9
50	29.3	40.4	51.9	52.3
60	39.1	52.9	55.7	56.4
70	50.1	54.8		
80	53.2			

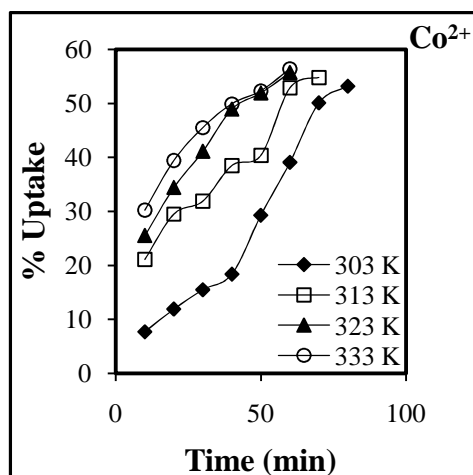


**Figure 2.27 % Uptake of  $Co^{2+}$**

**Reaction conditions:** Amount of TiATMP, 0.1 g; metal ion concentration, 0.001M; total volume of metal ion, 10 mL; pH,5;

**Table 2.22 % Uptake of  $Ni^{2+}$  using TiATMP**

Time Mins	% Uptake of $Ni^{2+}$			
	303 K	313 K	323 K	333 K
10	7.7	8.4	12.2	13.8
20	12.9	15.5	18.9	22.2
30	19.9	21.1	24.5	29.9
40	24.9	28.8	30.8	37.9
50	30.3	33.9	35.9	38.1
60	32.1	37.7	38.1	
70	35.5			

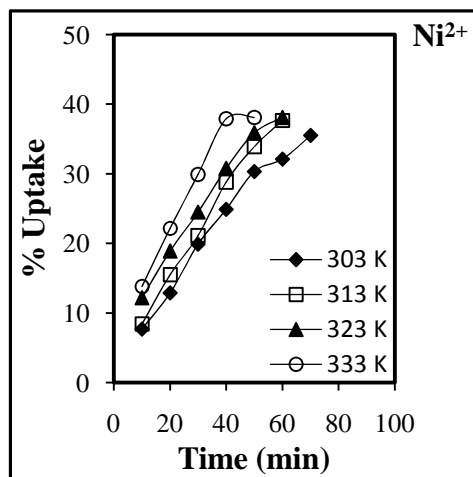


**Figure 2.28 % Uptake of  $Ni^{2+}$**

**Reaction conditions:** Amount of TiATMP, 0.1 g; metal ion concentration, 0.001M; total volume of metal ion, 10 mL; pH, 5;

**Table 2.23 % Uptake of  $\text{Cu}^{2+}$  using TiATMP**

Time Mins	% Uptake of $\text{Cu}^{2+}$			
	303 K	313 K	323 K	333 K
10	22.5	34.3	39.1	49.4
20	33.5	43.6	48.9	56.2
30	41.8	46.3	57.4	63.9
40	46.2	51.8	62.4	72.3
50	48.4	56.8	68.9	74.2
60	52.0	56.8	71.1	75.9
70	56.7	58.7	73.2	76.4
80	59.1	62.8	74.1	77.4
90	61.8	65.3		
100	62.9	69.3		
110	64.9	72.4		
120	66.9			
130	68.4			
140	69.4			
150	70.1			

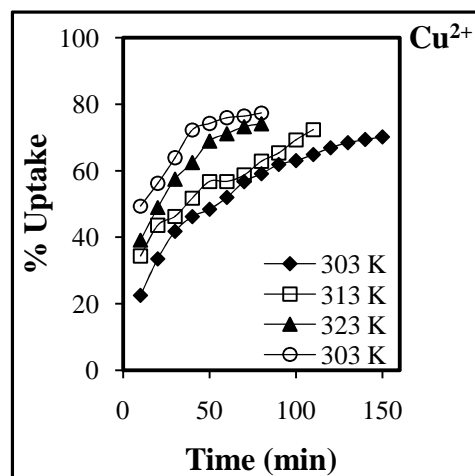


**Figure 2.29 % Uptake of  $\text{Cu}^{2+}$**

**Reaction conditions:** Amount of TiATMP, 0.1 g; metal ion concentration, 0.001M; total volume of metal ion, 10 mL; pH,3;

**Table 2.24 % Uptake of  $\text{Zn}^{2+}$  using TiATMP**

Time Mins	% Uptake of $\text{Zn}^{2+}$			
	303 K	313 K	323 K	333 K
10	15.6	18.8	22.3	30.4
20	19.8	22.1	25.6	33.8
30	25.6	27.8	29.9	39.8
40	29.9	31.9	33.2	48.9
50	34.3	36.8	38.5	53.8
60	42.2	43.4	44.3	58.3
70	49.8	51.1	48.3	63.8
80	52.2	54.3	55.3	65.9
90	57.9	58.7	63.8	68.3
100	62.2	63.3	67.4	69.9
110	64.9	66.9		
120	65.1			
130	65.7			

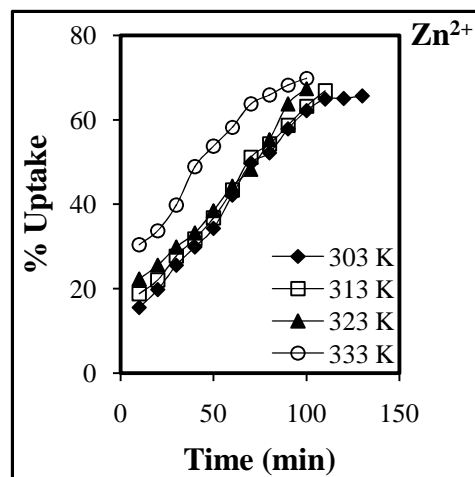


**Figure 2.30 % Uptake of  $\text{Zn}^{2+}$**

**Reaction conditions:** Amount of TiATMP, 0.1 g; metal ion concentration, 0.001M; total volume of metal ion, 10 mL; pH, 4;

**Table 2.25 % Uptake of Cd<sup>2+</sup> using TiATMP**

Time	% Uptake of Cd <sup>2+</sup>			
Mins	303 K	313 K	323 K	333 K
10	13.3	15.5	16.6	28.8
20	19.9	23.3	25.9	30.4
30	23.3	35.5	39.9	40.1
40	28.8	39.9	44.9	46.6
50	34.4	44.9	46.6	48.9
60	39.9	49.9	51.3	52.2
70	43.3	50.2	52.2	53.3
80	47.7	51.1	52.2	
90	49.9			

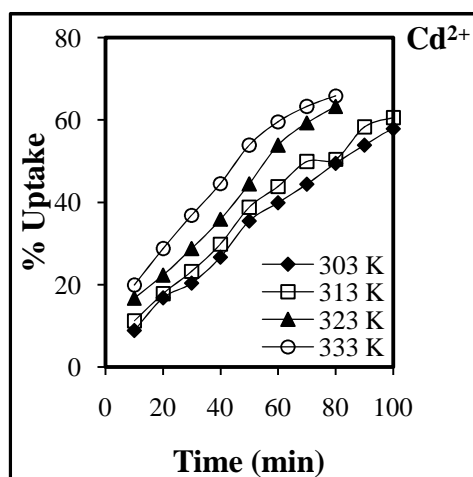


**Figure 2.31 % Uptake of Cd<sup>2+</sup>**

**Reaction conditions:** Amount of TiATMP, 0.1 g; metal ion concentration, 0.001M; total volume of metal ion, 10 mL; pH, 3;

**Table 2.26 % Uptake of Hg<sup>2+</sup> using TiATMP**

Time	% Uptake of Hg <sup>2+</sup>			
Mins	303 K	313 K	323 K	333 K
10	3.9	4.5	5.5	10
20	9.9	11.9	15.5	18.7
30	14.4	18.8	23.3	28.8
40	19.9	25.5	28.5	30.9
50	27.8	29.9	32.3	33.1
60	29.8	31.1		
70	30.0			

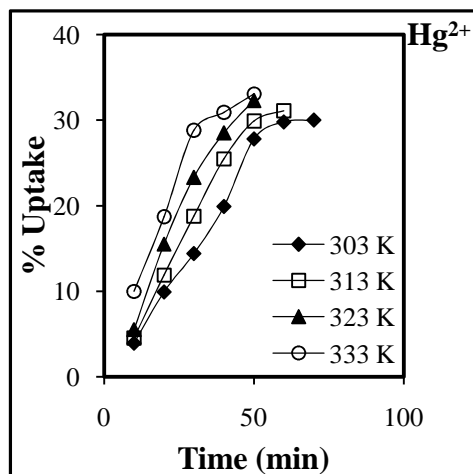


**Figure 2.32 % Uptake of Hg<sup>2+</sup>**

**Reaction conditions:** Amount of TiATMP, 0.1 g; metal ion concentration, 0.001M; total volume of metal ion, 10 mL; pH, 3;

**Table 2.27 % Uptake of  $Pb^{2+}$  using TiATMP**

Time Mins	% Uptake of $Pb^{2+}$			
	303 K	313 K	323 K	333 K
10	8.9	11.2	16.7	19.9
20	16.8	17.8	22.3	28.8
30	20.4	23.3	28.8	36.9
40	26.7	29.9	35.9	44.6
50	35.5	38.8	44.5	53.9
60	39.9	43.9	53.9	59.6
70	44.4	49.9	59.3	63.3
80	49.5	50.5	63.3	65.9
90	53.9	58.3		
100	57.9	60.6		
110	59.6			

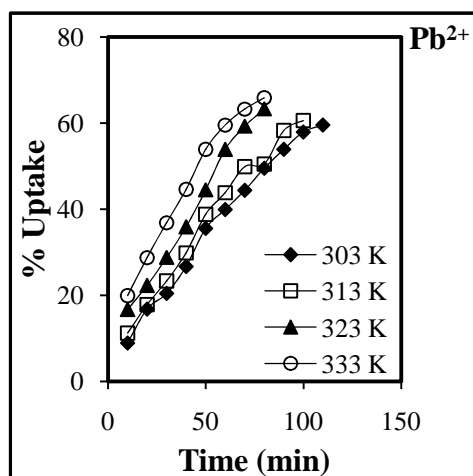


**Figure 2.33 % Uptake of  $Pb^{2+}$**

**Reaction conditions:** Amount of TiATMP, 0.1 g; metal ion concentration, 0.001M; total volume of metal ion, 10 mL; pH, 4;

**Table 2.28 Langmuir and Freundlich constants evaluated for transition and heavy metal ions using TiATMP**

Metal Ion	Temperature (K)	Langmuir Constants				Freundlich Constants		
		$R^2$	$b$ ( $\text{dm}^3 \cdot \text{mg}^{-1}$ )	$V_m$ ( $\text{mg} \cdot \text{g}^{-1}$ )	$R_L$ values	$R^2$	$K$	$1/n$
Co <sup>2+</sup>	303	0.994	0.0076	12.95	0.992	0.990	4.520	0.655
	313	0.980	0.0061	15.36	0.999	0.994	3.799	0.579
	323	0.960	0.0052	20.08	0.992	0.979	3.751	0.574
	333	0.998	0.0062	21.09	0.999	0.993	3.415	0.533
Ni <sup>2+</sup>	303	0.997	0.0018	15.77	0.999	0.992	2.512	0.689
	313	0.992	0.0034	17.57	0.992	0.996	4.501	0.568
	323	0.994	0.0045	18.11	0.991	0.999	1.148	0.824
	333	0.992	0.0098	18.31	0.991	0.991	9.232	0.395
Cu <sup>2+</sup>	303	0.993	0.0024	21.05	0.993	0.997	5.204	0.716
	313	0.987	0.0024	29.23	0.992	0.996	5.984	0.777
	323	0.992	0.0036	38.02	0.992	0.988	5.000	0.699
	333	0.997	0.0020	68.51	0.999	0.992	4.742	0.676
Zn <sup>2+</sup>	303	0.987	0.0026	16.75	0.999	0.992	3.157	0.791
	313	0.996	0.0047	19.45	0.999	0.935	2.891	0.895
	323	0.991	0.0073	20.00	0.999	0.932	2.841	0.926
	333	0.990	0.0081	39.57	0.991	0.982	4.137	0.616
Cd <sup>2+</sup>	303	0.992	0.0020	22.07	0.993	0.948	3.061	0.485
	313	0.959	0.0016	41.66	0.991	0.989	2.903	0.462
	323	0.972	0.0017	47.61	0.996	0.916	2.646	0.422
	333	0.992	0.0021	50.00	0.992	0.891	2.655	0.424
Hg <sup>2+</sup>	303	0.941	0.0039	23.25	0.997	0.961	3.784	0.578
	313	0.972	0.0052	22.72	0.996	0.973	3.380	0.529
	323	0.905	0.0036	35.71	0.992	0.976	4.246	0.628
	333	0.990	0.0041	43.47	0.991	0.998	6.368	0.804
Pb <sup>2+</sup>	303	0.994	0.0104	46.51	0.993	0.995	2.486	0.231
	313	0.995	0.0121	56.81	0.991	0.962	3.091	0.232
	323	0.993	0.0628	57.14	0.993	0.938	3.823	0.184
	333	0.992	0.1485	60.24	0.999	0.991	4.196	0.175

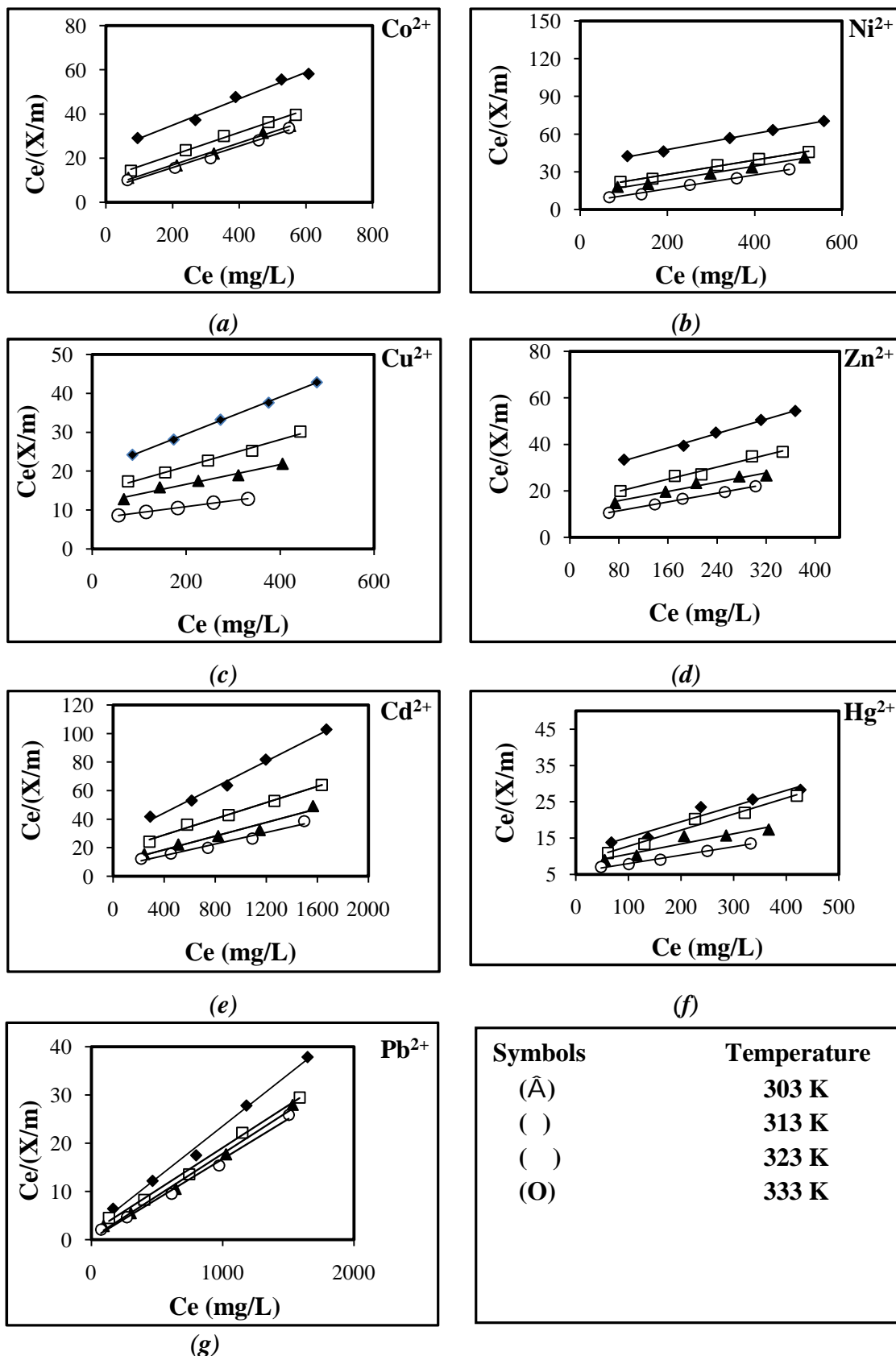


Figure 2.34 (a-g) Langmuir plots for transition metal ions (a)  $Co^{2+}$ ; (b)  $Ni^{2+}$ ; (c)  $Cu^{2+}$ ; (d)  $Zn^{2+}$  and heavy metal ions (e)  $Cd^{2+}$ ; (f)  $Hg^{2+}$ ; (g)  $Pb^{2+}$  using TiATMP

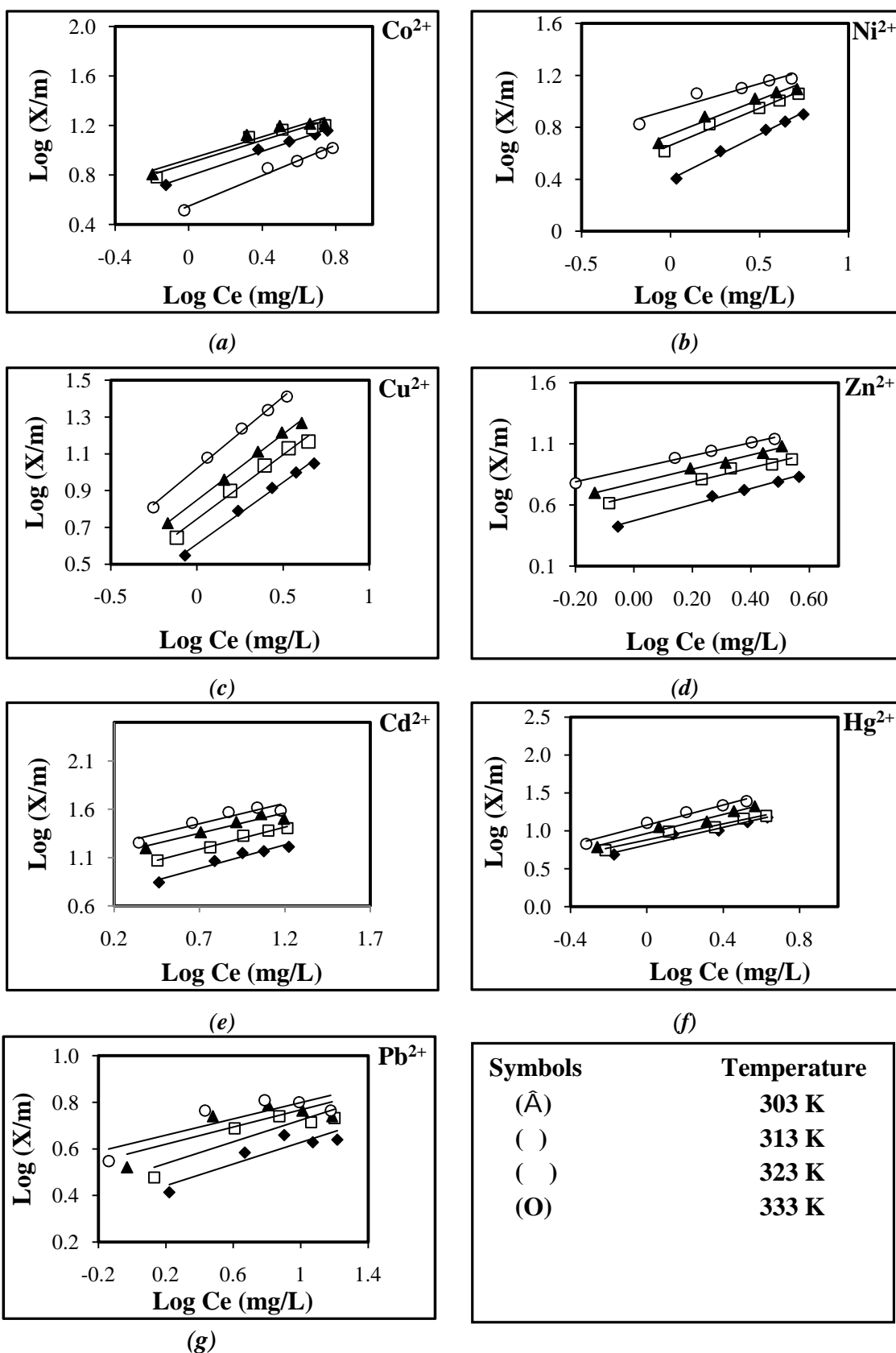


Figure 2.35 (a-g) Freundlich plots for transition metal ions (a)  $\text{Co}^{2+}$ ; (b)  $\text{Ni}^{2+}$ ; (c)  $\text{Cu}^{2+}$ ; (d)  $\text{Zn}^{2+}$  and heavy metal ions (e)  $\text{Cd}^{2+}$ ; (f)  $\text{Hg}^{2+}$ ; (g)  $\text{Pb}^{2+}$  metal ions using TiATMP

## **2.11 CONCEPTS IN ION EXCHANGE AND METAL SEPARATIONS**

Ion exchange is a physico-chemical process. Chemical variables include  $pH$ , nature of ions being separated, concentration of ions in solution, tendency of ions to hydrate, chemical composition of ion exchanger etc. The exchange capacity of a cation exchanger generally increases with increase in  $pH$  of the solution, while that of an anion exchanger decreases. Sorption ability of ions increases with increase in charges, atomic masses, ionic radii and ionic potential. Physical variables include rate of flow of solution in column, size of exchanger particles, the height of column, temperature of the solution, amount of ion exchanger etc.

Ion exchangers can be used, in both, batch and column operations. Since a column operation effects several equilibrations as the solution passes through the column, many difficult separations can be achieved relatively easily. The applications of an ion exchange column, offers some advantages such as: (a) simple working technique (b) elements concentrated on an ion exchanger can be eluted as whole or in separated groups or even as individual elements, using a suitable gradient elution procedure.

Practically, all ion-exchange reactions are reversible. At equilibrium, the favoured direction of an exchange reaction is determined by the relative affinity of the ion exchanger for the ions entering into the exchanger matrix. Better separation takes place if there is equilibrium between the ions in the solution and on the ion exchanger. An increase in the surface area of the ion exchanger also improves the attainment of an equilibrium and separation. A rise in temperature alters the equilibrium constant of the exchange which improves the separation in some cases.

### ***Factors Affecting Selectivity***

**Selectivity coefficient ( $K_c$ ):** Selectivity coefficient can also be used for describing ion exchange equilibria. The selectivity coefficient is defined as the ratio of the concentrations of the two ions, in the exchanger phase and solution phase, at equilibrium. It is thus a direct measure of the preference of the exchanger for one ion relative to the other. The exchange reaction between monovalent ions is represented as,

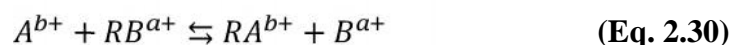


At equilibrium, selectivity coefficient is given by the expression,

$$K_c = \frac{[RA^+][B^+]}{[RB^+][A^+]} \quad (\text{Eq. 2.29})$$

where  $R$  is exchanger matrix and  $A$  and  $B$  are exchanging ions. In this respect, selectivity coefficient is quite different from separation factor when the valencies of the competing counter ions are not equal. Selectivity coefficient ( $K_c$ ) can be evaluated from experimental data for strongly acidic or strongly basic exchanger. The number of equivalent exchangeable ions in the exchanger is equal to total exchange capacity. If,  $K_c > 1.0$ , 'A' has more affinity for exchanger,  $K_c < 1.0$  indicates ion 'B' is held strongly by exchanger and needs strong external solution as an eluant to accomplish exchange reaction while  $K_c = 1.0$  indicates no preferential selectivity for both ions.

The exchange reaction between two ions of different valency as 'a' and 'b' is represented as,



At equilibrium, selectivity coefficient is given by the expression,

$$K_c = \frac{[RA^+]^b[B^+]^a}{[RB^+]^a[A^+]^b} \quad (\text{Eq. 2.31})$$

Selectivity coefficient contains the ionic valencies as exponents. In such cases, the selectivity coefficient remains more or less constant, when the experimental conditions, particularly the total solution concentration are varied. Selectivity coefficient depends upon the nature of the ion, the nature of the exchanger, external factors such as temperature, and the degree of saturation of the ion exchange material.

**Distribution coefficient ( $K_d$ ):** Distribution coefficient ( $K_d$ ) is a measure of fractional uptake of metal ions in solution, competing for  $H^+$  ions, in case of a cation exchange material. It can be determined by batch experiments, in which a small known quantity of the ion exchange material is shaken with a solution containing a known concentration of the solute (metal ion), followed by analysis of the two phases, after equilibrium has been attained.

The presence of other electrolytes in metal ion solution, strongly affects the  $K_d$  value of the metal ion.  $K_d$  values change, depending on the ionic strength and  $pH$  of the electrolyte. The degree of ionization of the ionogenic groups of the exchanger, depends on the acid or base strength of the groups, i.e. on their  $pK$  values and on the  $pH$ . When the  $pH$  drops below the  $pK$  value of the groups, the acid groups become predominantly nonionic, the apparent capacity and hence the  $K_d$  values thus fall off. Based on such a study, a proper electrolyte can be selected for the elution of a particular metal ion from the exchanger column.

**Breakthrough capacity (BTC):** The selectivity of an ion exchanger for a particular metal ion can also be assessed by break through capacity (BTC). BTC is expressed in millimoles, milligrams, micrograms, or other appropriate units related to 0.1 g of dry resin or 1 mL of swollen resin. For BTC determination, ion exchanger is taken in a column and fractions of metal ion solution passed through the column and effluent collected, till the amount of metal ion concentration is same in feed and effluent. The break through capacity depends on, flow rate of feed solution through the column, bed depth, selectivity coefficient, particle size and temperature. BTC is the dynamic capacity or operating capacity of a known amount of ion exchange material towards metal ion in column operation/ operating condition.  $K_d$  values also give an idea of affinity of metal ion towards ion exchanger. It is therefore expected that the selectivity order based on  $K_d$  values and BTC should be same. However, in practice, the selectivity order based on  $K_d$  values and BTC may not be matching due to the fact that  $K_d$  values are determined by batch process while BTC is determined by column process.

**Separation factor ( $\alpha$ ):** The preference of an ion exchanger for one of the two counter ions is also expressed by the separation factor. It is used as a measure of the chromatographic separation possible on an ion exchange column.  $K_d$  is an important factor for determining the analytical potential of an ion exchanger. Separation factor  $\alpha$  is the rate at which any two constituents separate on a column and is defined as the ratio of the two corresponding distribution coefficients  $K_{d1}$  and  $K_{d2}$ . The separation factor  $\alpha$  is given by the equation,

$$\alpha = K_{d1}/K_{d2} \quad \text{(Eq. 2.32)}$$

where,  $K_{d1}$  and  $K_{d2}$  are the distribution coefficients of the two constituents in a given medium. The greater the deviation of  $\alpha$  from unity, better is the separation.

### **Conclusions on factors affecting selectivity**

Selectivity/affinity of a particular metal ion towards an ion exchanger depends on (a) the ion exchanger: the factors responsible being particle size, the presence of functional groups that indicate the nature of the exchanger weak or strong, the ion exchange capacity, the degree of cross linking, and the structural complexity of the ion exchanger (b) the exchange media: the factors responsible being concentration, pH, and the nature of the electrolyte, weak or strong, as well as the temperature, and (c) the exchanging metal ion: the factors responsible being ionic radius and the ionic

charge on the metal ion, with higher valent ions having more affinity for the exchanger [95]. Over and above these three factors the exchange process itself, i.e., the rate of exchange and equilibrium also play an important role in determining the selectivity.

On immersing the exchanger in solution, equilibrium is established between the exchanger and the electrolyte solution, the rate of exchange depending on the size of the exchanging ion and the grain/particle size of the exchanger. Smaller the size of the cation, greater is its tendency to be hydrated and greater is the hydrated ionic radii. Larger ions being less hydrated, less energy is utilized for dehydration of the metal ions to occupy a site on the exchanger, which plays a prominent role in determining the selectivity of metal ions [96]. The overall effect is a result of the contribution of the above mentioned factors. Depending on the predominant factor, the affinity of metal ions towards the ion exchanger varies in each case.

***Other General Guidelines:***

- At low concentrations (aqueous) and ordinary temperatures, the extent of exchange increases with increasing valency of the exchanging ion: ( $\text{Na}^+ < \text{Ca}^{2+} < \text{Al}^{3+} < \text{Th}^{4+}$ ).
- At low concentrations (aqueous) ordinary temperatures and constant valence, the extent of exchange increases with increasing atomic number of the exchanging ion ( $\text{Li}^+ < \text{Na}^+ < \text{K}^+ < \text{Rb}^+ < \text{Cs}^+$ ;  $\text{Mg}^{2+} < \text{Ca}^{2+} < \text{Sr}^{2+} < \text{Ba}^{2+}$ ).
- At high concentrations, the difference in the exchange “potentials” of ions of different valence ( $\text{Na}^+$  versus  $\text{Ca}^{2+}$ ) diminish and, in some cases, the ion of lower valence has the higher exchange “potential”.
- The relative exchange “potentials” of various ions may be approximated from their activity coefficients - the lesser the activity coefficient, the greater the exchange “potential”.
- The exchange “potential” of the hydrogen ion ( $\text{H}_3\text{O}^+$  vs.  $\text{OH}^-$ ) vary considerably with the nature of the functional group, and depends on the strength of the acid or base formed between the functional group and either the hydroxyl or hydrogen ion. The stronger the acid or base, the lower the exchange potential.
- As a rule, the  $K_d$  values increase with increasing charge on the ion. There are however two contradictory factors, (a) an increase in charge increases the

attraction for the cation ( $K_d$  high), (b) an increase in charge also increases hydrated ionic radii ( $K_d$  low).

### ***Factors Affecting Separations***

An efficient ion exchange separation may be influenced by load of metal ion, electrolyte used for elution, flow rate of eluant, diffusion of metal ions in mobile and stationary phases,  $pH$ , nature of ion exchange material and the particle size and length of the column. Other factors responsible are distribution coefficient ( $K_d$ ), Breakthrough capacity (BTC), Separation factor ( $r$ ), Selectivity coefficient ( $K_c$ ), retardation factor ( $R$ ), retention volume ( $V_r$ ), column capacity and temperature.

Proper use of solution for sorption/elution, enhances the scope of an ion exchange separation which may be enhanced by using for fixation or for elution, a solution capable of complexing the ions exchanged. The formation of complexes may assist separations by diminishing the concentrations of free ions and also by producing complexes of different stabilities, thus leading to significantly different behaviour with selected eluants. As explained earlier, the presence of other electrolytes such as inorganic acids and certain salt solutions, strongly affects the  $K_d$  values of the metal ions. Thus, all investigations for the development of metal ion separations are based on  $K_d$  values, determined both in aqueous and various electrolyte media.

The efficiency of an ion exchange separation depends on the condition under which  $r$  has a useful value, or influencing in a direction favourable to separation. Since,  $r$  is the ratio of the  $K_d$  values of the constituent counter ions, the  $K_d$  values are determined under the expected solution conditions on the selected ion exchange material.

In many cases, the efficient separation of a mixture requires that the eluant concentration be changed during the course of elution, which may be done in a stepwise manner or by continuous change in the concentration, as in gradient elution.

To understand the behaviour of solute (such as metal ions in solutions), the following terminologies should be understood.

### ***Partition/Distribution coefficient ( $K_d$ ):***

$$K_d = C_S/C_M \quad \text{(Eq. 2.33)}$$

where,  $C_S$  and  $C_M$  are concentrations of solute in stationary and mobile phases, respectively.

**Retardation factor (R):** is the ratio of the displacement velocity of solute to velocity of solvent (electrolyte in present case).  $R$  represents fraction of time spent by species in mobile phase i. e.

$$R = t_M / (t_M + t_S) \quad \text{(Eq. 2.34)}$$

where,  $t_M$  and  $t_S$  represent retention time of solute in stationary and mobile phases respectively.

**Retention Volume ( $V_r$ ):** At appearance of peak, half of the solute is eluted in retention volume, while other half remains on the column in mobile phase, plus volume of stationary phase.

This indicates the time period for which solute/metal ion resides in mobile phase/electrolyte, which is expressed as,

$$V_r = L F (V_M + K_d V_S / v V_M) \quad \text{(Eq. 2.35)}$$

where,  $L$  = length of column,  $F$  = flow rate,  $v$  = linear flow rate or average velocity, and  $V_M$  and  $V_S$  are volume of mobile and stationary phase respectively.

**Column capacity:** Column capacity is related to retention volume. It is given by,

$$k = (V_r - V_M) / V_M \quad \text{(Eq. 2.36)}$$

where,  $V_r$  = retention volume and  $V_M$  = volume of mobile phase.

**Temperature:** Since temperature influences  $K_d$ , resolution is also affected by temperature.

**Elution behaviour:** When solution containing metal ions is passed through a column containing exchanger, based on differential affinity, the various species get strongly or weakly bound on the exchanger. During the elution process, pure electrolyte is eluted first, followed by weakly bound species and finally the strongly bound species. A plot of concentration of metal ion in stationary phase vs. mobile phase provides partition isotherm. Generally, three types of curves are observed (**Figure 2.36**).

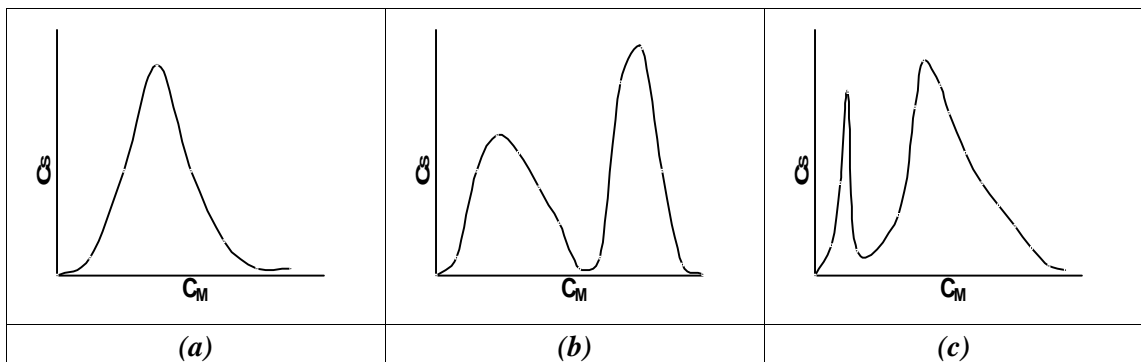


**Figure 2.36** Types of elution curve (a) linear isotherm (b) classical isotherm and (c) anti classical isotherm

**Linear isotherm:** is symmetric bell shaped Gaussian curve where  $C_S = C_M$ .

**Classical isotherm:** also referred to as Langmuir curve, is observed in adsorption chromatography.

**Anti classical isotherm:** is referred to as non Langmuir curve. Here, micro peak is followed by broad peak. Such curves are observed in cases where the solute has low solubility in stationary phase.

As seen from **Figure 2.36**, linear isotherm (**Figure 2.36a**) is considered to be best for chromatographic separation. In practice, for single ion elution, symmetrical bell shaped curves are observed. In binary and ternary separations, separation efficiency is indicated by (a) percentage recovery and (b) peak shapes/elution curves of the constituent metal ions, in terms of Langmurian/non-Langmurian which indicates how well one metal ion is separated in presence of another metal ion. However, in binary metal separations in columns, generally '**Figure 2.36b**' or '**Figure 2.36c**' type curves are obtained. Further tailing effects are attributed to (a) high  $K_d$  values (due to which the metal ion is retained for long time on stationary phase) and (b) irregular flow/flow rate.

**Zone spreading:** Another factor that affects peak shape is due to a phenomenon called "zone spreading" that occurs due to differential migration of solute in mobile phase. Separation efficiency depends on differential migration of metal ion in mobile/stationary phase. Deviations are observed referred to as "zone spreading", caused by diffusion of metal ion in stationary phase (eddy diffusion), concentration gradient in stationary/mobile phase (longitudinal diffusion) and mass transfer of metal ion in stationary phase (exchanger) and mobile phase (electrolyte).

**Eddy diffusion:** There are a multitude of pathways by which an ion finds its way through a packed column, which is directly proportional to the diameter of the particles making up the column.

**Longitudinal diffusion:** this is due to, concentration gradient of solutes, ahead and behind the zone center. Longitudinal diffusion is directly proportional to mobile phase diffusion coefficient and inversely proportional to mobile phase velocity.

**Mass transfer:** occurs in stationary as well as mobile phase. Time is required for solute molecules to diffuse from the interior of exchanger phases to the interface, where transfer occurs. This time lag results in the persistence of non equilibrium conditions. A column is always operated at non equilibrium condition. Thus metal ion

is swept ahead before they have time to equilibrate with the stationary phase. This unequal distribution in stationary and mobile phases also leads to zone spreading. Typical elution curves indicating separation efficiency is presented in **Figure 2.37**.

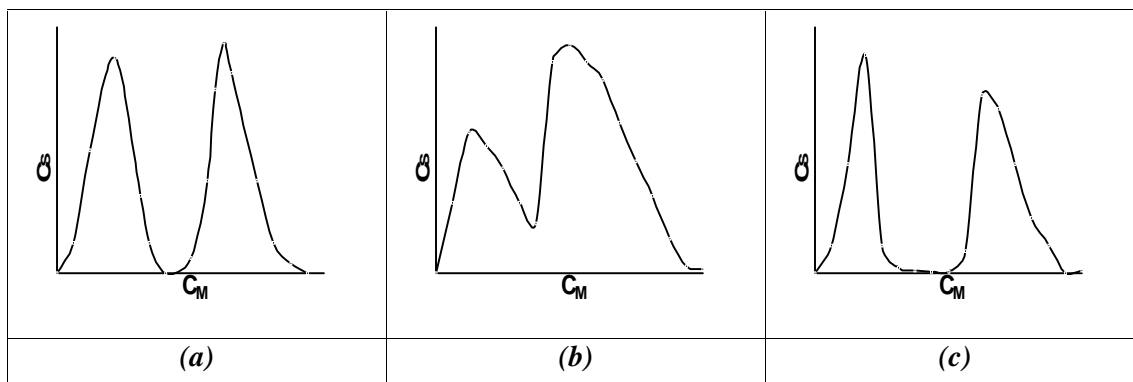


**Figure 2.37** Types of elution curve with (a) controlled flow (b) tailing/not good flow and (c) ideal time break.

A controlled flow rate gives good separation of peaks, however irregular flow rate results in tailing effect. Peak shapes with ideal time break between two peaks indicate efficient separation.

### ***Elution techniques***

Generally three types of elution techniques are practiced.

***Frontal:*** passing electrolyte containing metal ion continuously through a column. In this case, electrolytes are eluted first, followed by weakly bound/exchanged species and then strongly exchanged species.

***Elution:*** This is the most popular technique, wherein separation is effected due to differential migration of solute in mobile phase and the electrolyte, exhibits behaviour of symmetrical bell shaped curve in ideal case. Here, the eluant which may be a pure electrolyte is passed through the column, which in turn, leads to the differential migration of metal ion in mobile phase. If the flow rate is fixed, separation depends on  $K_d$ .

***Displacement:*** In this technique, separation is achieved by running a more strongly exchanged displacement agent into the column. The main advantage of this technique is that heavy loading of the column is possible. Gradient elution is the variation of eluting condition during the course of separation.

In the present study, with an aim to explore the utility of ZrATMP and TiATMP in separation of metal ions following studies were under taken,

- ✓ Distribution coefficient ( $K_d$ ) has been determined at optimized conditions (optimum pH, optimum metal ion concentration and optimum equilibrium time) in aqueous as well as various electrolyte media/concentration ( $\text{HNO}_3$ ,  $\text{NH}_4\text{NO}_3$ ,  $\text{HClO}_4$  and  $\text{CH}_3\text{COOH}$  of 0.2 M and 0.02 M).
- ✓ Breakthrough curves have been plotted, breakthrough capacity (BTC) determined and compared with  $K_d$  values to confirm the selectivity order of metal ions.
- ✓ Elution behaviour of metal ions has been studied using acids and electrolytes ( $\text{HNO}_3$ ,  $\text{NH}_4\text{NO}_3$ ,  $\text{HClO}_4$  and  $\text{CH}_3\text{COOH}$  of 0.2 M and 0.02 M). Based on the separation factor ( ) a few binary and ternary metal ion separations have been performed.
- ✓ The performance ability of ZrATMP and TiATMP has also been assessed by regenerating and reusing the exchangers.

## 2.12 EXPERIMENTAL

**Materials:** Chloride and nitrate salts of transition metal ions ( $\text{Co}^{2+}$ ,  $\text{Ni}^{2+}$ ,  $\text{Cu}^{2+}$ ,  $\text{Zn}^{2+}$ ) and heavy metal ions ( $\text{Cd}^{2+}$ ,  $\text{Hg}^{2+}$ ,  $\text{Pb}^{2+}$ ) of AR grade were obtained from E Merck, India. Disodium salt of ethylene diamine tetra acetic acid (EDTA) was procured from Fluka. Perchloric acid, acetic acid, ammonium nitrate, nitric acid, indicators and reagents used were of AR grade. DIW was used for all the studies. ZrATMP and TiATMP have been synthesized and characterized, as discussed earlier in text, **Section 2.6** and **2.7**. For distribution, elution and separation studies the exchanger (ZrATMP and TiATMP) particles of definite mesh size [30 - 60 mesh (ASTM)] in  $\text{H}^+$  form was used.

**Distribution Studies:** Effect of metal ion concentration on distribution coefficient ( $K_d$ ) for  $\text{Co}^{2+}$ ,  $\text{Ni}^{2+}$ ,  $\text{Cu}^{2+}$ ,  $\text{Zn}^{2+}$  (transition metals) and  $\text{Cd}^{2+}$ ,  $\text{Hg}^{2+}$ ,  $\text{Pb}^{2+}$  (heavy metals) has been determined in aqueous medium by batch method [57]. 0.1 g of ZrATMP/TiATMP in the  $\text{H}^+$  form was equilibrated with 20 mL of varying metal ion concentration (0.002-0.02 M with interval of 0.002M) for 6 h (optimum equilibrium time) at room temperature. The metal ion concentration before and after exchange was determined by EDTA titration.

$K_d$  has also been evaluated at optimum condition, (optimum metal ion concentration, pH of maximum adsorption and maximum equilibrium time) using 0.1 g of the exchanger in aqueous as well as various electrolyte media  $\text{NH}_4\text{NO}_3$ ,  $\text{HNO}_3$ ,  $\text{HClO}_4$  and  $\text{CH}_3\text{COOH}$  of 0.02 and 0.2 M concentration at room temperature.  $K_d$  was evaluated using the expression,  $K_d = [(I-F)/F] \times V/W$  ( $\text{mL}\cdot\text{g}^{-1}$ ) where,  $I$  = total amount of the metal ion in the solution initially;  $F$  = total amount of metal ions left in the solution after equilibrium;  $V$  = volume of the metal ion solution;  $W$  = weight of the exchanger in g.

**Column Preparation:** For determination of BTC, elution studies and separation studies, the column was prepared as follows. A dry glass column [30 cm (length)  $\times$  1 cm (internal diameter)] was filled with glass-wool at bottom (height = ~1 cm) and washed thoroughly with DIW. 0.5 g of the ion exchanger ZrATMP/TiATMP, was now introduced into the column (bed height = 1.3 cm), and packed with glass-wool (height = ~1 cm) at the top and washed thoroughly with DIW to remove air bubbles from the column and flow rate adjusted to  $0.5 \text{ mL}\cdot\text{min}^{-1}$  for all studies.

**Breakthrough Capacity (BTC):** For determination of BTC, 0.5 g of the ion exchanger, ZrATMP/TiATMP, was taken in a glass column (as prepared above), washed thoroughly with DIW and flow rate adjusted to  $0.5 \text{ mL}\cdot\text{min}^{-1}$ . 5 mL fractions of each individual metal ion  $\text{Co}^{2+}$ ,  $\text{Ni}^{2+}$ ,  $\text{Cu}^{2+}$ ,  $\text{Zn}^{2+}$ , (transition metal ions) and  $\text{Pb}^{2+}$ ,  $\text{Cd}^{2+}$ ,  $\text{Hg}^{2+}$  (heavy metal ions) of 0.002M concentration was passed through the column and effluent collected, till the amount of metal ion concentration was same in feed and effluent. A breakthrough curve was obtained by plotting the ratio  $C_e/C_0$  against the effluent volume, where  $C_0$  and  $C_e$  are the concentrations of the initial solution and effluent, respectively. BTC is calculated using formula,  $(C_0 V_{(10\%)})/W$ , ( $\text{mmol}\cdot\text{g}^{-1}$ ) where,  $C_0$  is initial concentration of metal ion in  $\text{mol}\cdot\text{L}^{-1}$ ,  $V_{(10\%)}$  is the volume of metal ion solution passed through column when exit concentration reaches 10 % of the initial concentration in mL and  $W$  is the weight of the exchanger in mg.

**Adsorption and Elution Studies:** For all metal ions under study (0.001 M, 10 mL) of each metal ion, was loaded onto the column. Each metal ion loaded was eluted with reagents like  $\text{HNO}_3$ ,  $\text{HClO}_4$ ,  $\text{CH}_3\text{COOH}$  and  $\text{NH}_4\text{NO}_3$  of 0.02 M and 0.2 M concentration. The amount of metal ion eluted (% E) was calculated using the expression,

$$\% \text{ Metal eluted ( \% E) } = \frac{\text{Concentration of metal ion eluted (Ce)}}{\text{Concentration of metal ion loaded (Co)}} \times 100 \quad (\text{Eq. 2.37})$$

**Binary and Ternary Separation Studies:** For binary or ternary separations, the mixture of the metal ions (0.001 M, 10 mL of each metal ion) to be separated was loaded onto the column. Metal separations were achieved by passing suitable eluants through the column. For a given metal ion pair, the eluant was selected based on  $K_d$  values of respective metal ions (in a particular medium) in which separation factor was highest. Metal ion concentration was determined quantitatively by EDTA titration. For every experimental point in graphs, two identical sets are prepared to compare/verify the obtained values. Reproducibility in values for same experimental point was assessed by again preparing two identical sets. The amount of each metal ion eluted (% E) was calculated using (Eq. 2.37) above.

**Regeneration and Reusability Studies:** Regeneration and reuse of ion exchanger ZrATMP/TiATMP was performed in the case of Copper ion by batch method. 10 mL of  $\text{Cu}^{2+}$  solution (0.004M for ZrATMP and 0.014M for TiATMP, optimum concentration) was treated with 0.1 g of ZrATMP/TiATMP and kept for 6 h (maximum equilibrium time) after which metal ion concentration was determined by EDTA titration and  $K_d$  value determined. The  $\text{Cu}^{2+}$  exchanged ZrATMP/TiATMP was treated with  $\text{HNO}_3$  (1 M, 50 mL) for 30 min with occasional shaking. The sample ZrATMP/TiATMP was separated from acid by decantation and treated with DIW to remove adhering acid. This process was repeated at least five times to ensure complete removal of  $\text{Cu}^{2+}$  from exchanger. This regenerated ZrATMP/TiATMP was used to determine  $K_d$  values. The process was repeated till wide variation in  $K_d$  values was observed. % retention in  $K_d$  values  $K_{d(R)}$  was determined using the expression,  $K_{d(R)} = K_{d(C)}/K_d \times 100$  where  $K_d$  = Initial value obtained,  $K_{d(C)}$  =  $K_d$  determined in each subsequent cycle.

## 2.13 RESULTS AND DISCUSSION

### *Metal Ion Separations Using ZrATMP*

The effect of metal ion concentration on distribution coefficient ( $K_d$ ) studied in aqueous medium (Table 2.29) shows that with increase in concentration,  $K_d$  values increase. Above a particular concentration  $K_d$  values are constant which could be explained to be due to the fact that at lower concentrations, almost all the ions are

exchanged due to availability of exchangeable sites, which are not available at higher concentrations.

$K_d$  values were also evaluated in various electrolyte media ( $\text{HNO}_3$ ,  $\text{NH}_4\text{NO}_3$ ,  $\text{HClO}_4$  and  $\text{CH}_3\text{COOH}$  of 0.2 M and 0.02 M) at optimum conditions (optimum metal ion concentration, optimum pH and optimum equilibrium time) (**Table 2.30**). In general, it is observed that the  $K_d$  values are lower in high concentration of electrolyte and vice versa. In strong electrolyte media  $K_d$  values are lower as compared to weak electrolyte and aqueous media. This may be attributed to the high competition amongst ions for exchange in strong electrolyte media.  $K_d$  values in aqueous medium follows the order:  $\text{Cu}^{2+} > \text{Ni}^{2+} > \text{Zn}^{2+} > \text{Co}^{2+}$  amongst the transition metal ions and  $\text{Pb}^{2+} > \text{Cd}^{2+} > \text{Hg}^{2+}$  amongst the heavy metal ions. The most promising features of ZrATMP are, high  $K_d$  values observed in case of  $\text{Cu}^{2+}$ ,  $\text{Ni}^{2+}$  and  $\text{Pb}^{2+}$  in aqueous medium.

Breakthrough curves (a plot of  $C_e/C_0$  vs. effluent volume) for transition metal ions and heavy metal ions are presented in {**Figure 2.38(a-g)**}. Breakthrough capacity (BTC) is the dynamic capacity or operating capacity of a known amount of ion exchange material towards metal ion in column operation.  $K_d$  values also give an idea of affinity of metal ion towards ion exchanger, which is determined by a batch process. It is expected that the metal ion affinity towards the exchanger based on  $K_d$  and BTC should be same, which is observed (**Table 2.30**) in the present study.

The elution behaviour of transition metal ions and heavy metal ions (under study) have been carried out using different electrolytes such as  $\text{HNO}_3$ ,  $\text{HClO}_4$ ,  $\text{CH}_3\text{COOH}$ , and  $\text{NH}_4\text{NO}_3$  of 0.02 and 0.2M concentration and results presented in **Table 2.31**. The % metal eluted in all cases is in the range 79 to 99 %. Good elution is observed due to presence of single metal ion and non interference of elements. Higher concentration of eluent and acids in general, are better eluents. 0.2 M  $\text{HNO}_3$  is the best eluent for most metal ions. Using 0.2 M  $\text{HNO}_3$ , order of % metal eluted amongst transition metal ions is  $\text{Zn}^{2+}(99\%) > \text{Co}^{2+}(98\%) > \text{Ni}^{2+}(91\%) > \text{Cu}^{2+}(85\%)$  and amongst heavy metal ions is  $\text{Hg}^{2+}(96\%) > \text{Cd}^{2+}(93\%) > \text{Pb}^{2+}(87\%)$ . This observation is in keeping with the fact that metal ions with high  $K_d$  values are less eluted and vice-versa. All elution curves are symmetrical bell shaped {**Figure 2.39(a-g)**}, indicating elution efficiency.

Binary separations for following metal ion pairs (under study)  $\text{Ni}^{2+}$ -  $\text{Cu}^{2+}$  ,  $\text{Co}^{2+}$ -  $\text{Cu}^{2+}$ ,  $\text{Zn}^{2+}$ - $\text{Ni}^{2+}$ ,  $\text{Co}^{2+}$ -  $\text{Ni}^{2+}$ ,  $\text{Hg}^{2+}$ - $\text{Pb}^{2+}$ ,  $\text{Hg}^{2+}$ -  $\text{Cd}^{2+}$ ,  $\text{Cd}^{2+}$ -  $\text{Pb}^{2+}$  have been performed using concept of high separation factor in a particular medium as discussed earlier in the text. In binary separations, separation efficiency is in the range 75–93 % amongst transition metal ions and 74-91%, amongst heavy metal ions (**Table 2.32**). Efficient separation is also supported by symmetrical bell shaped curves **Figure 2.40(a-g)**. In all cases of binary separation, irrespective of metal ion pair, maximum % metal eluted is  $\text{Cu}^{2+}$  (75%),  $\text{Ni}^{2+}$  (85%),  $\text{Co}^{2+}$  (90%),  $\text{Zn}^{2+}$  (93%) (amongst transition metal ions) and  $\text{Pb}^{2+}$  (75%),  $\text{Cd}^{2+}$  (82%),  $\text{Hg}^{2+}$  (91%), (amongst heavy metal ions). This observation is in keeping with separation factor ( ) and  $K_d$  values of metal ions. % metal eluted decreases with decreasing separation factor and increases with increasing separation factor and as explained earlier, metal ions with high  $K_d$  values are less eluted and vice-versa.

In ternary separations for  $\text{Co}^{2+}$ -  $\text{Ni}^{2+}$ - $\text{Cu}^{2+}$ , (transition metal ions) and  $\text{Hg}^{2+}$  -  $\text{Cd}^{2+}$ -  $\text{Pb}^{2+}$ , (heavy metal ions) % metal eluted is in the range 59-73% and 62-75% respectively (**Table 2.33**). In all cases, three distinct peaks are observed (**Figure 2.41**) however, with tailing effects for every metal ion eluted. % metal eluted is also lower as compared to single and binary metal ion separations. Probably the separation process becomes complex, attributed to the loss of metal ions during the changeover of the eluent, interference of metal ions, pH, simultaneous elution of two or more metal ions with the same eluent, and lastly, experimental errors involved in the determination of metal ions in the presence of other ions, etc.

A study on regeneration and reuse was performed as described in experimental section. It is observed that the exchanger, once used, can be converted back to its original form by desorption of the metal ions with concentrated nitric acid. A plot of % retention in  $K_d$  values vs number of cycles is presented in **Figure 2.42**, which shows that % retention in  $K_d$  values is almost the same upto 4 cycles, indicating that ZrATMP could be regenerated and reused without much decline in performance.

**Table 2.29 Distribution coefficient ( $K_d$ ) values ( $\text{mL}\cdot\text{g}^{-1}$ ) evaluated varying metal ion concentration in aqueous medium using ZrATMP**

Metal ions	$K_d$ values at different concentration ( $\text{mol}\cdot\text{L}^{-1}$ ) of metal ions							
	0.002	0.004	0.006	0.008	0.01	0.012	0.014	0.016
$\text{Co}^{2+}$	690	751	825	901	992	1185	1250	1296
$\text{Ni}^{2+}$	1650	1789	1978	2090	2100	2501	2980	2980
$\text{Cu}^{2+}$	C.S	C.S	C.S	9844	9856	9840	9810	9848
$\text{Zn}^{2+}$	620	660	738	1209	1490	1734	1810	1815
$\text{Cd}^{2+}$	1037	1189	1290	1389	1589	1598	1601	1601
$\text{Hg}^{2+}$	59	70.3	85.3	95	101	120	125	125
$\text{Pb}^{2+}$	1290	1492	1830	2290	2488	2619	2672	2672

*C.S. = Complete sorption*

**Table 2.30 BTC ( $\text{mmol}\cdot\text{g}^{-1}$ ) and  $K_d$  ( $\text{mL}\cdot\text{g}^{-1}$ ) values evaluated in aqueous and various electrolyte media using ZrATMP**

Metal Ion	BTC	$K_d^*$ values in aqueous and various electrolyte media/concentration at optimum conditions								
		DIW	$\text{NH}_4\text{NO}_3$		$\text{HNO}_3$		$\text{HClO}_4$		$\text{CH}_3\text{COOH}$	
			0.02M	0.2 M	0.02M	0.2M	0.02M	0.2 M	0.02M	0.2M
$\text{Co}^{2+}$	0.24	1250	1120	340	704	172	960	129	1951	940
$\text{Ni}^{2+}$	0.40	2980	1710	649	880	53	730	92	4931	2750
$\text{Cu}^{2+}$	0.64	CS	5940	2920	3320	289	2130	209	3930	2928
$\text{Zn}^{2+}$	0.20	1810	8423	2750	3329	350	3720	369	3820	4201
$\text{Cd}^{2+}$	0.28	1601	2620	1780	8290	1620	1250	1300	2230	690
$\text{Hg}^{2+}$	0.09	125	780	129	140	430	470	640	301	139
$\text{Pb}^{2+}$	0.37	3612	2301	1090	2500	2198	2710	1620	4600	3601

$K_d^*$  Values obtained at optimum condition (Optimum metal ion concentration, Optimum pH of solution and maximum equilibrium time); DIW = Deionized water,

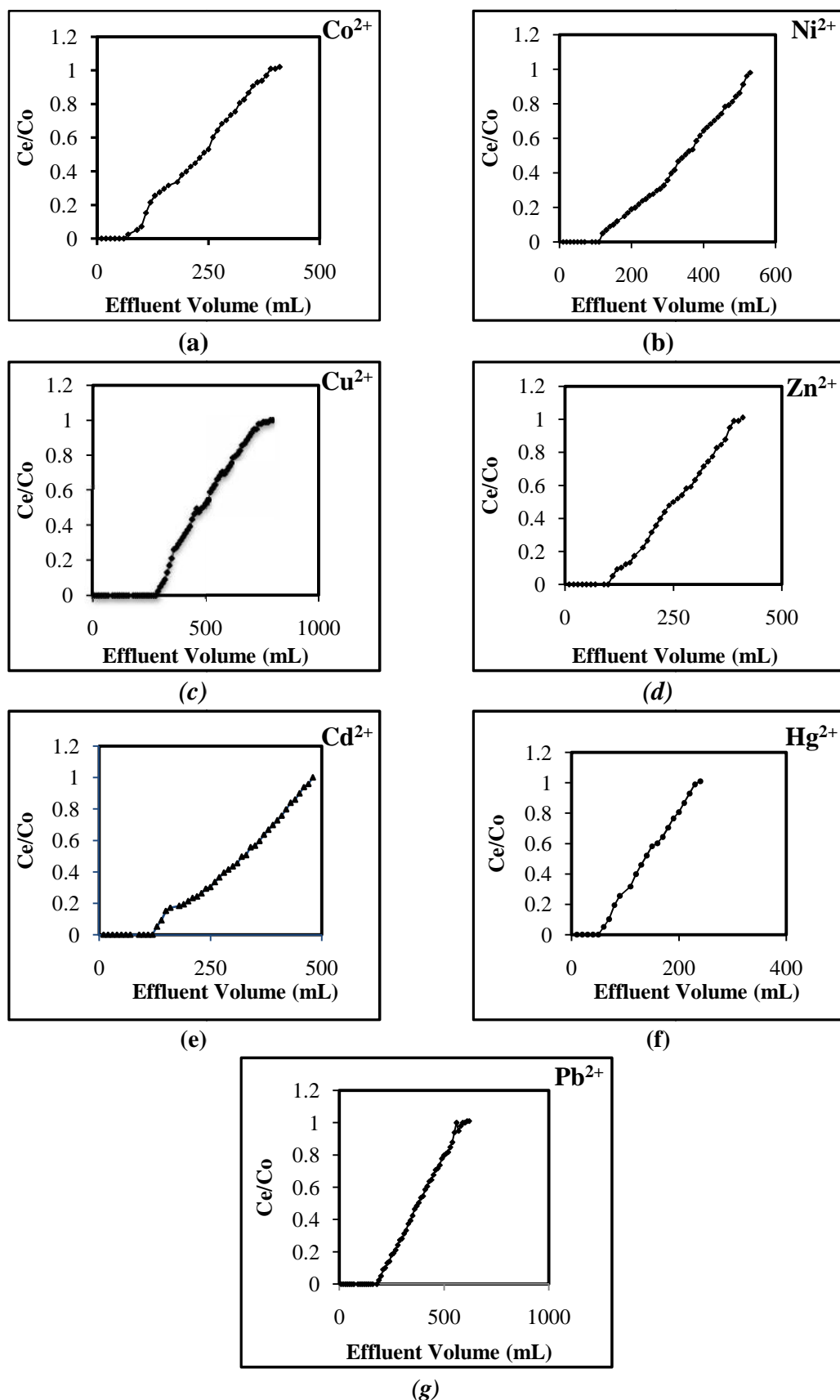


Figure 2.38 (a-g) Breakthrough curves for transition metal ions (a)  $\text{Co}^{2+}$ ; (b)  $\text{Ni}^{2+}$ ; (c)  $\text{Cu}^{2+}$ ; (d)  $\text{Zn}^{2+}$ ; and heavy metal ions (e)  $\text{Cd}^{2+}$ ; (f)  $\text{Hg}^{2+}$ ; (g)  $\text{Pb}^{2+}$  using ZrATMP

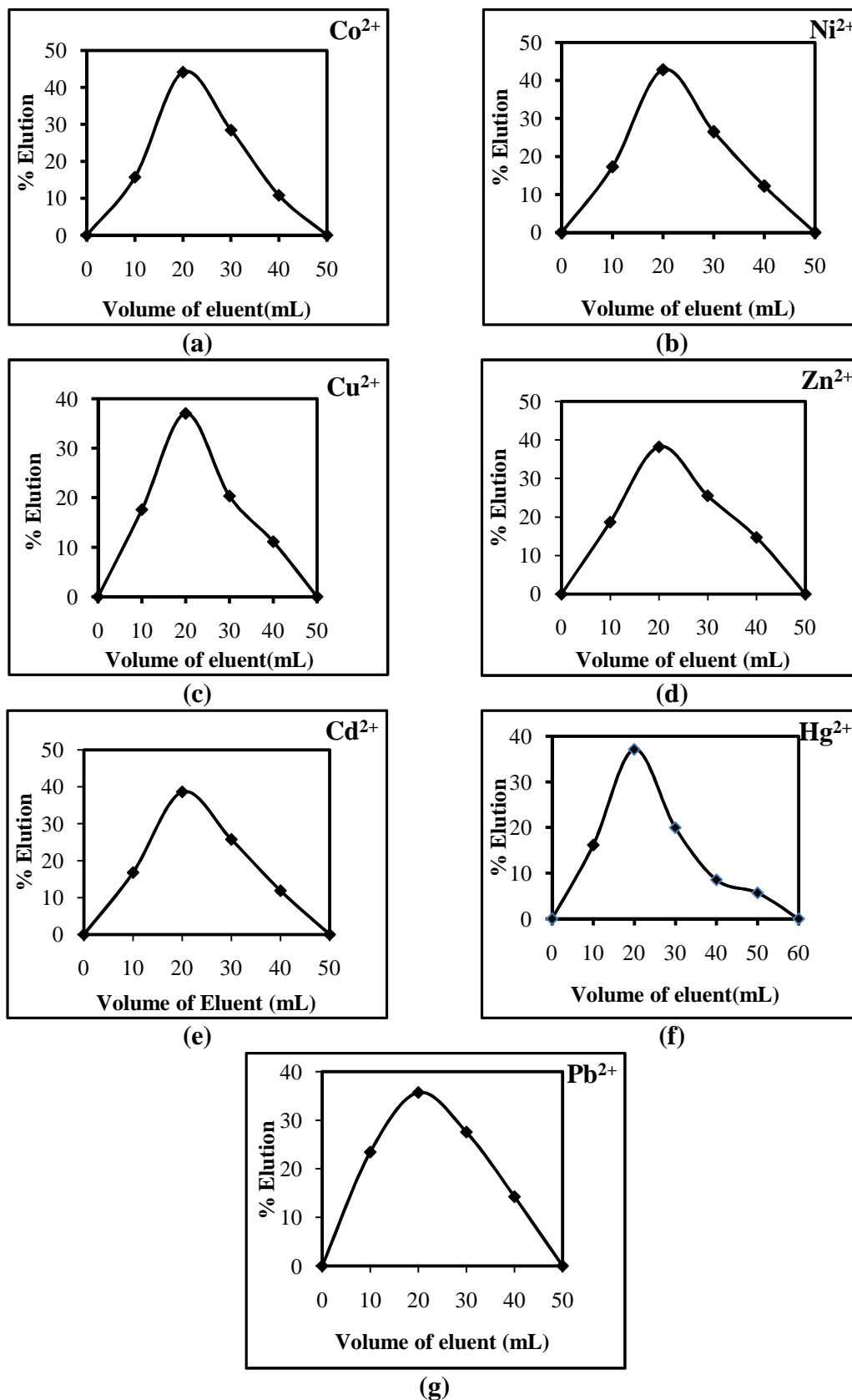


Figure 2.39(a-g) Elution behaviour of transition and heavy metal ions using 0.2 M HNO<sub>3</sub> as eluent (a) Co<sup>2+</sup>; (b) Ni<sup>2+</sup>; (c) Cu<sup>2+</sup>; (d) Zn<sup>2+</sup>; (e) Cd<sup>2+</sup>; (f) Hg<sup>2+</sup> and (g) Pb<sup>2+</sup> using ZrATMP

**Table 2.31 Percentage elution (% E) of metal ions in various electrolyte media using ZrATMP**

Metal ion	NH <sub>4</sub> NO <sub>3</sub>		HNO <sub>3</sub>		HClO <sub>4</sub>		CH <sub>3</sub> COOH	
	0.02M	0.2M	0.02M	0.2M	0.02M	0.2M	0.02M	0.2M
Co <sup>2+</sup>	98	95	99	98	96	98	94	96
Ni <sup>2+</sup>	94	97	96	91	96	97	90	96
Cu <sup>2+</sup>	91	92	97	85	97	98	87	79
Zn <sup>2+</sup>	94	98	96	99	95	98	85	90
Cd <sup>2+</sup>	97	96	91	93	97	88	97	98
Hg <sup>2+</sup>	99	97	90	96	83	87	97	99
Pb <sup>2+</sup>	90	94	93	87	91	96	89	90

\*Eluent volume = 60 mL and 50 mL for 0.02 M and 0.2 M electrolytes respectively  
 Maximum deviation in % elution of metal ions = ±2

**Table 2.32 Binary separations of transition and heavy metal ions using ZrATMP**

Metal ion pairs	Separation factor( )	Eluant	Metal ion loaded [mg]	Metal ion Eluted [mg]	Elution [%]
Ni <sup>2+</sup> -Cu <sup>2+</sup>	3.30	a) 0.2 M HNO <sub>3</sub> (Ni <sup>2+</sup> )	0.5893	0.4916	83
		b) 0.2 M HClO <sub>4</sub> (Cu <sup>2+</sup> )	0.6354	0.5463	75
Co <sup>2+</sup> -Cu <sup>2+</sup>	7.88	a) 0.2 M HClO <sub>4</sub> (Co <sup>2+</sup> )	0.5869	0.5458	89
		b) 0.2 M HNO <sub>3</sub> (Cu <sup>2+</sup> )	0.6354	0.5401	75
Zn <sup>2+</sup> -Ni <sup>2+</sup>	1.64	a) 0.2 M HClO <sub>4</sub> (Zn <sup>2+</sup> )	0.6539	0.5763	93
		b) 0.2 M HNO <sub>3</sub> (Ni <sup>2+</sup> )	0.5893	0.5016	85
Co <sup>2+</sup> -Ni <sup>2+</sup>	2.38	a) 0.2 M HClO <sub>4</sub> (Co <sup>2+</sup> )	0.5869	0.5282	90
		b) 0.2 M HNO <sub>3</sub> (Ni <sup>2+</sup> )	0.5893	0.4995	84
Hg <sup>2+</sup> -Pb <sup>2+</sup>	28.89	a) 0.2 M NH <sub>4</sub> NO <sub>3</sub> (Hg <sup>2+</sup> )	2.0059	1.8454	91
		b) 0.2 M HClO <sub>4</sub> (Pb <sup>2+</sup> )	2.0720	1.8337	74
Hg <sup>2+</sup> -Cd <sup>2+</sup>	12.88	a) 0.2 M NH <sub>4</sub> NO <sub>3</sub> (Hg <sup>2+</sup> )	2.0059	1.8053	90
		b) 0.2 M CH <sub>3</sub> COOH (Cd <sup>2+</sup> )	1.1241	0.9217	82
Cd <sup>2+</sup> -Pb <sup>2+</sup>	2.24	a) 0.2 M CH <sub>3</sub> COOH (Cd <sup>2+</sup> )	1.1241	0.9105	81
		b) 0.2 M HClO <sub>4</sub> (Pb <sup>2+</sup> )	2.0720	1.6369	75

Maximum deviation in %elution = ±2

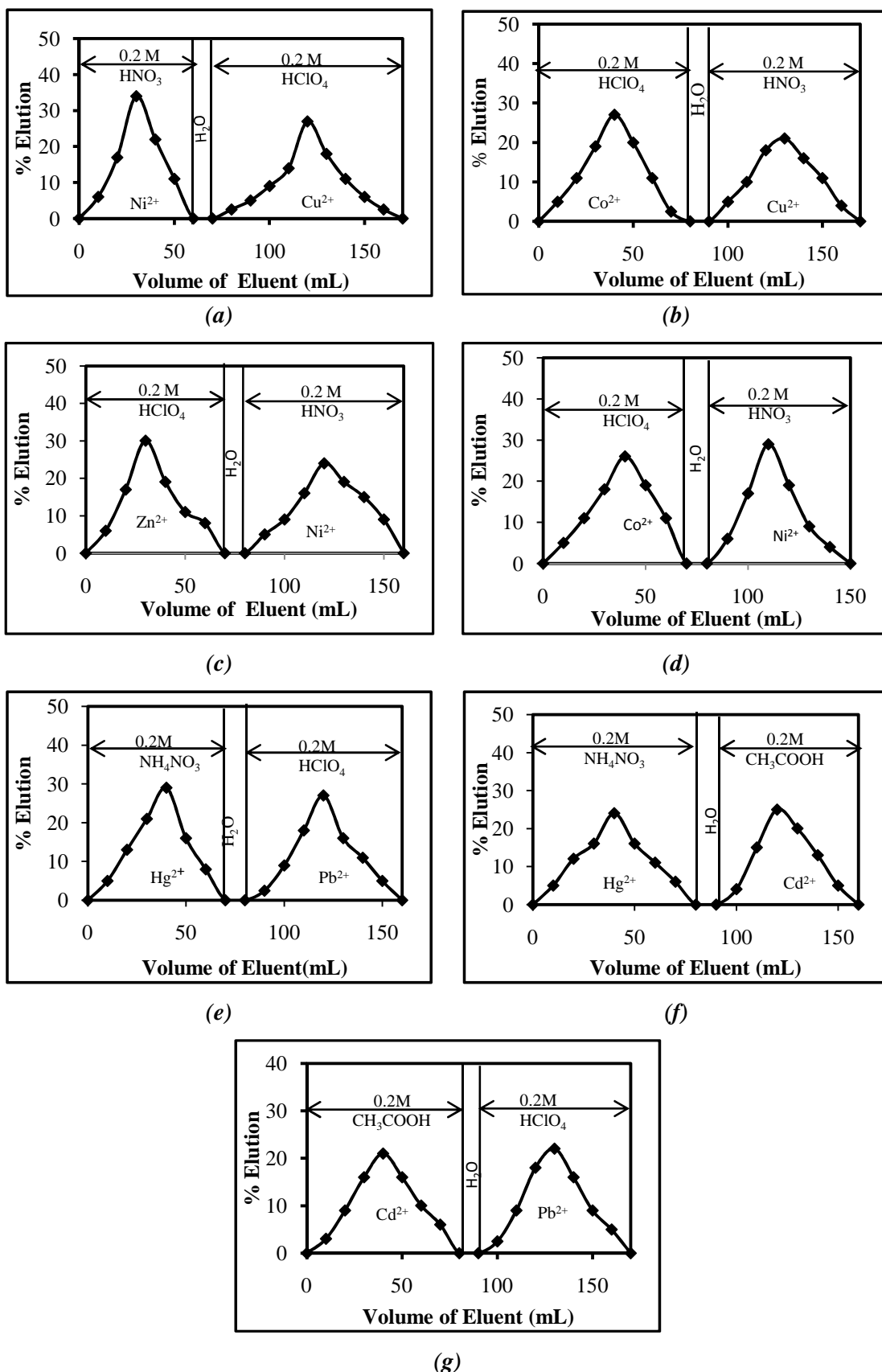
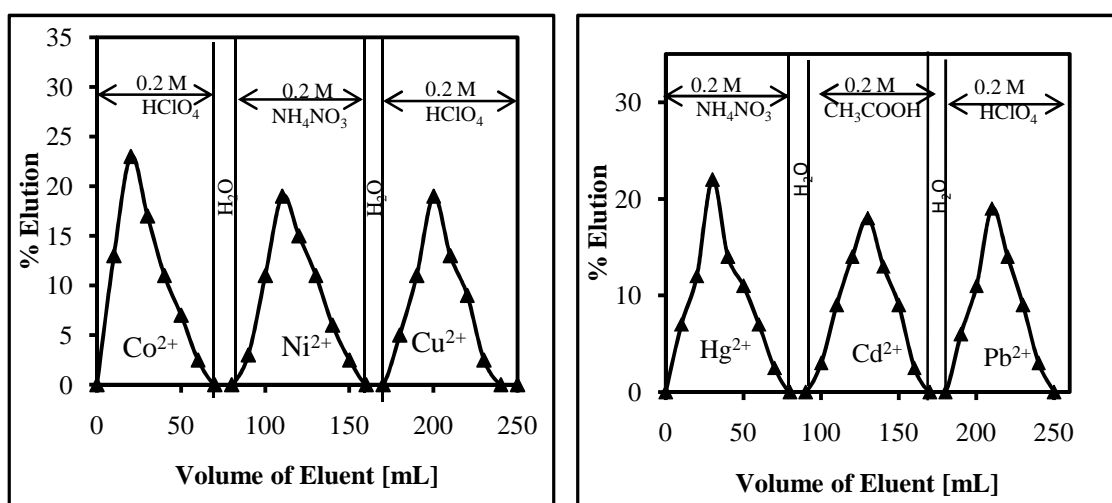


Figure 2.40(a-g) Binary separations of transition and heavy metal ions using ZrATMP (a)  $\text{Ni}^{2+}$  -  $\text{Cu}^{2+}$  (b)  $\text{Co}^{2+}$  -  $\text{Cu}^{2+}$ , (c)  $\text{Zn}^{2+}$  -  $\text{Ni}^{2+}$ , (d)  $\text{Co}^{2+}$  -  $\text{Ni}^{2+}$  (e)  $\text{Hg}^{2+}$  -  $\text{Pb}^{2+}$  (f)  $\text{Hg}^{2+}$  -  $\text{Cd}^{2+}$  (g)  $\text{Cd}^{2+}$  -  $\text{Pb}^{2+}$

Table 2.33 Ternary separations of transition and heavy metal ions using ZrATMP

Metal ion pairs	Eluant	Metal ion loaded [mg]	Metal ion Eluted [mg]	Elution [%]
$\text{Co}^{2+}$ - $\text{Ni}^{2+}$ - $\text{Cu}^{2+}$	a) 0.2 M $\text{HClO}_4$ ( $\text{Co}^{2+}$ )	0.5869	0.431	73
	b) 0.2 M $\text{NH}_4\text{NO}_3$ ( $\text{Ni}^{2+}$ )	0.5893	0.398	67
	c) 0.2 M $\text{HClO}_4$ ( $\text{Cu}^{2+}$ )	0.6354	0.378	59
$\text{Hg}^{2+}$ - $\text{Cd}^{2+}$ - $\text{Pb}^{2+}$	a) 0.2 M $\text{NH}_4\text{NO}_3$ ( $\text{Hg}^{2+}$ )	2.0059	1.514	75
	b) 0.2 M $\text{CH}_3\text{COOH}$ ( $\text{Cd}^{2+}$ )	1.1241	0.777	68
	c) 0.2 M $\text{HClO}_4$ ( $\text{Pb}^{2+}$ )	2.0720	1.285	62

Maximum deviation in %elution =  $\pm 2$



(a)

(b)

Figure 2.41 Ternary separations of transition and heavy metal ions using ZrATMP (a)  $\text{Co}^{2+}$ - $\text{Ni}^{2+}$ - $\text{Cu}^{2+}$  and (b)  $\text{Hg}^{2+}$ - $\text{Cd}^{2+}$ - $\text{Pb}^{2+}$

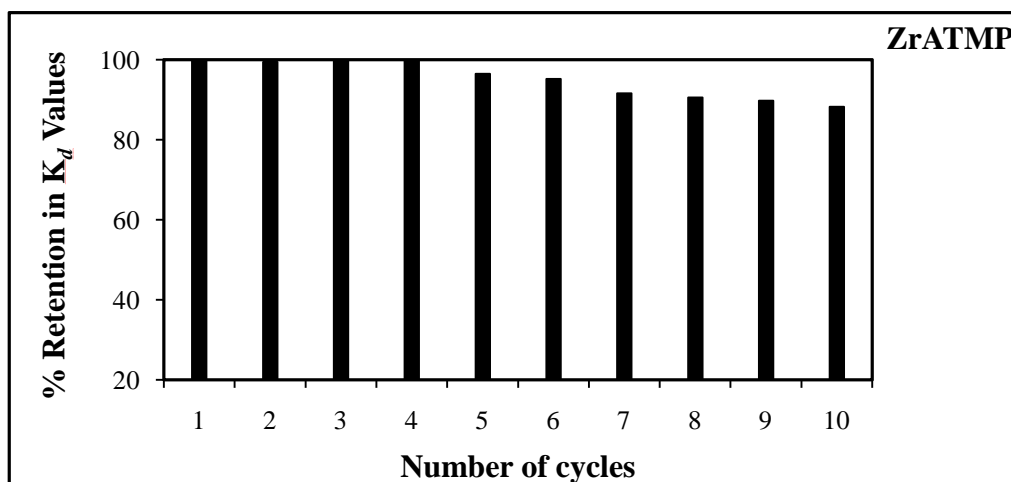


Figure 2.42 Plot of % retention in  $K_d$  values versus number of cycles using ZrATMP

### ***Metal Ion Separations using TiATMP***

The effect of metal ion concentration on distribution coefficient ( $K_d$ ), studied in aqueous medium (**Table 2.34**) shows that with increase in concentration,  $K_d$  values increase. Above a particular concentration  $K_d$  values are constant which could be explained to be due to the fact that at lower concentrations, almost all the ions are exchanged due to availability of exchangeable sites, which are not available at higher concentrations.

$K_d$  values have also been evaluated in various electrolyte media (HNO<sub>3</sub>, NH<sub>4</sub>NO<sub>3</sub>, HClO<sub>4</sub> and CH<sub>3</sub>COOH of 0.2 M and 0.02 M) at optimum conditions (optimum metal ion concentration, optimum pH and optimum equilibrium time) (**Table 2.35**). In general, it is observed that the  $K_d$  values are lower in high concentration of electrolyte and vice versa. In strong electrolyte media  $K_d$  values are lower as compared to weak electrolyte and aqueous media. This may be attributed to the high competition amongst ions for exchange in strong electrolyte media.  $K_d$  values in aqueous medium follows the order: Cu<sup>2+</sup> > Zn<sup>2+</sup> > Co<sup>2+</sup> > Ni<sup>2+</sup> amongst the transition metal ions and Pb<sup>2+</sup> > Cd<sup>2+</sup> > Hg<sup>2+</sup> amongst the heavy metal ions. The most promising features of TiATMP are, high  $K_d$  values observed in case of Cu<sup>2+</sup>, Zn<sup>2+</sup> and Pb<sup>2+</sup> in aqueous medium.

Breakthrough curves (a plot of  $C_e/C_0$  vs. effluent volume) for transition metal ions and heavy metal ions are presented in (**Figure 2.43 (a-g)**). Breakthrough capacity (BTC) is the dynamic capacity or operating capacity of a known amount of ion exchange material towards metal ion in column operation.  $K_d$  values also give an idea of affinity of metal ion towards ion exchanger, which is determined by a batch process. It is expected that the metal ion affinity towards the exchanger based on  $K_d$  and BTC should be same, which is observed (**Table 2.35**) in the present study.

The elution behaviour of transition metal ions and heavy metal ions (under study) have been carried out using different electrolytes such as HNO<sub>3</sub>, HClO<sub>4</sub>, CH<sub>3</sub>COOH, and NH<sub>4</sub>NO<sub>3</sub> of 0.02 and 0.2M concentration and results presented in (**Table 2.36**). The % metal eluted in all cases is in the range 70 to 99 %. Good elution is observed due to presence of single metal ion and non interference of elements. Higher concentration of eluent and acids in general, are better eluents. 0.2 M HNO<sub>3</sub> is the best eluent for most metal ions. Using 0.2 M HNO<sub>3</sub>, order of % metal eluted amongst transition metal ions is Ni<sup>2+</sup> (99%) > Co<sup>2+</sup> (95%) > Zn<sup>2+</sup> (92%) > Cu<sup>2+</sup> (90%)

and amongst heavy metal ions is  $\text{Hg}^{2+}$  (99%) >  $\text{Cd}^{2+}$  (96%) >  $\text{Pb}^{2+}$  (90%). This observation is in keeping with the fact that metal ions with high  $K_d$  values are less eluted and vice-versa. All elution curves are symmetrical bell shaped (**Figure 2.44**), indicating elution efficiency.

Binary separations for following metal ion pairs (under study)  $\text{Ni}^{2+}$ -  $\text{Cu}^{2+}$ ,  $\text{Co}^{2+}$ -  $\text{Cu}^{2+}$ ,  $\text{Zn}^{2+}$ - $\text{Cu}^{2+}$ ,  $\text{Ni}^{2+}$ -  $\text{Zn}^{2+}$ ,  $\text{Hg}^{2+}$ -  $\text{Pb}^{2+}$ ,  $\text{Cd}^{2+}$ -  $\text{Pb}^{2+}$  and  $\text{Hg}^{2+}$ -  $\text{Cd}^{2+}$  have been performed using concept of high separation factor in a particular medium as discussed earlier in the text. In binary separations, separation efficiency is in the range 69–93 % amongst transition metal ions and 64-95% amongst heavy metal ions (**Table 2.37**). Efficient separation in terms of % metal eluted is observed and also well supported by symmetrical bell shaped curves {**Figure 2.45(a-g)**}. In all cases of binary separation, irrespective of metal ion pair, maximum % metal eluted is  $\text{Cu}^{2+}$  (80%),  $\text{Zn}^{2+}$  (84%),  $\text{Co}^{2+}$  (88%),  $\text{Ni}^{2+}$  (93%) (amongst transition metal ions) and  $\text{Pb}^{2+}$  (75%),  $\text{Cd}^{2+}$  (87%),  $\text{Hg}^{2+}$  (95%), (amongst heavy metal ions). This observation is in keeping with separation factor ( ) and  $K_d$  values of metal ions. % metal eluted decreases with decreasing separation factor and increases with increasing separation factor and as explained earlier, metal ions with high  $K_d$  values are less eluted and vice-versa.

In ternary separations for  $\text{Co}^{2+}$ -  $\text{Ni}^{2+}$ - $\text{Cu}^{2+}$ , (transition metal ions) and  $\text{Hg}^{2+}$  -  $\text{Cd}^{2+}$ -  $\text{Pb}^{2+}$ , (heavy metal ions) % metal eluted is in the range 55-70% and 61-72% respectively (**Table 2.38**). In all cases, three distinct peaks are observed (**Figure 2.46**) however, with tailing effects for every metal ion eluted. % metal eluted is also lower as compared to single and binary metal ion separations. Probably the separation process becomes complex, attributed to the loss of metal ions during the changeover of the eluent, interference of metal ions, pH, simultaneous elution of two or more metal ions with the same eluent, and lastly, experimental errors involved in the determination of metal ions in the presence of other ions, etc.

A study on regeneration and reuse was performed as described in experimental section. It is observed that the exchanger, once used, can be converted back to its original form by desorption of the metal ions with concentrated nitric acid. A plot of % retention in  $K_d$  values vs number of cycles is presented in **Figure 2.47**, which shows that % retention in  $K_d$  values is almost the same upto 5 cycles, indicating that TiATMP could be regenerated and reused without much decline in performance.

**Table 2.34** *Distribution coefficient ( $K_d$ ) values ( $\text{mL}\cdot\text{g}^{-1}$ ) evaluated varying metal ion concentration in aqueous medium using TiATMP*

Metal ions	$K_d$ values at different concentration of metal ions									
	0.002	0.004	0.006	0.008	0.01	0.012	0.014	0.016	0.018	0.02
$\text{Co}^{2+}$	146	251	425	681	1292	1185	1093	1093	-	-
$\text{Ni}^{2+}$	153	260	438	700	842	870	842	864	865	-
$\text{Cu}^{2+}$	2022	2300	3800	4244	6466	9800	9890	9784	9769	9776
$\text{Zn}^{2+}$	382	660	842	1450	1685	1680	1680	1687	-	-
$\text{Cd}^{2+}$	188	250	307	482	742	734	732	-	-	-
$\text{Hg}^{2+}$	29	51	83	118	184	181	184	-	-	-
$\text{Pb}^{2+}$	292	345	521	678	863	1353	1685	1689	1685	-

**Table 2.35** *BTC ( $\text{mmol}\cdot\text{g}^{-1}$ ) and  $K_d$  ( $\text{mL}\cdot\text{g}^{-1}$ ) values evaluated in aqueous and various electrolyte media using TiATMP*

Metal Ions	BTC	$K_d^*$ values in aqueous and various electrolyte media/concentration at optimum conditions								
		DIW	$\text{NH}_4\text{NO}_3$		$\text{HNO}_3$		$\text{HClO}_4$		$\text{CH}_3\text{COOH}$	
			0.02M	0.2M	0.02	0.2 M	0.02 M	0.2 M	0.02M	0.2 M
$\text{Co}^{2+}$	0.51	2630	2501	435	681	630	879	170	730	69
$\text{Ni}^{2+}$	0.32	2390	1260	498	460	70	729	40	3075	2740
$\text{Cu}^{2+}$	0.72	19820	5539	3190	1498	129	1290	169	4780	4290
$\text{Zn}^{2+}$	0.56	3280	3229	1029	780	679	910	360	9230	4330
$\text{Cd}^{2+}$	0.21	2340	3989	2190	1820	1690	1480	559	1890	2298
$\text{Hg}^{2+}$	0.08	610	249	79	295	104	332	121	250	69
$\text{Pb}^{2+}$	0.40	3590	2698	2198	4479	224	4021	1169	7612	5190

$K_d^*$  Values obtained at optimum condition (Optimum metal ion concentration, Optimum pH of solution and maximum equilibrium time); DIW = Deionized water,

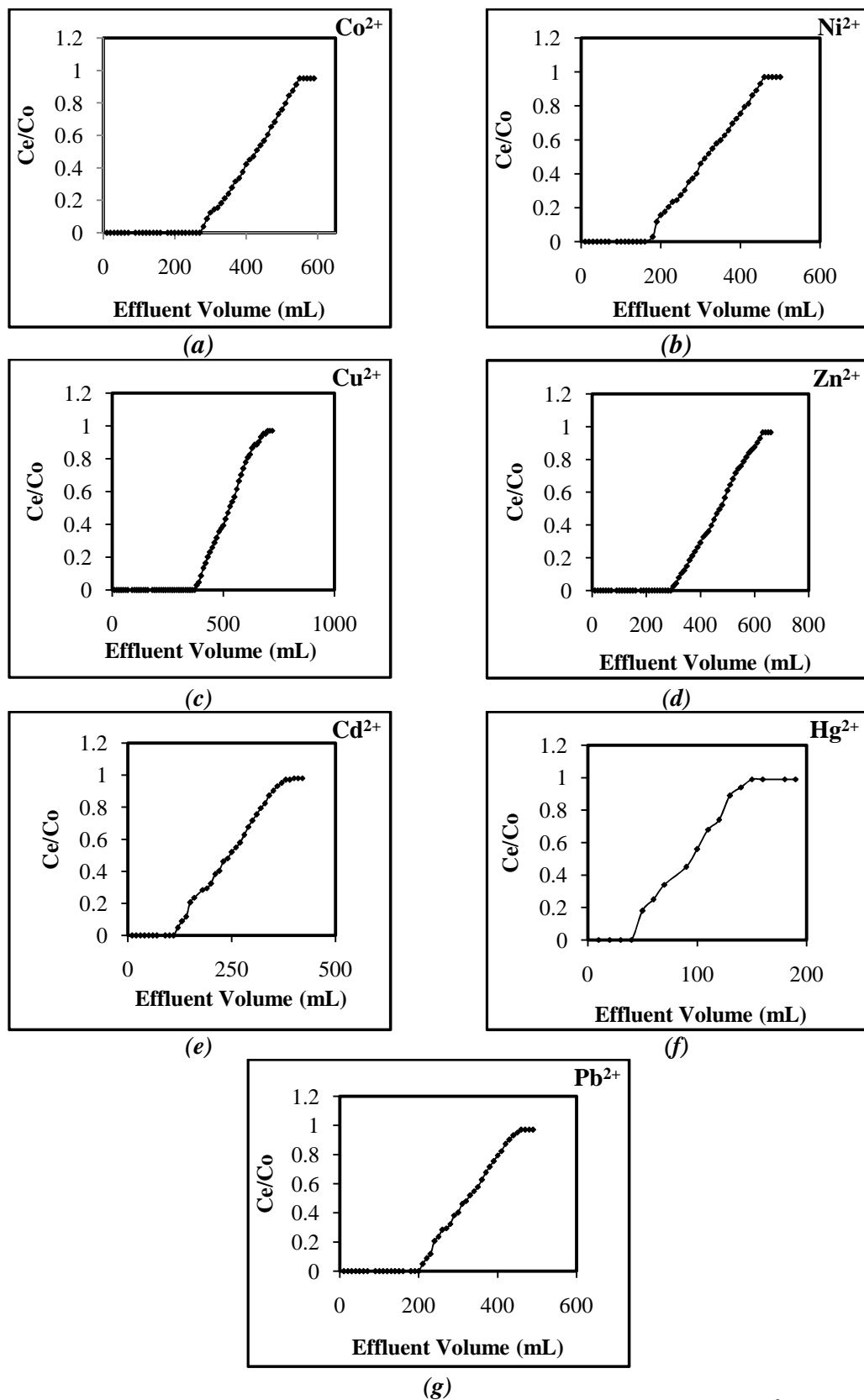


Figure 2.43(a-g) Breakthrough curves for transition metal ions (a)  $Co^{2+}$ ; (b)  $Ni^{2+}$ ; (c)  $Cu^{2+}$ ; (d)  $Zn^{2+}$ ; and heavy metal ions (e)  $Cd^{2+}$ ; (f)  $Hg^{2+}$ ; (g)  $Pb^{2+}$  metal ions using TiATMP

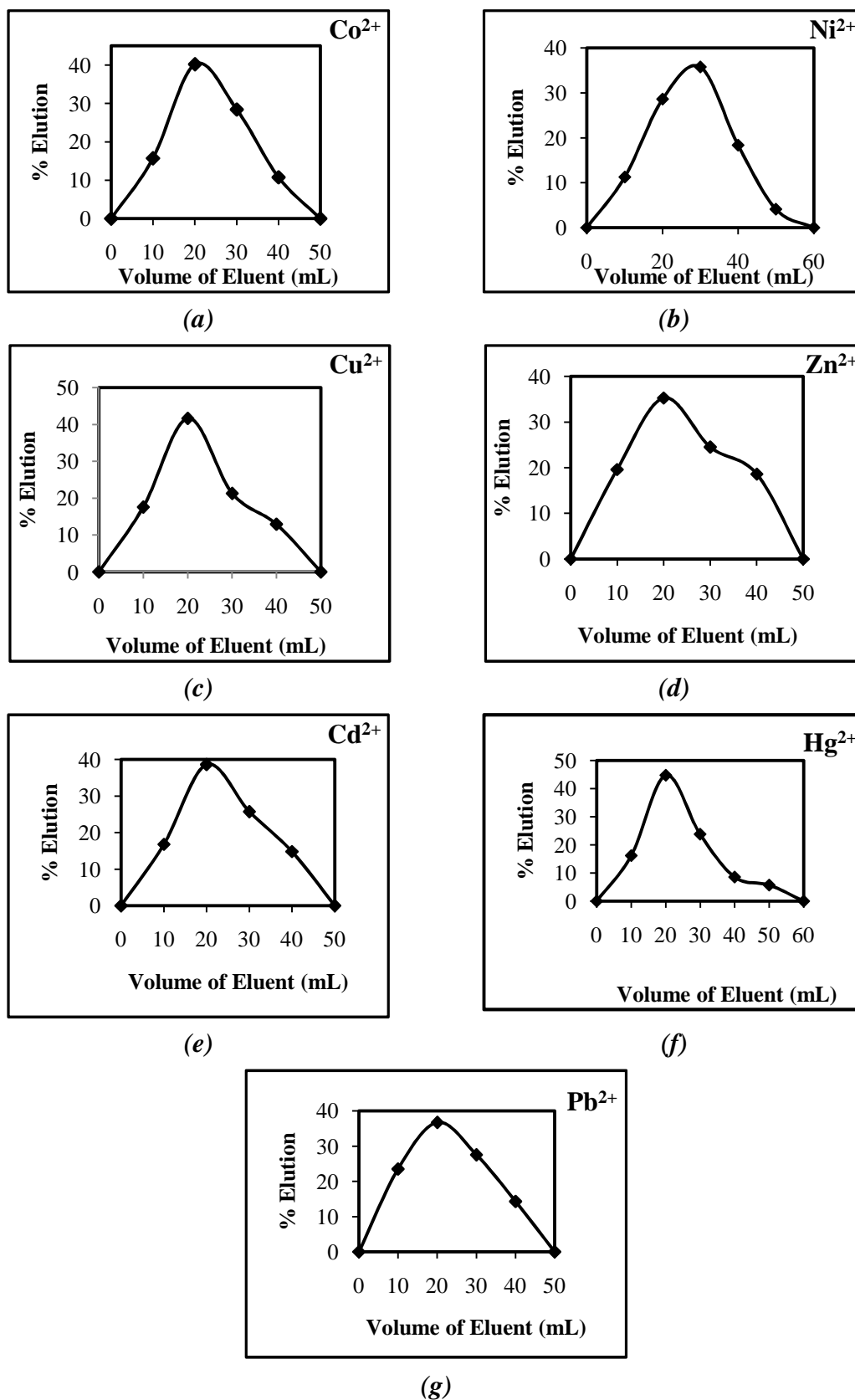


Figure 2.44 (a-g) Elution behaviour of transition and heavy metal using 0.2 M HNO<sub>3</sub> as eluent (a) Co<sup>2+</sup>; (b) Ni<sup>2+</sup>; (c) Cu<sup>2+</sup>; (d) Zn<sup>2+</sup>; (e) Cd<sup>2+</sup>; (f) Hg<sup>2+</sup> and (g) Pb<sup>2+</sup> using TiATMP

**Table 2.36 Percentage elution (%E) of metal ions in different electrolyte media using TiATMP**

Metal ion	NH <sub>4</sub> NO <sub>3</sub>		HNO <sub>3</sub>		HClO <sub>4</sub>		CH <sub>3</sub> COOH	
	0.02M	0.2M	0.02M	0.2M	0.02M	0.2M	0.02M	0.2M
Co <sup>2+</sup>	91	94	91	95	90	94	95	96
Ni <sup>2+</sup>	93	98	94	99	91	94	98	99
Cu <sup>2+</sup>	86	91	88	90	89	90	70	75
Zn <sup>2+</sup>	82	90	89	92	88	90	90	89
Cd <sup>2+</sup>	89	93	95	96	86	91	91	92
Hg <sup>2+</sup>	98	97	98	99	94	98	95	98
Pb <sup>2+</sup>	89	90	87	90	85	88	87	88

*Eluent volume = 60 mL and 50 mL for 0.02 M and 0.2 M electrolytes respectively*

*Maximum deviation in % elution of metal ions = ±2*

**Table 2.37 Binary separations of transition and heavy metal ions using TiATMP**

Metal ion pairs	Separation factor( )	Eluents	Metal ion loaded [mg]	Metal ion Eluted [mg]	Elution [%]
Ni <sup>2+</sup> - Cu <sup>2+</sup>	8.29	a) 0.2 M HClO <sub>4</sub> (Ni <sup>2+</sup> )	0.5893	0.5375	91
		b) 0.2 M HNO <sub>3</sub> (Cu <sup>2+</sup> )	0.6354	0.5097	80
Co <sup>2+</sup> - Cu <sup>2+</sup>	7.53	a) 0.2 M CH <sub>3</sub> COOH (Co <sup>2+</sup> )	0.5869	0.5211	88
		b) 0.2 M HNO <sub>3</sub> (Cu <sup>2+</sup> )	0.6354	0.4477	70
Zn <sup>2+</sup> -Cu <sup>2+</sup>	6.04	a) 0.2 M HClO <sub>4</sub> (Zn <sup>2+</sup> )	0.6539	0.5434	83
		b) 0.2 M HNO <sub>3</sub> (Cu <sup>2+</sup> )	0.6354	0.4445	69
Ni <sup>2+</sup> - Zn <sup>2+</sup>	1.37	a) 0.2 M HClO <sub>4</sub> (Ni <sup>2+</sup> )	0.5893	0.5485	93
		b) 0.2 M NH <sub>4</sub> NO <sub>3</sub> (Zn <sup>2+</sup> )	0.6539	0.5534	84
Hg <sup>2+</sup> - Cd <sup>2+</sup>	3.83	a) 0.2 M NH <sub>4</sub> NO <sub>3</sub> (Hg <sup>2+</sup> )	2.0059	1.8973	94
		b) 0.2 M HClO <sub>4</sub> (Cd <sup>2+</sup> )	1.1241	0.9878	87
Cd <sup>2+</sup> - Pb <sup>2+</sup>	1.53	a) 0.2 M HClO <sub>4</sub> (Cd <sup>2+</sup> )	1.1241	0.9728	86
		b) 0.2 M HNO <sub>3</sub> (Pb <sup>2+</sup> )	2.0720	1.3465	64
Hg <sup>2+</sup> -Pb <sup>2+</sup>	5.88	a) 0.2 M NH <sub>4</sub> NO <sub>3</sub> (Hg <sup>2+</sup> )	2.0059	1.9179	95
		b) 0.2 M HNO <sub>3</sub> (Pb <sup>2+</sup> )	2.0720	1.5647	75

*Maximum deviation in %elution = ±2*

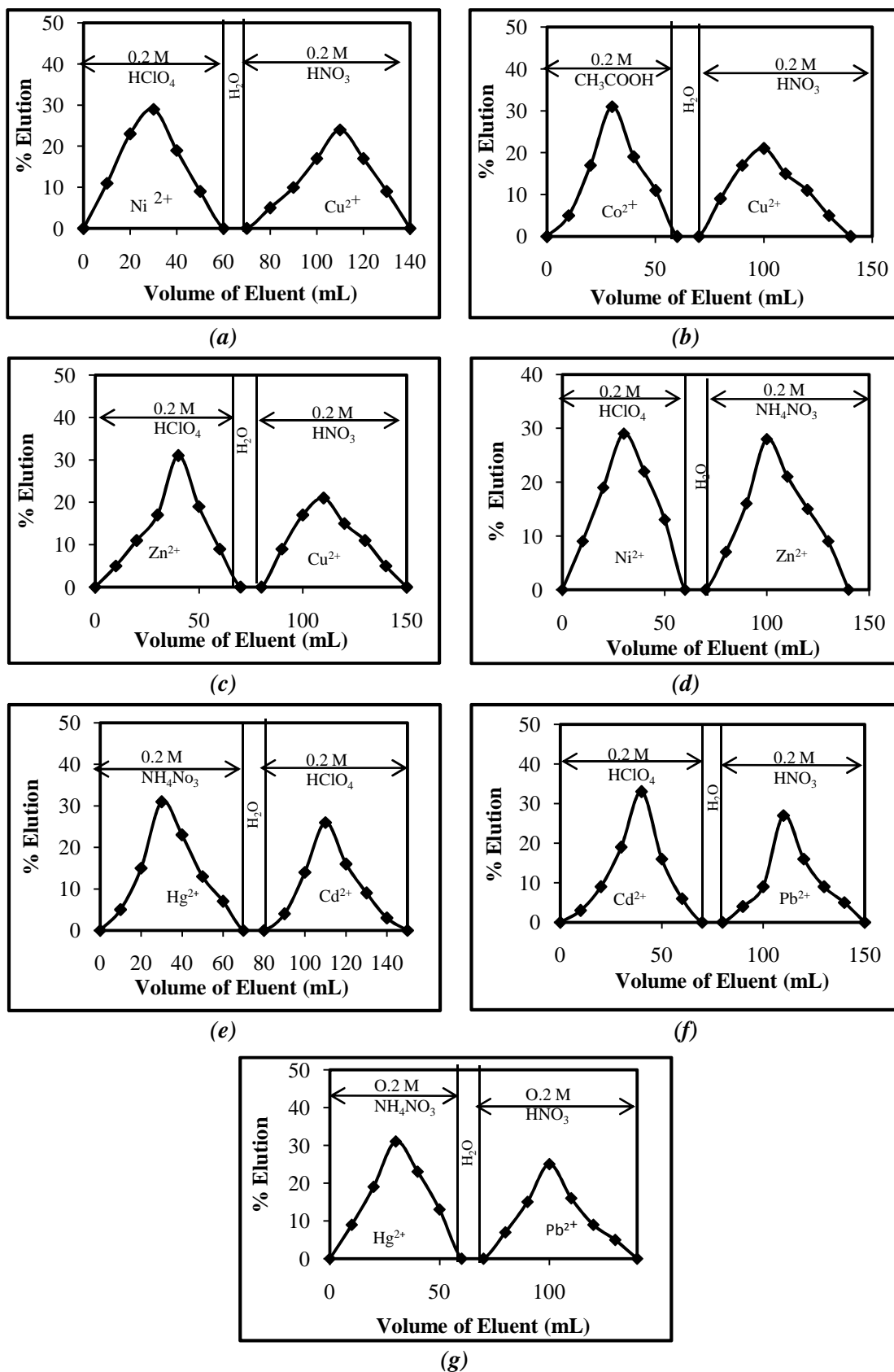


Figure 2.45(a-g) Binary separations of transition and heavy metal ions using TiATMP (a)  $Ni^{2+}$ -  $Cu^{2+}$  (b)  $Co^{2+}$ -  $Cu^{2+}$ , (c)  $Zn^{2+}$ - $Cu^{2+}$ , (d)  $Ni^{2+}$ -  $Zn^{2+}$  (e)  $Hg^{2+}$ -  $Cd^{2+}$  (f)  $Cd^{2+}$ - $Pb^{2+}$  (g)  $Hg^{2+}$ -  $Pb^{2+}$

Table 2.38 Ternary separations of transition and heavy metal ions using TiATMP

Metal ion pairs	Eluents	Metal ion loaded [mg]	Metal ion Eluted [mg]	Elution [%]
Ni <sup>2+</sup> -Co <sup>2+</sup> - Cu <sup>2+</sup>	a) 0.2 M HClO <sub>4</sub> (Ni <sup>2+</sup> )	0.5893	0.4132	70
	b) 0.2 M CH <sub>3</sub> COOH (Co <sup>2+</sup> )	0.5869	0.3954	67
	c) 0.2 M HNO <sub>3</sub> (Cu <sup>2+</sup> )	0.6354	0.3494	55
Hg <sup>2+</sup> -Cd <sup>2+</sup> -Pb <sup>2+</sup>	a) 0.2 M NH <sub>4</sub> NO <sub>3</sub> (Hg <sup>2+</sup> )	2.0059	1.4400	72
	b) 0.2 M HClO <sub>4</sub> (Cd <sup>2+</sup> )	1.1241	0.7808	69
	c) 0.2 M HNO <sub>3</sub> (Pb <sup>2+</sup> )	2.0720	1.2639	61

Maximum deviation in %elution = ±2

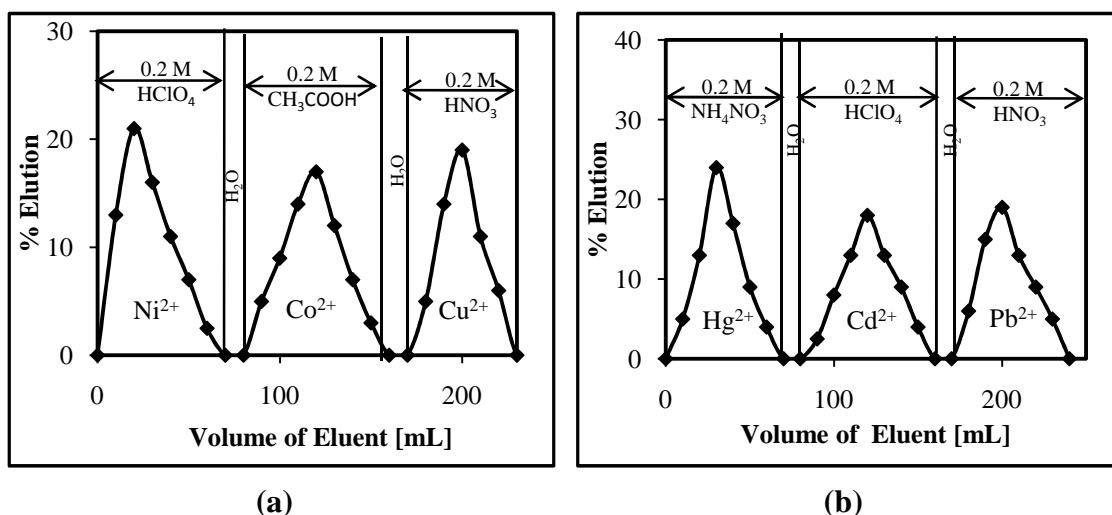


Figure 2.46 Ternary separations of transition and heavy metal ions using TiATMP (a) Ni<sup>2+</sup>-Co<sup>2+</sup>-Cu<sup>2+</sup> and (b) Hg<sup>2+</sup>-Cd<sup>2+</sup>-Pb<sup>2+</sup>

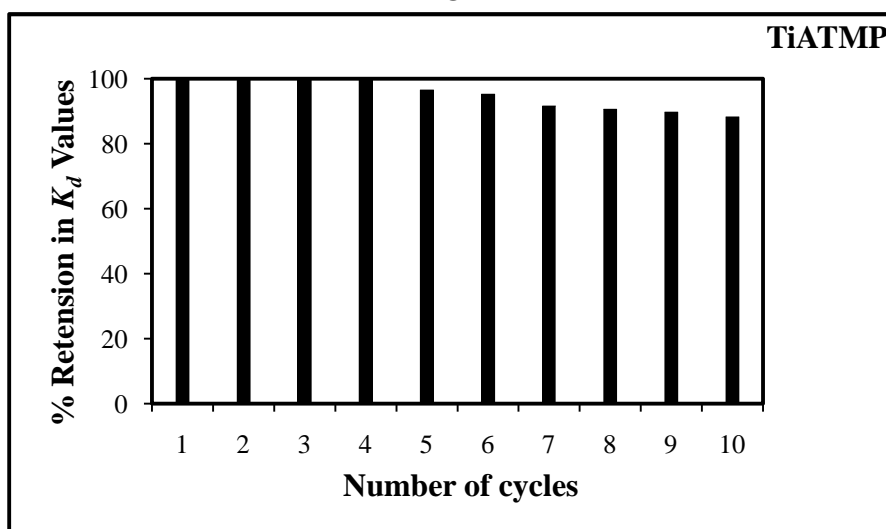


Figure 2.47 Plot of % retention in  $K_d$  values versus number of cycles using TiATMP

## 2.14 CONCLUSIONS

- ❖ The synthesized materials ZrATMP and TiATMP exhibit promising ion exchange characteristics - good CEC values,  $3.61 \text{ meq.g}^{-1}$  and  $4.01 \text{ meq.g}^{-1}$  respectively, granular nature suitable for column operation, good chemical (insoluble in aqueous, acid and organic solvent media) and thermal stability.
- ❖ Thermodynamic studies reveal that for both ZrATMP and TiATMP, equilibrium constant ( $K$ ) values increase with increase in temperature for all metal ions under study, indicating that the metal ions have higher affinity for the exchanger and that the mechanism is ion exchange.  $G^\circ$  values for all the exchange reactions are negative and become more negative with increasing temperature indicating increase in feasibility and spontaneity of the exchange process.  $H^\circ$  is positive in all cases indicating complete dehydration of ions for exchange to take place.
- ❖ Kinetic studies indicate the  $M^{2+} - H^+$  exchange to be an ion exchange process, favouring a particle diffusion-controlled mechanism.
- ❖ For both ZrATMP and TiATMP,  $R^2$  values are found to be close to unity (for both Langmuir and Freundlich isotherms) providing a good fit to the experimental data for sorption of all the metal ions studied.
- ❖ The most promising property is high selectivity for  $\text{Cu}^{2+}$ ,  $\text{Ni}^{2+}$ ,  $\text{Pb}^{2+}$  (ZrATMP) and  $\text{Cu}^{2+}$ ,  $\text{Zn}^{2+}$ ,  $\text{Pb}^{2+}$  (TiATMP) which suggests the possibility of their application for separation of these metal ions from other pollutants.
- ❖ Efficient binary metal ion separations carried out using ZrATMP and TiATMP indicate good potential for these materials to be used as cation exchangers.

## REFERENCES

- [1] Alberti G, *Layered metal phosphonates and covalently pillared diphosphonates* in *Comprehensive Supramolecular Chemistry*, (Eds.) Alberti G, Bein T, Pergamon Press, Oxford, Vol 7, 1996, p. 151.
- [2] Clearfield A, Costantino U, *Layered metal phosphates and their intercalation chemistry* in *Comprehensive Supramolecular Chemistry*, (Eds.) Alberti G, Bein T, Pergamon Press, Oxford, vol. 7, 1996, p. 107.
- [3] Clearfield A, *Recent advances in metal phosphonate chemistry*, **Curr. Opin. Solid State Mater. Sci**, 1 (1996) 268-278.
- [4] Clearfield A, *Metal phosphonate Chemistry in progress in inorganic chemistry*, (Ed.) Karlin K D, John Wiley & Sons, New York, Vol. 47, 1998, p. 374.
- [5] Clearfield A, *Coordination chemistry of phosphonic acids with special relevance to rare earths*, **J Alloys Compds**, 418 (2006) 128-138.
- [6] Vivani R, Alberti G, Costantino F, Nocchetti M, *New advances in zirconium phosphate and phosphonate chemistry: Structural archetypes*, **Microporous and Mesoporous Materials**, 107 (2008) 58–70.
- [7] Sanchez C, Soler-Illia G J de A A, Ribot F, Lalot T, Mayer C R, Cabuil V, *Designed hybrid organic-inorganic nanocomposites from functional nanobuilding blocks*, **Chem Mater**, 13 (2001) 3061-3083.
- [8] Wu Z, Liu Z, Tian P, He Y, Xu L, Yang Y, Zhang Y, Bao X, Liu X, Liu X, *Template-assisted syntheses of two novel porous zirconium methylphosphonates*, **Microporous and Mesoporous Materials**, 81(2005)175-183.
- [9] Zhang B, Clearfield A, *Crown ether pillared and functionalized layered zirconium phosphonates: A new strategy to synthesize novel ion selective materials*, **J Am Chem Soc**, 119 (1997) 2751-2752.
- [10] Leenstra W R, Amicangelo J C, *Synthesis, characterization, and interlayer distance study of zirconium phosphonates with stoichiometric variation of Methyl and p-Aminobenzyl Pendant Groups*, **Inorg Chem**, 37 (1998) 5317-5323.
- [11] Yin P, Zheng L M, Gao S, Xin X Q,  *$Cu_4\{CH_3C(OH)(PO_3)_2\}_2(C_4H_4N_2)(H_2O)_4$ : a novel, three-dimensional copper diphosphonate with metamagnetism*, **Chem Commun**, (2001) 2346-2347.

- [12] Morizzi J, Hobday M, Rix C, *Some bidentate amine adducts of indium(III) organophosphonates*, **J Mater Chem**, 11 (2001) 794-798.
- [13] Mao J G, Wang Z, Clearfield A, *Building layered structures from hydrogen bonded molecular units and 1D metal phosphonate chains: synthesis, characterization and crystal structures of N,N -dimethyl-N,N -ethylenediamine-bis(methylenephosphonic acid), its Ni(II) and Pb(II) complexes*, **J Chem Soc Dalton Trans**, (2002) 4541-4546.
- [14] Bauer S, Bein T, Stock N, *High-Throughput investigation and characterization of cobalt carboxy phosphonates*, **Inorg Chem**, 44 (2005) 5882-5889.
- [15] Varshney K G, Pandith H A, *Thermodynamics of the Na(I)-H(I), K(I)-H(I) and Ca(II)-H(I) exchanges on zirconium(IV)aluminophosphate cation exchanger*, **Coll Surf A**, 201 (2002) 1-7.
- [16] Zhilei Y, Yasuhiro S, Jihong Y, Sixiu S, Osamu T, Ruren X, *microemulsion-based synthesis of titanium phosphate nanotubes via amine extraction system*, **J Am Chem Soc**, 126 (2004) 8882-8883.
- [17] Kijima T, Yamaguchi M, Imaizumi K, Yada M, Machida M, *Carbon number-dependent intercalation and interlayer amidation properties of  $n$ -alkanediamines for  $n$ -titanium (2-carboxyethyl) phosphonate phosphate*, **J Chem Soc Dalton Trans**, (1998) 1633-1638.
- [18] Gomez-Alcántara M M, Cabeza A, Martínez-Lara M, Miguel A G A, Suau R, Bhuvanesh N, Clearfield A, *synthesis and characterization of a new bisphosphonic acid and several metal hybrids derivatives*, **Inorg Chem**, 43 (2004) 5283-5293.
- [19] Zhang B, Poojary D M, Clearfield A, *Synthesis, characterization, and amine intercalation behavior of zirconium N-(Phosphonomethyl)iminodiacetic acid layered compounds*, **Chem. Mater**, 8 (1996) 1333-1340.
- [20] Yamanaka S, Matsunaga M, Hattori M, *Preparation and structure of n-alkyl ester derivatives of zirconium bis(monohydrogen orthophosphate) dehydrate with layered structure*, **J Inorg Nucl Chem**, 43 (1976) 1343.
- [21] Yamanaka S, Tsujimoto M, *synthesis of the organic derivatives of  $n$ -zirconium phosphate by the reaction with propylene oxide*, Tanaka M, **J Inorg Nucl Chem**, 41 (1978) 605.

- [22] Hix G B, Turner A, Kariuki B M, Tremayne M, MacLean E J, *Strategies for the synthesis of porous metal phosphonate materials*, **J. Mater. Chem.**, 2002, 12, 3220-3227.
- [23] Mitchell M C, Kee T P, *Recent development in phosphono transfer Chemistry*, **Coordination Chemistry Reviews**, 158 (1997) 359-383.
- [24] Murugavel R, Gogoi N, *Structural variations in layered alkaline earth metal cyclohexyl Phosphonates*, **Bull Mater Sci**, 32 (2009) 321-328.
- [25] Holz R C, Meister G E, Horrocks W D Jr, *Spectroscopic characterization of a series of europium(III) amino phosphonate complexes in solution*, **Inorg. Chem**, 29 (1990) 5183-5189.
- [26] Ma T Y, Lin X Z, Zhang X J, Yuan Z Y, *Periodic mesoporous titanium phosphonate hybrid materials*, **J Mater Chem** (2010), DOI: 10.1039/c0jm01442g. (view online)
- [27] Ma T Y, Yuan Z Y, *Functionalized periodic mesoporous titanium phosphonate monoliths with large ion exchange capacity*, **Chem. Commun.**, 2010, 46, 2325-2327.
- [28] Ma T Y, Lin X Z, Zhang X J, Yuan Z Y, *High surface area titanium phosphonate materials with hierarchical porosity for multi-phase adsorption*, **New J Chem**, 34 (2010) 1209-1216.
- [29] Ma T Y, Zhang X J, Shao G S, Cao J L, Yuan Z Y, *Ordered macroporous titanium phosphonate materials: Synthesis, photocatalytic activity and heavy metal ion adsorption*, **J Phys Chem C**, 112 (2008) 3090-3096.
- [30] Ma T Y, Yuan Z Y, *Organic-additive-assisted synthesis of hierarchically Meso-/Microporous titanium phosphonates*, **Eur J Inorg Chem** (2010) 2941-2948.
- [31] Guerrero G, Mutin P H, Vioux A, *Organically modified aluminas by grafting and sol-gel processes involving phosphonate derivatives*, **J Mater Chem**, 11 (2001) 3161-3165.
- [32] Mehring M, Guerrero G, Dahan F, Mutin P H, Vioux A, *Synthesis, characterizations, and single crystal X-ray structures of soluble titanium alkoxide phosphonates*, **Inorg Chem**, 39 (2000) 3325-3332.
- [33] Tsai T Y, Wu Y J, Hsu F J, *Synthesis and properties of epoxy/layered zirconium phosphonate (Zr-P) nanocomposites*, **J Phys Chem Solids**, 69 (2008) 1379-1382.

- [34] Zhang X J, Ma T Y, Yuan Z Y, *Titania-phosphonate hybrid porous materials: preparation, photocatalytic activity and heavy metal ion adsorption*, **J Mater Chem**, 18 (2008) 2003-2010.
- [35] Zeng R, Fu X, Sui Y, Yang X, Sun M, Chen J, *Synthesis, characterization and intercalation property of layered zirconium benzylamino-N,N-dimethyl phosphonate phosphate materials*, **J Organometallic Chem**, 693 (2008) 2666-2672.
- [36] Chessa S, Claydon N J, Bochmann M, Wright J A,  *$\gamma$ -zirconium phosphonates: versatile supports for N-heterocyclic carbenes*, **Chem commun** (2009) 797-799.
- [37] Ma X, Liu J, Xiao L, Chen R, Zhou J, Fu X, *Novel organosoluble filiform zirconium phosphonates with a layered mesoporous backbone*, **J Mater Chem**, 19 (2009) 1098-1104.
- [38] Shimizu G K H, Vaidhyanathan R, Taylor J M, *Phosphonate and sulphonate metal organic frameworks*, **Chem Soc Rev**, 38 (2009) 1430-1449.
- [39] Subbiah A, Pyle D, Rowland A, Huang J, Narayanan R A, Thiagarajan P, Zon J, Clearfield A, *A family of microporous materials formed by Sn(IV) phosphonate Nanoparticles*, **J Am Chem Soc**, 127(2005)10826-10827.
- [40] Christian Serre and Gerard Ferey, *Hydrothermal synthesis and structure determination from powder data of new three-dimensional titanium(IV) diphosphonates  $Ti(O_3P-(CH_2)_n-PO_3)$  or MIL-25<sub>n</sub> ( $n = 2,3$ )*, **Inorg Chem**, 40(2001)5350-5353.
- [41] Tian-Yi Ma, Xiu-Zhen Lin, and Zhong-Yong Yuan, *Cubic mesoporous titanium phosphonates with Multifunctionality*, **Chem Eur J**, 16(2010)8487–8494.
- [42] Faghihian, Hossein, Yaghobb, Nejadasl, Hooman, *Synthesis, characterization and application of a novel zirconium phosphonate ion-exchanger for removal of  $Ni^{2+}$ ,  $Cu^{2+}$  and  $Zn^{2+}$  from aqueous Solutions*, **Iran J Chem Eng**, 30(2)(2011) 23-31.
- [43] Xiu-Zhen Lin and Zhong-Yong Yuan, *Synthesis of mesoporous zirconium organophosphonate solid-acid catalysts*, **Eur J Inorg Chem**,(2012)2661–2664.
- [44] Yunjie Jia, Yuejuan Zhang, Ruiwei Wang, Jianjun Yi, Xu Feng, and Qinghong Xu, *Mesoporous zirconium phosphonate hybrid material as adsorbent to heavy metal ions*, **Ind Eng Chem Res**, 51(2012)12266-12273.

- [45] Jonghyun Choi, Andreas Ide, and Rachel A. Caruso Yen B. Truong, Ilias L. Kyratzis, *High surface area mesoporous titanium–zirconium oxide nanofibrous web: a heavy metal ion adsorbent*, **J Mater Chem A**, 1(2013)5847-5853.
- [46] Marco Taddei, Anna Donnadio, Ferdinando Costantino, Riccardo Vivani, Mario Casciola, *Synthesis, crystal structure, and proton conductivity of one dimensional, two-dimensional, and three-dimensional zirconium phosphonates based on glyphosate and glyphosine*, **Inorg Chem**, 52(2013) 12131-12139.
- [47] Alain Graillet, Denis Bouyer, Sophie Monge, Jean-Jacques R, Catherine F, *Removal of nickel ions from aqueous solution by low energy-consuming sorption process involving thermosensitive copolymers with phosphonic acid groups*, **J of Hazar Mater**, 244(2013), 507–515.
- [48] Zengdi Wang, Ping Yin, Zhi Wang, Qiang Xu, Rongjun Qu, and Qinghua Tang, *Removal of Pb(II) and Cu(II) Ions From Aqueous Solutions by Manganese Phosphonate*, **Sep Sci Tech**, 48(2013), 281–287.
- [49] Aurelia Visa, Bianca Maranescu, Alexandra Bucur, Demadis Smaranda Iliescu and Konstantinos D. *Synthesis and Characterization of a Novel Phosphonate Metal Organic Framework Starting from Copper Salts*. View online.
- [50] Lu-Lu Dai, Cui-Ying Huang, Rui Li, Zhen-GangSun, Cheng-Qi Jiao, Shao-Ping Shi, Wei Zhou, Yan-YuZhu, *Synthesis, structure, and surface photovoltage property of two new cobalt (II) phosphonates with 2D layered structure*, **Inorganic Chemistry Communications**, 40, 2014, 181–186.
- [51] Inamuddin, Khan S A, Siddiqui W A, Khan A A, *Synthesis, characterization and ion-exchange properties of a new and novel ‘organic-inorganic’ hybrid cation-exchanger: Nylon-6,6, Zr(IV) phosphate*, **Talanta**, 71 (2007) 841-847.
- [52] K. G. Varshney, M. A. Khan, *Inorganic Ion Exchangers in Chemical Analysis*, M. Qureshi and K. G. Varshney, Eds., CRC Press, Boca Raton Florida (1991)117.
- [53] A. Bhaumik & S. Inagaki, *Mesoporous Titanium Phosphate Molecular Sieves with Ion-Exchange Capacity*, **J Am. Chem Soc**, 123 (2001) 691-696.
- [54] A. Jayswal & U. Chudasama, *Synthesis and characterization of a novel metal phosphonate, zirconium (IV)-hydroxy ethylidene diphosphonate, and its application as an ion exchanger*, **Turk J Chem**, 32(2008)63-74.

- [55] K. Maheria & U. Chudasama, *Synthesis and characterization of a new phase of titanium phosphate and its application in separation of metal ions*, **Indian J Chem Technol**, 14 (2007) 423-426.
- [56] P Patel, U Chudasama, *Synthesis, characterization and ion exchange characteristics of a novel hybrid ion exchange material*, **Desalination and water treatment**, 12 (2009) 87-92.
- [57] Thakkar R, Chudasama U, *Synthesis and Characterization of Zirconium Titanium Hydroxy Ethylidene Diphosphonate and Its Application in Separation of Metal Ions*, **Separation Science and Technology**, 44 (2009) 3088-3112.
- [58] Patel P, Chudasama U, *Synthesis and Characterization of a Novel Hybrid Cation Exchange Material and its Application in Metal Ion Separations*, **Ion Exchange Letters**, 4 (2011) 7-15.
- [59] Patel P, Chudasama U, *Application of a Novel Hybrid Cation Exchange Material in Metal Ion Separations*, **Separation Science and Technology**, 46 (2011)1346-1357.
- [60] Gupta V K, Singh P, Rahman N, *Synthesis, characterization and analytical application of zirconium (IV) selenoiodate: a new cation exchanger*, **Anal Bioanal Chem**, 381 (2005) 471-476.
- [61] Hiavacek V, Puszynski J, *Chemical Engineering Aspects of Advanced Ceramic Materials*, **Ind Eng Chem Res**, 35 (1996) 349-377.
- [62] Martinola F, Kune G, *Int Conf on Ion Exchange*, London (1969).
- [63] Helfferich F, *Ion Exchange*, McGraw Hill, New York (1962).
- [64] Nabi S A, Rao R K, *Synthesis and ion exchange properties of cerium (IV) tellurite*, **J Indian Chem Soc**, 11 (1981) 1030-1032.
- [65] Schlocl R, Schurig H, *Eine experimentelle Methode zur Bestimmung der Porengrößen in Ionenaustauschern*, **Z Elektrochem**, 65 (1961) 863-870.
- [66] Seip C T, Granroth G E, Meisel M W, Talham D R, *Langmuir-Blodgett Films of Known Layered Solids: Preparation and Structural Properties of Octadecylphosphonate Bilayers with Divalent Metals and Characterization of a Magnetic Langmuir-Blodgett Film*, **J Am Chem Soc**, 119 (1997) 7084-7094.
- [67] Slade R C T, Knowels J A, Jones D J, Roziere J, *The isomorphous acid salts -  $Zr(HPO_4)_2 \cdot H_2O$ ,  $-Ti(HPO_4)_2 \cdot H_2O$  and  $-Zr(HAsO_4)_2 \cdot H_2O$  Comparative*

- thermochemistry and vibrational spectroscopy*, **Solid State Ionics**, 96 (1997) 9-19.
- [68] Varshney K G, Pandith H A, *Thermodynamics of the Na(I)-H(I), K(I)-H(I) and Ca(II)-H(I) exchanges on zirconium(IV) aluminophosphate cation exchanger*, **Coll Surf A: Physicochem and Engg Aspects**, 201 (2002) 1-7.
- [69] Manov G G, Bates R G, Hamer W J, Acree S F, *Values of the Constants in the Debye-Hückel Equation for Activity Coefficients*, **J Am Chem Soc**, 65 (1943) 1765-1767.
- [70] Gaines G L, Thomas H C, *Adsorption Studies on Clay Minerals. II. A Formulation of the Thermodynamics of Exchange Adsorption*, **J Chem Phys**, 21 (1953) 714-718.
- [71] Pehlivan E, Ersoz M, Pehlivan M, Yildiz S, Duncan H J, *The Effect of pH and Temperature on the Sorption of Zinc(II), Cadmium(II) and Aluminum(III) onto New Metal-Ligand Complexes of Sporopollenin*, **J Coll Inter Sci**, 170 (1995) 320-325.
- [72] Yuh-Shan H, *Removal of copper ions from aqueous solution by tree fern*, **Wat Res**, 37 (2003) 2323-2330.
- [73] Brown P A, Gill S A, Allen S J, *Metal removal from wastewater using peat*, **Wat Res**, 34 (2000) 3907-3916.
- [74] Tagami L, Santos O, Sousa-Aguiar E, Arroyo P, Barros M, *NaY and CrY zeolites ion exchange. Thermodynamics*, **Acta Scientiarum Maringa**, 23 (2001) 1351-1357.
- [75] Boyd G E, Adamson A W, Myers L S, *The Exchange Adsorption of Ions from Aqueous Solutions by Organic Zeolites. II. Kinetics*, **J Am Chem Soc**, 69 (1947) 2836-2848.
- [76] Varshey K G, Khan A R, Alam K Z, Ahmad A, *Evaluation of the dimensionless time parameter for some particle diffusion controlled forward and reverse OH(I)-Anion(I) and OH(I)-Anion(II) exchanges*, **Coll Surf**, 48 (1990) 373-378.
- [77] Kullberg L H, Clearfield A, *Thermodynamics of Alkali and Alkaline Earth Metal Ion-Exchange on Zirconium Sulphophosphonates*, **Solv Extr Ion Exch**, 8 (1990) 187-197.

- [78] Varshney K G, Gupta U, Maheshwari S M, *Kinetics of ion-exchange of alkaline earth metals on antimony(V) phosphate cation exchanger*, **React Kinet Catal Lett**, 61 (1997) 127-132.
- [79] Barrer R M, *Diffusion in and through Solids*, Cambridge University Press, New York (1941) 29.
- [80] Helfferich F, Plesset M S, *Ion Exchange Kinetics. A Nonlinear Diffusion Problem*, **J Chem Phys**, 28 (1958) 418-424.
- [81] Plesset M S, Helfferich F, Franklin J N, *Ion Exchange Kinetics. A Nonlinear Diffusion Problem. II. Particle Diffusion Controlled Exchange of Univalent and Bivalent Ions*, **J Chem Phys**, 29 (1958) 1064-1069.
- [82] Barrer R M, Fender B E F, *The diffusion and sorption of water in zeolites-II. Intrinsic and self-diffusion*, **J Phys Chem Solids**, 21 (1961) 12-24.
- [83] Gupta A P, Qureshi M, Rawat J P, *Ion Exchange Equilibrium Studies in Niobium Arsenate*, **Indian J Chem Soc**, 58 (1981) 855-857.
- [84] Altin O, Özbelge H Ö and Dogu T, **J Colloid Interface Sci**, **198** (1998) 130.
- [85] Voudrias E, Fytianos K, Bozani E, *Sorption - desorption isotherms of dyes from aqueous solutions and waste waters with different sorbent materials*, **Global Nest: The Int J**, 4(1)(2002) 75-83.
- [86] Akpomie G K, Ogbu I C, Osunkunle A A, Abuh M A, Abonyi M N, *Equilibrium isotherm studies on the sorption of Pb(II) from solution by ehendiagu clay*, **J Emerg Trends Eng App Sci**, 3(2)(2012)354-358.
- [87] Kinniburgh G D, Barker A J and Whitefuekd M J, *A comparison of some simple adsorption isotherms for describing divalent cation adsorption by ferrihydrite*, **J Coll, Interface Sci.**, 95(1983) 370-375.
- [88] Kunin, R. 1958. *Ion Exchange Resin*, Wiley, London.
- [89] P. Patel and U. Chudasama, *Thermodynamics and kinetics of ion exchange of a hybrid cation exchanger, titanium diethylene triamine pentamethylene phosphonates*, **J Sci & Ind Rese**, **69**(2010)756-766.
- [90] Kurtoglu, A. E. and G. Atun., *Determination of kinetics and equilibrium of Pb/Na exchange on clinoptilolite*, **Sep Puri Tech**, 50(2006)62-70.
- [91] Barrer R M, Bartholomew R F, Ress L V C, *Ion exchange in porous crystals part I. Self- and exchange-diffusion of ions in chabazites*, **J Phys Chem Solids**, 24(1963)51-62.

- [92] Benyamin K, *Self-diffusion of sodium and cesium ions in hydrous titanium oxide*, **Solid State Ionics**, 73(1994)303-308.
- [93] Thind P S, Mittal S K, *Particle diffusion kinetics of exchnage for transition metal ions in crystalline Tin(IV) Antimonophosphate*, **Transition Met Chem**, 10 (1985) 69-73.
- [94] El-Batouti M, Zaghoul A A, Hanna M T J, *A Kinetic Study of the Copper Exchange Reaction on a Sodium-Montmorillonite Clay Mineral in Acetonitrile and Dimethylformamide*, **J Coll Inter Sci**, 180(1996)106-110.
- [95] Sasaki T, Komatsu Y, Fujiki T, *Ion-exchange properties of hydrous titanium dioxide with a fibrous form obtained from potassium dititanate*, **Solv Extr Ion Exch**, 1(1983)775-790.
- [96] Abou-Mesalam M M, *Sorption kinetics of copper, zinc, cadmium and nickel ions on synthesized silico-antimonate ion exchanger*, **Colloid Surf A**, 225 (2003) 85-94.